Characterizing effects of puromycin selection on enrichment of astrocyte subtypes and extracellular matrix (ECM) generation with ECM incorporation in hyaluronic-acid (HA)-based hydrogels for axon growth of V2a interneurons

Sangamithra Vardhan

A dissertation

submitted in partial fulfillment of the

requirements for the degree of

Doctor of Philosophy

University of Washington

2025

Reading Committee:

Shelly Sakiyama-Elbert

Andre Berndt

Drew Sellers

Program Authorized to Offer Degree:
Bioengineering

University of Washington

Abstract

Characterizing effects of puromycin selection on enrichment of astrocyte subtypes and extracellular matrix (ECM) generation with ECM incorporation in hyaluronic-acid (HA)-based hydrogels for axon growth of V2a interneurons

Sangamithra Vardhan

Chair of the Supervisory Committee:

Shelly Sakiyama-Elbert

Bioengineering Department

Astrocyte subtypes are key cellular players to study *in vitro* for identifying specific cues that increase axon growth of neuron populations in potential translation to develop a scalable astrocyte-derived solution for axon regeneration post SCI. I characterized the use of transgenic puromycin selectable cell lines to enrich protoplasmic and fibrous astrocytes differentiated from mouse embryonic stem cells (mESCs) through viability and glutamate uptake assays, immunocytochemistry, flow cytometry, quantitative polymerase chain reaction (qPCR), and calcium imaging. It was demonstrated that selected astrocyte subtypes maintain low levels of other cell types (mature neurons and oligodendrocytes and undifferentiated stem cells) and high levels of astrocyte markers with functionality by glutamate uptake, inflammatory response, and calcium transients. Furthermore, selected protoplasmic astrocyte components, specifically ECM,

demonstrated significant increases in axon growth of mESC-derived V2a interneurons, a critical excitatory neuron population found in grey matter of spinal cord, compared to selected fibrous astrocytes in both 2D and 3D HA-based hydrogel setting. With bulk-RNA sequencing of astrocyte subtypes and proteomic analysis of selected astrocyte subtype ECM, selected protoplasmic astrocytes demonstrated upregulation of critical adhesion and ECM-related genes and proteins that could contribute to the positive impact on axon growth. Based on the criteria of protein availability and manufacturing, 5 selected protoplasmic ECM proteins at defined combinations and concentrations (based on design of experiments- DoE approach) in HA-based hydrogel were shown to significantly increased axon growth of V2a interneurons compared to selected protoplasmic ECM hydrogel. Overall, this thesis demonstrates the importance of studying *in vitro* properties of astrocyte subtypes for axon growth and the use of astrocyte-derived factors in developing a scalable, cell-free permissive biomaterial for supporting axon regeneration in future SCI applications.

Table of Contents

List of Figures

List of Tables

Appendix A: Supplemental figures and tables for chapter 2

Appendix B: Supplemental figures and tables for chapter 3

Supplemental Table 2.3: Custom DoE output for fifth-order interactions perlecan, col18a1, laminin-1, fibronectin, and anti-thrombin-III at low for K_d and high at 50µg/mL

Abbreviations

N-[*N*-(3,5-difluorophenacetyl-l-alanyl)]-(*S*)-phenylglycine t-butyl ester- **DAPT**
Adeno-associated virus- **AAV**
Adenosine triphosphate- **ATP**
Aldehyde dehydrogenase L1- **Aldh1L1**
AMPA receptor- **AMPAR**
Analysis of variance- **ANOVA**
Aquaporin 4- **Aqp4**
β-mercaptoethanol- **BME**
Basso-Beattie- Bresnahan- **BBB**
Basic helix-loop-helix- **bhlh**
Bicinchoninic acid- **BCA**
Blood-brain barrier- **BBB**
Blood-spinal cord barrier- **BSCB**
Brain lipid binding protein- **BLBP**
Biotinylated dextran amine- **BDA**
Bone morphogenic protein- **BMP4**
Brain-derived neurotrophic factor- **BDNF**
Central nervous system- **CNS**
Central pattern generator- **CPG**
Clozapine-N-oxide- **CNO**
Chondroitin sulfate proteoglycans- **CSPGs**
Chondroitinase ABC – **ChABC**
Chordin-like 1- **Chrdl1**
Ciliary neurotrophic factor- **CNTF**
Complete media-**CM**
Connexin-30- **Cx-30**
Connexin-43- **Cx-43**
Cortical spinal tract- **CST**
Damage-associated molecular patterns- **DAMPs**
Design of experiments- **DoE**
Diphtheria toxin- **DTA**
Dorsal root ganglion- **DRG**
Dulbecco's modified Eagle's Medium- **DMEM**
Embryoid bodies- **EBs**
Enhanced green fluorescent protein- **eGFP**
Epidermal growth factor- **EGF**
Equilibrium dissociation constant- **K_d**
Ethylenediaminetetraacetic acid- **EDTA**
Extracellular matrix -**ECM**
Excitatory post synaptic current- **EPSC**
False discovery rate- **FDR**
Fetal bovine serum- **FBS**

Fibroblast growth factor-1- **FGF-1**
Fibroblast growth factor-2- **FGF-2**
Ganciclovir- **GCV**
Gamma-aminobutyric acid- **GABA**
Genetically encoded calcium indicator- **GCaMP**
Gene ontology biological process- **GObp**
Glial-derived neurotrophic factor- **GDNF**
Glial restricted progenitors- **GRPs**
Glial fibrillary acidic protein- **GFAP**
Glutamate transporter- **GLT-1**
Glutamate aspartate transporter- **GLAST**
Glutamine synthetase- **GS**
Glyceraldehyde 3-phosphate dehydrogenase- **GAPDH**
Growth associated protein- **GAP-43**
4-(2-hydroxyethyl)-1-piperazineethanesulfonic acid- **HEPES**
HA and methylcellulose- **HAMC**
Hank's balanced salt solution- **HBSS**
Heparan sulfate proteoglycans- **HSPGs**
Human induced pluripotent stem cells- **hiPSCs**
Hyaluronic acid- **HA**
Hyaluronic acid- methylfuran- **HA-mF**
Human induced pluripotent stem cells- **hiPSCs**
Immunocytochemistry- **ICC**
Inhibitory designer receptors exclusively by designer drugs- **(G_i)DREADD**
Janus kinase- **JAK**
Junction PCR- **jPCR**
Kyoto Encyclopedia of Genes and Genomes- **KEGG**
Leukemia inhibitory factor- **LIF**
Lipopolysaccharide- **LPS**
Liquid chromatography- mass spectrometry- **LC-MS**
Long-term potentiation- **LTP**
Matrix metalloprotease 9- **MMP 9**
Methylfuran- **mF**
Motor neurons- **MNs**
Mouse embryonic stem cell lines- **mESCs**
Myelin basic protein- **MBP**
Neomycin phosphotransferase II- **Neo**
Neurotrophin-3- **NT3**
Neural progenitor cell- **NPCs**
Neural stem cells- **NSCs**
Nuclear magnetic resonance- **NMR**
Oligodendrocyte precursor cells- **OPCs**
Perineuronal nets- **PNNs**
Polyethylene glycol-dimaleimide- **PEG-diMal**
Phosphate buffer saline solution- **PBS**
Phrenic motor neurons- **PhMN**

Platelet-derived growth factor receptor- **PDGFRα**
Progenitor motor neuron- **pMN**
Polyethylene glycol- **PEG**
Poly(lactic acid co-glycolic acid)- **PLGA**
Purmorphamine- **Pur**
Puromycin- **Puro**
Puromycin N-acetyl transferase- **PAC**
Quality control- **QC**
Quantitative polymerase chain reaction- **qPCR**
Reactive oxygen species- **ROS**
Receptor for HA-mediated mobility- **RHAMM**
Regions of interest- **ROIs**
Retinoic acid- **RA**
Retinal ganglion cell- **RGC**
Ribonucleic acid- **RNA**
Secreted protein acidic and rich in cysteine- **SPARC**
Smoothened agonist- **SAG**
Sonic hedgehog- **Shh**
Spinal cord injury- **SCI**
Src homology 3- **SH3**
Td-Tomato fluorescent protein- **tdTomato**
Telomerase reverse transcriptase- **Tert**
Toll-like receptor- **TLRs**
Transgenic- **TG**
Thymidine kinase- **TK**
Ultra-performance liquid chromatography- **UPLC**
University of Washington Proteomics Resource Center- **UWPRC**
Vesicular glutamate transporter 2- **vGlut2**
Vimentin- **Vim**
Wingless integrants- **Wnts**

Acknowledgements

This journey has been incredibly rewarding with the help of so many wonderful people at both the University of Texas at Austin and University of Washington who have guided me through exploration of science in my dissertation project. My first thanks and immense gratitude goes to Dr. Sakiyama-Elbert for her mentorship, support, encouragement, and guidance through these years. You have shown me not only how to be a better scientist and writer, but also how to be a better person and leader. Through all my personal difficulties, you have been someone that has shown care, and I deeply appreciate it. Thank you for letting me explore my own interests in the world of astrocytes and giving me the support to find my own way as a female scientist. I extend my deepest gratitude to my professors on my UW committee and as well as my UT Austin committee for supporting my potential as a scientist and encouraging me through my dissertation studies with constructive, insightful feedback that allowed me to approach my project from different perspectives.

My joy in the Sakiyama-Elbert Lab not only came from the science but also from working with people that I am so honored to call my friends. I am thankful for the support and research advice from all former lab members and colleagues: Dr. Pablos Ramos Ferrer, Dr. Nicholas White, Dr. Jennifer Pardieck, Dr. Bill Wang, Dr. Thomas Wilems, Dr. Jaewon Lee, Dr. Russell Thompson, Vanessa Page Barth, Aditi Merchant, Dr. Nikita Ghosh, Dr. Manwal Harb, and Mary Salazar. You have all helped me to grow as a scientist with better communication skills. An immense thanks to Hayley Lindsay for being my close friend, listening ear, and advisor in and out of the lab and always being there for me. You have been beyond helpful and kept me cheerful. Thank you to Tyler Jordan, Lori Won, Evelyn Chang, and Anna Cramer for being a joy to work with. I

would like to give huge thanks to Dr. Mary Regier, Dr. Ashley Baltes, Dr. Prisk von Haller, and Jimmy Eng for their valuable assistance and guidance in major techniques for my thesis. These skill sets will help me to be a better researcher in industry.

My time at University of Texas at Austin and University of Washington was further enriched through participation in student organizations and allowed me to interact with wonderful, driven individuals in graduate school. I had the pleasure of being part of Society of Women in Engineering and Society for Advancing Gender Equity in STEM and meeting wonderful female scientists and graduate students who continued to motivate me in my own research goals. Furthermore, I would like to thank Mellie Price of Texas Venture Labs Practicum for instilling in me the business concepts and consultant skill sets that molded me into being a leader in my team during my two semesters. I hope to translate those skills into the future at a management position in the science industry. I would also like to thank all my previous teachers and professors for instilling my curiosity and love of science.

None of this would be possible without the love and support of my parents. They have tirelessly worked to provide me with the best life and joyful memories to foster my interest in science and math. Your endless support at my elementary, middle-school, and high school science fairs made me realize my dream of being a scientist. I know that whatever comes in future, I can face it with confidence because I have my parents by my side always. Thank you to all my wonderful friends at UT Austin for happy memories around Austin pre and post pandemic throughout graduate school. Special shoutout to my friends in Seattle at University of Washington- Lily Torp, Madelyn Shelby, Kylie Gallagher, and Katherine Meinhold. I also would like to massively thank

my aunt, Subhi Ravi, for always inviting me to her home and festival celebrations with open arms and caring for me as my mother would have. You have all made my transition away from my parents in Austin to the new City of Seattle the best time possible. You have become my family away from home and I cannot thank you enough for making me feel loved and comfortable in Seattle, thus helping me transition to graduate school in a new environment. Lastly, I would like to thank my family in India for their constant love and endearing support. Their life experiences have taught me important lessons that I will carry into the future to be the best human being I can be.

Sangamithra Vardhan

University of Washington

July 2025

“No matter what happens in life, be good to people. Being good to people is a wonderful legacy to leave behind.”- Taylor Swift

Dedicated to my parents, Sundara R. Vardhan and Usha S. Vardhan, who always believe in me and continue to be my main support and source of encouragement in life

Chapter 1: Introduction

1.1 Overview

Research for treatments of spinal cord injury (SCI) is focused on ameliorating the inhibitory microenvironment in injured spinal cord to promote increased axon connections and neuron viability. The axon bridging and integration with host neural circuitry can help patients regain lost sensory and motor functions. The current research strategies include electric stimulation, rehabilitation, cellular transplantation, biomaterial implantation, and neurotrophic growth factor delivery. Our lab focuses on developing differentiation protocols for neural and glial cell types to study neural plasticity and glial-derived factors as potential drivers of promoting axon in SCI. The long-term goal is to understand the mechanisms of interneuron-neuron connections and the effects of glial-derived growth factors and ECM proteins that promote axon growth and functional outcomes after SCI. These findings can ultimately help us develop biomaterial platforms incorporating glial- derived factors that provide a regenerative niche in an injured spinal cord.

Previous research initially thought astrocytes, a key glial cell in healthy and injured spinal cord microenvironment, were harmful cellular players in SCI as they undergo reactive astrogliosis and secrete axon-growth inhibitory chondroitin sulfate proteoglycans (CSPGs). However, reactive astrocytes and astrocyte subtypes can limit secondary damage and inflammation to the host tissue, suggesting there are beneficial factors provided by astrocyte phenotypes that can play a role in neural repair.

In this chapter, I convey the rationale and significance of this thesis based on the foundation of past research of astrocyte roles in SCI. The sections that follow demonstrate the motivation of this thesis work, the importance of microenvironment changes for neurons in the spinal cord, the impacts of astrocytes on neuronal populations, biomaterial strategies for SCI applications, and the use of stem cell platforms to study astrocytes.

1.2 Spinal cord injury

Spinal cord injury (SCI) is a severe, debilitating condition with complex pathophysiology that renders patients to endure permanent disabilities with complete or partial loss of sensory and motor functions depending on the severity and location of injury[1–4]. The main causes of falls, car accidents, violence, and sports injuries result in more than 90% of SCI being traumatic (SCI produced by a physical impact) and predominantly (~60%) cervical SCI[1,2,5–7]. Traumatic SCI currently affects 305,000 people in the United States with an incidence rate of nearly 18,000[5]. SCI patients experience a spectrum of impaired neurological outcomes with other complications such as respiratory dysfunction and frequent bladder and kidney infections[1]. In addition, SCI patients in the US face significant social and financial burdens with medical care costs ranging from $1.1 to 4.6 million per patient, causing additional stress on the patient and their support system[2,7].

While it is possible for incomplete SCI to result in neural sprouting that promote plasticity for functional recovery, complete SCI results in severed ascending and descending neural pathways and create a microenvironment harsh for plasticity and functional improvements[1,4,8,9]. With no current effective treatments for SCI, there is an

imminent research need to discover strategies that promote a regenerative microenvironment for restoring neural connections and facilitating functional recovery. This section describes the key cellular players contributing to microenvironment changes from SCI, the loss of neural connections that result in disabilities for patients, and different research strategies for SCI treatments.

1.2.1 Pathophysiology of spinal cord injury

After the immediate physical impact, SCI progresses through two stages, primary and secondary, that result in an inhibitory microenvironment detrimental to central nervous system (CNS) cell types, such as neural connections[2,6,7,9,10]. This occurs over a timescale that defines acute stages as less than 48 hours, subacute as 2 days to 2 weeks, intermediate as 2 weeks to 6 months, and chronic as more than 6 months in mammals[6,7,11]. During the primary phase, the traumatic forces result in buildup of inflammation, cytokine release, disruption of ion homeostasis, free radical formation, neural cell death, and demyelination of axons through apoptosis of oligodendrocytes[1,2,10]. The secondary phase continues the disruption of ion homeostasis, free radical formation, and astrocyte and fibroblast proliferation at the injury site to form the glial border and fibrotic core. The formation of these boundaries changes the ECM composition to include axon -growth inhibitory proteins, such as chondroitin sulfate proteoglycans (CSPGs). Overall, these two phases create a microenvironment imbalance in the spinal cord.

The definition of glial border has changed to provide nuanced definitions of perivascular fibrotic lesion core and astrocyte glial scar as an astrocyte border instead[4,8,12]. The injury site is divided into fibrotic scar consisting of proliferative

fibroblasts secreting collagen matrix and astrocyte border that surround this fibrotic core. The border serves to protect the spared neural projections in host tissue from increases in inflammatory cells. The research is ongoing to tease out the different development and microenvironment cues that trigger reactive astrocytes for therapeutic target identification to regain lost neural connections[8].

1.2.2 Key glial cell types in spinal cord injury

There are three major types of glial cell that exist in the central nervous system: astrocytes, oligodendrocytes, and microglia[13]. Each cell type performs specific functions throughout the brain and spinal cord to support neurons and other glial cells. These three glial cell types undergo morphological and molecular changes, enabling them to play complex roles in SCI and modify the microenvironment that impacts axon growth.

Astrocytes

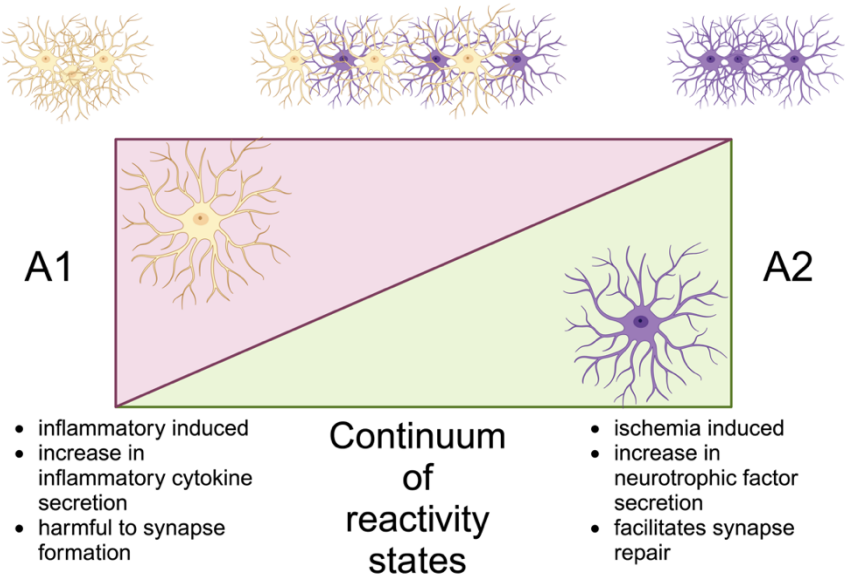

Figure 1.1 Schematic diagram demonstrating the concept of astrocyte reactivity on a spectrum
There are two main observed reactive astrocyte subtypes, A1 (neurotoxic) and A2 (neurorepair), that develop under inflammatory stimuli and ischemia. It is believed in the astrocyte field that astrocytes adopt a reactivity state in a spectrum between A1 and A2 due to a mixture of signals in the SCI microenvironment.

Under normal physiological conditions, astrocytes are considered the CNS helper cells providing support for neuron viability, synapse formation, neural metabolism, blood-brain barrier maintenance, and axon guidance[14–17]. Astrocytes are sensitive to cytokines (such as tumor necrosis factor (TNF)-α), chemokines, and reactive oxygen species (ROS) in the injured spinal cord microenvironment and can adopt reactive subtypes[18–20]. Reactive astrocytes have altered key cellular functions, such as decreased glutamate uptake, an ion imbalance, and loss of contacts with endothelial cells, resulting in losing their capacity to support neurons[2,10,20]. Researchers are forming clear definitions of A1 reactivity (inflammation-induced) as neurotoxic and A2 (ischemia-induced) reactivity as neurorepair, in which A1 reactive astrocytes are more in the acute SCI phase and A2 reactive astrocytes are more present during chronic phases of SCI[19,21] (Fig 1.1). Specifically, reactive border astrocytes secrete neuro-repulsive components, such as chondroitin sulfate proteoglycans (CSPGs), detrimental to axon and oligodendrocyte survival in intermediate and chronic phases of SCI[1,3,7,14]. More nuanced definitions show that astrocytes adopt reactivity states in the continuum spectrum between A1 and A2 as a response to SCI.

For a long time, the field considered astrocytes to be a harmful player and ablation of astrocytes could be the key for functional recovery. However, studies have shown that disruption of reactive astrocytes in the scar-border worsens the functional outcomes and axon growth potential *in vivo*[22–27]. Pekny *et al.* demonstrated that mice containing null mutations for both glial fibrillary acidic protein (GFAP) and vimentin (Vim), which are intermediate filaments commonly expressed by reactive astrocytes, produced aberrant glial scar structure post dorsal transection upper thoracic SCI. Furthermore, the

aberrant astrocytes led to observed fissures containing blood vessels and debris that caused more bleeding[22,23,27]. Thus, border-forming astrocytes are beneficial in limiting inflammation to the SCI injury site.

A pivotal study by Anderson *et al.* illustrated the benefits of astrocyte border around the lesion post severe crush SCI at T10 using targeted loss of astrocyte function in adult mice to produce losses of scar-forming reactive astrocytes, glial border formation, and chronic astrocytic scar processes. The mouse model with astrocyte expression of herpes-virus thymidine kinase (TK) plus ganciclovir (GCV) was used to kill scar-forming reactive astrocytes and the mouse model knock-out of *Stat3* in astrocytes led to disruption of scar formation[26]. Both these types of mice failed to produce astrocyte borders in 2-8 weeks post SCI and did not have any axon growth of descending CST axons in spared tissue, leading to further potential functional deficits at 8 weeks[26]. In addition, RNA-sequencing of border-forming astrocytes demonstrated gene expression of axon growth-permissive factors such as laminin, syndecan, decorin, and glypicans, indicating beneficial properties of astrocytes post SCI[26].

There are multiple key astrocyte phenotypes in the spinal cord that support different neuron populations[28]. Current research is involved in understanding various axon-growth permissive properties of these astrocyte phenotypes and reactive states for SCI[17,29]. It is also important to consider the maturity states of the astrocyte phenotypes since it has been shown that immature astrocytes can support more axon growth[19].

Oligodendrocytes

Oligodendrocytes are critical in generating myelin sheath for surrounding axons and facilitating transmission of electric signals across neural circuits for motor and

sensory functions[13]. This glia arise from oligodendrocyte precursor cells (OPCs), or NG2-glia, which are self-renewing cells that replace mature oligodendrocytes[30]. The inflammatory cascade activates microglia, generating a harmful milieu through apoptosis of neurons and oligodendrocytes[31]. Furthermore, high glutamate and calcium levels in the microenvironment contribute to oligodendrocyte apoptosis and thus demyelination[32].

One strategy to increase axon growth and regain functional improvement is to increase remyelination with oligodendrocyte or OPC transplantation. In response to SCI, $NG2^+$ progenitors can differentiate into phagocytic and reactive astrocytes that help in phagocytosis of myelin debris and contribute to inhibitory microenvironment[33]. After a week post SCI, $NG2^+$ progenitors differentiate into proliferating immature oligodendrocytes (APC^+), but more studies are needed to determine if new oligodendrocytes can remyelinate[32,33]. Research into oligodendrocyte differentiation and transplantation with signals promoting mature oligodendrocyte formation can play roles in SCI repair.

Microglia

Microglia are the resident immune cells of the CNS and adopt specific reactive phenotypes (between M1 pro-inflammatory and M2 anti-inflammatory spectrum) dependent upon the chemical and immunological conditions of the CNS microenvironment[13]. These cells constantly monitor physiological condition of the CNS and secrete cytokines in reaction to vascular damage, changes in blood-spinal cord barrier (BSCB) permeability, and damaged axons[34,35]. In addition, microglia are activated to M1 phenotype through TNF- α activating toll-like receptor (TLRs) on

microglia and M1 secrete inflammatory cytokines, such as interleukin Il-6 and IL-1β, in acute SCI[36,37]. The role of microglia has also been explored *in vitro* with lipopolysaccharide (LPS) exposure to quiescent microglia[36,38]. Activated microglia secrete IL-1α that continues immune cell infiltration at the injury site and leads to oligodendrocyte death and myelin loss[39]. The phagocytic function of M2 microglia in acute SCI phase helps uptake of myelin debris, reducing factors contributing to axon growth inhibition[38]. Neurotoxic M1 microglia secreting TNF-α and Il-α causes activation of astrocytes and adoption of A1 astrocytes[40]. On the other hand, anti-inflammatory cytokines from M2 microglia can suppress the reactivity in astrocytes and could have implications in neuron survival and axon growth[40]. Both microglia phenotypes are essential for SCI and potential functional improvements.

1.3 Protoplasmic and fibrous astrocytes in spinal cord

Protoplasmic astrocytes interact with capillaries and provide functional synaptic support (Fig. 1.2)[40]. Fibrous astrocytes support nodes of Ranvier along axons (Fig 1.2)[40]. The main astrocyte subtypes are conserved through different organisms with humans having complexity of astrocyte subtypes mainly found in the cerebral cortex with highly specific roles[41]. Studies demonstrated that these two phenotypes can differ in axon regeneration *in vitro* and *in vivo* with protoplasmic astrocytes being more axon-growth regenerative[42–44]. Thus, this thesis focuses on studying stem cell derived astrocyte phenotypes for their axon-growth related components.

1.3.1 Astrocyte phenotypes in spinal cord development

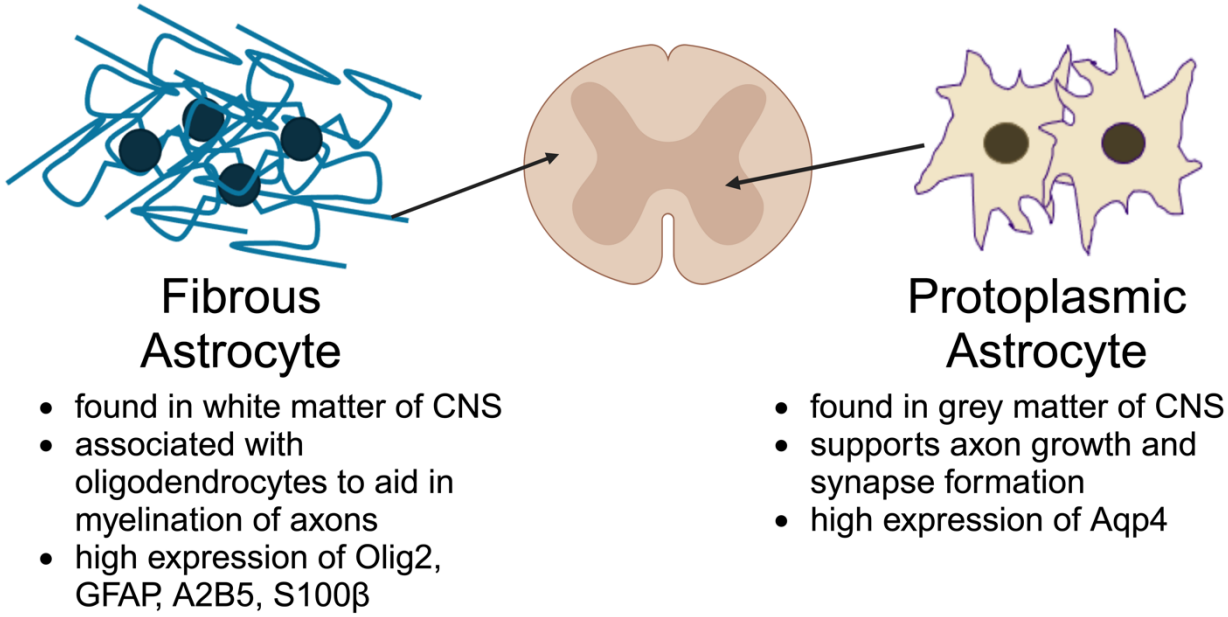

Figure 1.2 Two main astrocyte subtypes to study for understanding astrocyte-specific roles
Fibrous and protoplasmic astrocytes reside in white and gray matter of spinal cord respectively with different properties impacting axon health and express different levels of key astrocyte markers that help distinguish these phenotypes as more researchers explore astrocyte phenotypic properties.

In the developing spinal cord and neural tube, competing gradients of ventral sonic hedgehog signaling and dorsal BMP signaling are critical in patterning of the neural tube to establish the dorsal-ventral axis of progenitor domains. The ventral progenitor domains of p1-p3 and progenitor motor neuron (pMN) differentiate into the ventral spinal interneurons, motor neurons, and astrocytes. Different combinations of transcription factors Pax6 and Nkx6.1 expressions in progenitors lead to astrocyte heterogeneity during differentiation[45–47]. Pax6 is dominant in progenitors for VA1 and VA2 and Nkx6.1 is needed for VA3[47]. The positionality of these astrocyte subtypes is influenced by Reelin (extracellular glycoprotein) and Slit1 (ligand protein)[45,47]. The patterning of spinal cord in development is the foundation for astrocyte heterogeneity.

Radial glia are important intermediate cells to characterize markers of astrocyte progenitors, immature astrocytes, and mature astrocytes. These cells demonstrate a

bipolar, elongated morphology with extensions starting within the cell soma in the ventricular zone and ending away from the apical surface[25]. Radial glia is a heterogeneous population of neural and glial progenitors with various gene expressions. Radial glia express markers shared with astrocytes, such as the intermediate filaments vimentin and GFAP, glutamate aspartate transporter (GLAST), brain lipid binding protein (BLBP), and calcium binding protein S100β at the onset of neurogenesis[48,49]. In fact, the expression of BLBP is in response to activation of Notch signaling in radial glia and regulates neuronal migration[49]. Both neuroepithelial progenitors and radial glia do share some markers, such as nestin, despite being intermediate populations[48]. Radial glia are complex cell types with the ability to differentiate into different CNS cell types.

A key marker that plays a complicated role in gliogenesis is Olig2, a basic helix-loop-helix (bhlh) transcription factor. Olig2 expression in the pMN domain gives rise mainly to motor neurons and oligodendrocytes but can also be involved in astrocyte production[47,50,51]. Certain mature astrocytes are identified by $GFAP^+/Olig2^+$ particularly in white matter[52]. In addition, Olig2 lineage tracing demonstrates that Olig2 is co-expressed with platelet-derived growth factor receptor $(PDGFR\alpha)^+$ and $NG2^+$ (cell surface glycoprotein) OPCs and continued expression in mature oligodendrocytes[53,54]. Overall, Olig2 is a critical factor in deriving white and gray matter astrocytes and demonstrates how motor neuron and oligodendrocyte lineages are intertwined with astrocyte fate.

Since it is important to study astrocyte heterogeneity for identifying beneficial glial cues in SCI repair, mESC and PSC differentiation protocols mimic mouse astrocyte development to generate astrocyte phenotypes in 30-plus day period[15,44,55]. Most

protocols differentiate into fibrous ($A2B5^+/GFAP^+$) and protoplasmic astrocytes ($A2B5^-/GFAP^+$) using neuroepithelial progenitors, NSCs, or glial restricted progenitors (GRPs) as an intermediate point and then addition of CNTF or BMP4 respectively[42–44]. Our lab protocol utilizes chemicals Shh agonist (smoothened agonist- SAG) and retinoic acid (RA) to provide patterning cues for generation of ventral spinal cord progenitors[250]. The proliferation of these progenitors is mediated by time and the addition of epidermal and fibroblast growth factors (EGF and FGF)[15,44,56]. Specifically, CNTF and BMP4 are key in activating the janus kinase (JAK) signal cascades in progenitor cells to commit for astrocyte fate and inhibit oligodendrocyte lineage[57]. The resulting astrocytes express mature astrocyte markers GFAP, Aquaporin-4 (Aqp4), and GLT-1 and mostly demonstrate neuron support[58]. Furthermore, astrocyte differentiation has included exposure to serum, such as fetal bovine serum (FBS), and FGFs to produce a more mature phenotype, while low percentage of serum can give rise to more immature and reactive astrocytes[15,59]. Furthermore, pivotal studies demonstrate that protoplasmic astrocytes support more axon regeneration *in vivo* compared to fibrous[42,43,60]. This demonstrates astrocyte phenotypic differences in molecular expressions and functionality for axon growth and the need for stem cell protocols to produce an unlimited source of fibrous and protoplasmic astrocytes for identifying axon growth permissive astrocyte-derived cues.

1.3.2 Properties and markers of astrocyte phenotypes

After development from radial glia, the two main astrocyte phenotypes migrate away from the ventricular zone into final destinations of white and gray matter in different regions of CNS, including spinal cord[28,61]. One of the first indications of two

main types of GFAP+ astrocytes was found in cultures of developing rat optic nerves in which some astrocytes (type 1) did not express A2B5 (cell surface ganglioside) and others (type 2) did express A2B5[62]. As the field grew, the morphology and protein expression correlated with classification of type 1 and type 2 astrocytes into protoplasmic and fibrous respectively[63]. Protoplasmic astrocytes have more branches that spread from the cell body to form a large, flat morphology while fibrous have longer, fiber-like extensions with less complex and smaller cell body[47,61,64,65]. Bushong *et al.* found protoplasmic astrocyte processes form clear boundaries ('tiling') parallel to dendrites from pyramidal neurons[66,67]. However, the neighboring processes and intermediate filaments of fibrous astrocytes interact with each other in no clear organization[61]. Furthermore, fibrous astrocytes have variable lengths of processes that interact with oligodendrocytes[61,67]. In response to SCI, processes of protoplasmic astrocytes adjacent to the lesion overlap spatial domains to form the astrocyte border[61,68]. The astrocyte morphology is critical for functionality.

The astrocyte phenotypes contribute to the diverse roles in support of neuron health through regulation of neurotransmitters and metabolites, blood-brain barrier maintenance, and synaptogenesis. Protoplasmic and fibrous astrocyte processes and end feet are in contact with blood vessels to control blood flow in the CNS[61]. There are more capillaries present in the gray than white matter, suggesting protoplasmic astrocytes might impact vascularization[69]. Aqp4, a water channel membrane protein, is most abundantly expressed in the end feed of astrocytes that contacts with blood vessels in the spinal cord[70]. Protoplasmic astrocytes express more Aqp4 than fibrous in rodents and thus can be a characteristic astrocyte marker[69–71]. SCI causes Aqp4 to be

redistributed away from the end feet, contributing to astrocyte swelling and disrupted blood flow[71]. In addition, Aqp4 knockout mice demonstrate reduced magnitudes of long-term potentiation (LTP), a measurement of synaptic plasticity in brain slices, suggesting the role of Aqp4 in synapse formation[72].

Astrocytes are key in regulating metabolic support for neurons through glutamate uptake via glutamate transporters in astrocyte membranes to prevent excitotoxicity for neurons[73]. Glutamate transporter 1 (GLT-1) is found in both subtypes and is used as marker with GFAP to isolate two astrocyte populations: $GLT^+/GFAP^-$ (protoplasmic) and $GLT^+/GFAP^+$ (fibrous) from murine cortex[74]. Developing mouse spinal cord sections show GLAST and GLT-1 are present in postnatal spinal cord astrocytes. GLT-1 corresponded to axon pathways in the spinal cord, indicating the astrocytic glutamate transporter playing a role in axon growth[75]. GLAST is also present in cell bodies of radial glia and astrocyte precursor cells[76]. Furthermore, glutamine synthetase (GS), an enzyme catalyzing conversion of glutamate, ammonia, and adenosine triphosphate (ATP) into glutamine, is present in all astrocyte types with co-expression of Aqp4 in rat spinal cord and is increased in reactive astrocytes 7 days post SCI[77,78]. Interestingly, GS is found in oligodendrocytes and OPCs in the white matter tracts[77–79]. These markers are critical in demonstrating the metabolic functions of astrocytes.

Lastly, astrocytes support neurons through calcium signaling in response to ATP stimulation. Astrocytes mainly express gap junction proteins connexin 30 and 43 (Cx30, 43) to couple astrocytes for transmitting calcium transients[80,81]. Furthermore, astrocyte targeted deletion of Cx30 and 43 in double knockout mice from postnatal day 23 and older displayed edema in hippocampal protoplasmic astrocytes and widespread

vacuolation of oligodendrocytes in white matter tracts[81]. This led to functional deficits in double knockout mice, such as falling off the rotarod more frequently, suggesting the importance of astrocyte calcium signaling[81]. Immunohistochemical staining of rat brain slices at various ages demonstrates Cx43 is widely expressed with more prominent staining observed in fibrous astrocytes[82]. In addition, Cx30 can be expressed higher in mature protoplasmic than mature fibrous astrocytes[83]. Overall, calcium signaling in astrocytes is facilitated by gap junction proteins that modulates the polarization of neuron membrane in synaptic units for neurotransmitter release and action potential production, establishing astrocyte-neuron crosstalk[84].

As astrocyte differentiation protocols are developed, it is critical to characterize expression of astrocyte markers in the resulting cell cultures to understand the composition for tailoring studies of astrocyte phenotypic functions. The most prominent astrocyte marker is GFAP. While GFAP is a general astrocyte marker, there is evidence that GFAP expression is higher in white matter astrocyte populations than gray matter[53]. In addition, there is an astrocyte population that is characterized as $Olig2^+$ and $GFAP^+$ [85]. In fact, the astrocyte differentiation protocol developed by Thompson *et al.* produces fibrous astrocytes that express high levels of Olig2, suggesting this astrocyte phenotype resembles white matter astrocytes[44]. Olig2 is used as a selection marker for the transgenic selectable cell line in the thesis to enrich fibrous astrocytes[44]. Other general astrocyte markers are aldehyde dehydrogenase L1 (Aldh1L1) and S100β, a calcium binding protein. S100β, has greater expression in protoplasmic astrocytes and developing oligodendrocytes in the white matter[14,68,86]. However, S100β is expressed by $GFAP^+$ and $A2B5^+$ astrocytes, suggesting these astrocytes are from the $Olig2^+$

progenitor lineage in development[87]. This resembles the expression profile of differentiated fibrous astrocytes in this thesis. It is important to highlight that S100β is also expressed by Schwann cells[87,88]. A2B5 is expressed both in radial glia and immature astrocytes and differentiates into brain lipid binding protein (BLBP)$^+$ protoplasmic and A2B5$^+$ fibrous astrocytes[42,44,63,89]. However, A2B5 is also expressed by O4$^+$ immature oligodendrocytes[90]. Overall, the markers GFAP, S100β, Olig2, A2B5, GLAST, GLT-1, Aqp4, Cx30, and Cx43 are mainly used to characterize astrocytes phenotypic cultures in the spinal cord.

Immature astrocytes favor interactions with neural growth cones and promote axon growth[91–93]. Immature astrocyte markers originate from glial precursors in spinal cord development. A selective marker of immature astrocytes and astrocyte precursor cells is CD44, a hyaluronate receptor that biases progenitors to an astrocyte fate. The number of CD44$^+$ cells and astrocytes increase with exposure to BMP-4 and FGF-2, indicating these two factors are important for astrocyte differentiation[94]. Specifically, CD44$^+$ cells in postnatal development do not express CC1, a mature oligodendrocyte marker, and can co-express Olig2 that ultimately undergo astrocyte differentiation[95]. Vimentin, another intermediate filament protein, has greater expression in developing fibrous astrocytes with staining also in fibroblasts[89]. There still needs to be more characterization of gene and protein expressions of immature versus mature astrocytes to expand the current toolkit of markers.

Table 1.1 Key markers for characterizing protoplasmic and fibrous astrocytes used in this thesis

Marker	Hypothesis
Aqp4	Present in astrocyte subtypes with higher expression in protoplasmic than fibrous
Olig2	Higher in fibrous astrocytes
GFAP	Present in astrocyte subtypes with higher expression in fibrous than protoplasmic
Aldh1L1	Present in both astrocyte subtypes
CD44	Immature astrocyte marker
Vimentin	Immature astrocyte marker with higher expression in fibrous
A2B5	Higher expression in fibrous
GLT-1	Present in both astrocyte subtypes with higher expression in fibrous
Cx30	Present in both astrocyte subtypes
S100β	Present in both astrocyte subtypes

1.3.3 Multi-omics approach to characterize astrocytes

To identify more astrocyte specific markers and proteins that impact functionality, researchers are utilizing bulk and single-cell ribonucleic acid (RNA) sequencing and proteomics. RNA-sequencing studies have been conducted with single-cell resolution to identify specific characteristics of astrocytes compared to other CNS cell types[28,96–100]. Andersen *et al.* conducted transcriptomic mapping of the developing human spinal cord over 22 weeks of gestation to profile single cell and nuclei from samples[100]. The study produced different clusters based on gene expression for different CNS cell types, such as motor neurons, oligodendrocytes and OPCs and astrocytes. The clustering analysis identified ventral and dorsal glial progenitor populations with *Sox9* expression and lower levels of mature astrocyte markers, *Aqp4*[100]*.* Clusters were characterized as either fibrous astrocytes with higher expression of *GFAP*, *CRYAB*, and *ATP1A1* (ATPases for sodium and potassium exchange) or protoplasmic astrocytes with *SLC7A10* (amino-acid transporter involved with neurotransmitters), *GLUL* (glutamine synthetase), and

SLC1A2 [100]. This demonstrated the presence of astrocyte heterogeneity in the developing spinal cord.

Transcriptomics elucidates gene expression differences between primary and stem cell-derived astrocyte phenotypes[59,96,101–103]. Zhang *et al.* isolated purified astrocyte precursor cells and astrocytes from fetal and adult brain tissue samples with immunopanning using HepaCAM (cell adhesion glycoprotein) antibody and utilized RNA-sequencing with differential gene expression analysis to show proliferation genes were upregulated in astrocyte precursors and gap junction genes, *aldh1l1*, and *glul* were upregulated in mature astrocytes[96]. Furthermore, analysis of differentiated astrocytes from human NPCs exposed to serum, CNTF, and BMP4 demonstrated genes in pathways related to gliogenesis, proteoglycan metabolic process, and negative regulation of MAP kinase activity[59]. In addition, *GFAP, CD44, Notch1* (known to inhibit neuron maturation), and chemokine *CCL2* were upregulated in the astrocytes[59]. RNA-sequencing can aid understanding genes that define immature and mature astrocyte presence in cell cultures.

Proteomic studies of isolated primary and stem cell-derived astrocytes provide more insights into the composition of astrocyte ECM and membrane proteins under various conditions of healthy and injured CNS to further identify potential targets[104–107]. For example, Dowell *et al.* analyzed the secretome of cultured primary postnatal day 1 murine astrocytes with liquid chromatography and electrospray mass spectrometry (LC-MS) to focus on astrocyte extracellular signaling pathway targets[104]. It demonstrated overall 423 proteins identified in astrocyte conditioned media with expression of

SPARC, nidogen-2, spondin-1, and biglycan being potential protein targets for modulating axon growth pathways[105].

Proteomics can be done in parallel with transcriptomics to gain insight on translated protein targets expressed by astrocytes for neuron communication. Chai *et al.* analyzed striatal and hippocampal astrocytes from P30 *Aldh1l1*-eGFP mice with both mass spectrometry and transcriptomics to show 2879 common proteins in both types of -omics data sets[108]. Gene ontology analysis shows that these proteins are involved in cell cycle, cytoskeleton, and metabolite generation and might prove to be astrocyte-secreted factors affecting axon growth[108]. Proteomic studies are also instrumental in identifying proteins associated with inflammatory responses to elucidate proteins that inhibit axon growth after SCI. Keene *et al.* exposed primary neonatal cortical astrocytes to inflammatory stimuli (TNF-α, IL-1β, and interferon-γ) for 1 day (acute) or 7 days (sustained) and utilized LC-MS analysis to analyze astrocyte conditioned media to identify secreted protein abundance in response to inflammation mimics[109]. Complement C3, chemokine ligand 1, MMP3, Il-6, and nerve growth factor were discovered in the stimulated astrocyte secretome and might play complex roles in astrocyte disruption of neural support post SCI[109]. The proteomic analysis of astrocyte subtype ECM can thus provide protein target insights for modulation axon growth of various neuron populations.

1.3.4 Astrocyte-neuron interactions for axon growth

Astrocytes in the healthy CNS have been shown to support neurite growth of various types of neurons and has led to investigating molecular and cellular mechanisms involved in the astrocyte-neuron interactions[110–113]. Effects of astrocytes

purified from newborn mouse forebrain on embryonic and adult dorsal root ganglion and retina neurons were assessed[111]. It was demonstrated that only embryonic neurons extended axons profusely on astrocytes, suggesting maturity state of neurons might have certain protein expression that can interact with astrocytes[111]. Secreted astrocyte proteins influence synapse formation and axon growth. Thrombospondins are prominently secreted by astrocytes and increase synaptic puncta of synaptotagmin and PSD95 colocalizations in retinal ganglion cell (RGC) culture[114]. In addition to secreted protein acidic and rich in cysteine (SPARC), Hevin is expressed in mostly mouse Aldh1l1$^+$ protoplasmic astrocytes and is necessary for regulating excitatory synapse formation in size and number[115]. Furthermore, biochemical fractionation of rat cortical astrocyte conditioned medium identified glypican 4 and 6, which is part of the heparan sulfate proteoglycan family, as astrocyte-secreted proteins that increase amplitude and frequency of excitatory postsynaptic current (EPSC), AMPA receptor (AMPAR) clustering at synapses, and synapse size observed in RGC cultures *in vitro*[116]. In addition, mass spectrometry analysis of mouse astrocyte conditioned media identified chordin-like 1 (Chrdl1) is expressed in upper cortical layers through developing postnatal mouse brain and induces mature synapse formation observed by VGlut staining[117]. Chrd1 increased AMPAR clustering at synapses of RGCs *in vitro* and cortical synapses *in vivo* with decrease in EPSC decay time[117]. These previous studies show secreted factors influence synapse formation and activity.

1.4 Astrocyte purification from stem cell sources

It is important to study the biochemical and functional properties of astrocyte phenotypes *in vitro* to understand potential roles on axon growth of neuron populations

during SCI and recovery. *In vitro* stem cell-derived cultures of astrocyte phenotypes are promising for investigating nonreactive and reactive astrocyte phenotypes (Fig 1.3). Classic astrocyte isolation procedures based on McCarthy & DeVellis can produce more reactive astrocytes during tissue dissection[118]. Stem cell-derived astrocyte cultures can be a great alternative to primary astrocytes that are plagued with low viability during tissue extraction and post-isolation methods, as well as the potential to be non-reactive[13] (Fig 1.3). Previously, our lab developed a protocol generating fibrous and protoplasmic astrocytes from mESCs lines utilizing glial-restricted progenitors with application of CNTF and BMP4, respectively[44]. In this thesis, we utilize these fibrous and protoplasmic astrocytes to study phenotypic properties important for axon growth.

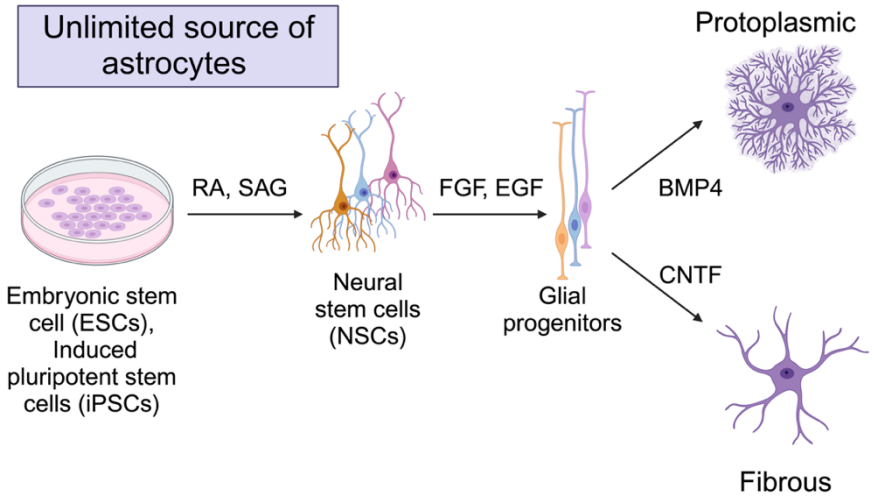

Figure 1.3 Stem cell sources for differentiating glia Stem cells have proven to be an unlimited source of astrocyte phenotypes with differentiation protocols developed to produce protoplasmic and fibrous astrocytes from using an intermediate precursor cell stage such as neural stem cells and glial restricted progenitors. The main growth factor used to generate protoplasmic is BMP4 and fibrous is CNTF.

1.4.1 Purification methods to remove other cell types

Similar to primary astrocytes, stem cell-derived astrocyte cultures are heterogeneous, containing other cell types that might make astrocyte-specific effects difficult to discern[58]. Thus, it is crucial to purify these stem cell-derived astrocyte cultures

with reduction of other cell types. Furthermore, it is important to characterize the purified astrocytes with expression of astrocyte markers, transcriptomic profiling, and cellular functionality to validate purified stem cell-derived astrocyte cultures as models for studying CNS physiology and disease. Specifically, characterization of astrocyte phenotypes in immature and mature astrocyte states can elucidate roles of astrocyte development on axon growth.

There are a few common purification methods that have been applied to isolate astrocytes from tissue. Fluorescence and magnetic flow sorting are based on astrocyte cell surface antigen expression[119–121]. The binding specificity of antibodies and magnetic beads to specific markers are still being investigated. It is important to include astrocyte specific markers for either reactive or quiescent astrocytes to properly study certain states. Certain antigens for cell surface markers can be affected during post-trypsinization and heating in isolation procedures[122]. Immunopanning is another common method for purifying isolated primary astrocytes resulting in high purity in astrocyte cultures. The protocols require several antibodies to remove other cell types from cultures and thus can be expensive[21,123]. Specifically, immunopanning results in decreased viability of white matter astrocytes providing potential phenotypic differences in purification methods[21]. Thus, it is crucial to utilize an easy, quick, inexpensive method for selection of *in vitro* derived astrocyte cultures with removal of other cell types, such as antibiotic selection.

1.4.2 Puromycin selection with genetic engineering of stem cells for purification

Puromycin selection is a common method in cloning experiments that allow researchers to verify proper transfection of transgenic cassettes into cells[124,125].

Puromycin selection is mediated through the expression of puromycin N-acetyl transferase (PAC- enzyme that results in cells being puromycin resistant) under the control of specific promoter expressed in transfected cells[126]. Thus, the cells that express PAC survive under puromycin exposure. There have been multiple studies utilizing transfection or insertion with CRISPR of PAC enzyme that results in cells being puromycin resistant) to purify variety of cell types such as stem cell-derived cardiomyocytes[127–129].

Our lab has employed this puromycin selection to generate transgenic selectable cell line for enriching various interneuron, motor neuron, and neural progenitor populations to study circuitry and other neuron interactions[51,130–133]. This thesis utilized transgenic selectable cell lines with PAC under the promoter of specific genes, *Olig2* and *Aqp4* to aim for enriched populations of mESC-derived fibrous and protoplasmic astrocytes. This purification method has the advantage of ease with puromycin addition and ability to determine optimal selection parameters by temporally identifying maximal PAC expression and testing effects of various puromycin concentrations on cell viability[126]. Generating selected astrocytes can then be used as a platform for studying astrocyte cues important in axon regeneration.

1.5 V2a interneurons in spinal cord

V2a interneurons in the spinal cord are well-characterized and are known to be part of the central pattern generator (CPG) that controls right-left alternation and other rhythmic locomotor movements, such as walking and respiratory functions. This thesis utilizes astrocyte phenotype-derived ECM proteins as potential axon-growth permissive

factors in a biomaterial platform to support V2a interneurons *in vitro* and may have implications for cervical SCI treatments *in vivo*.

1.5.1 Neural plasticity in injured spinal cord

The key detriments of SCI are the significant apoptosis of neurons and loss of axon connectivity for motor and sensory functions, caused by SCI cascades[6]. The physical force itself can disrupt neuronal membrane permeability leading to necrosis at the injury site[134]. While there is significant death of neurons in incomplete SCI, there are neural projections in the spared tissue near the astrocyte border (caudal or rostral) that contains potential for synaptic plasticity and sprouting with new synapse formations amongst both motor and sensory neuron pathways [8,31,135,136]. These reorganizations are possible due to the circuits below and above the SCI lesion site being anatomically intact and is more observed in incomplete SCI models[4,136]. There is significant ongoing research to understand the molecular signals that support axon growth of specific tracts that are instrumental to functional recovery. Axon guidance and growth with proper connections between neuron populations in ascending and descending axon pathways are key to adaptive plasticity mechanisms.

A critical population to activate for neural connectivity and synapse formation are spinal cord interneurons[7,137–140]. Interneuron plasticity for functional improvements was demonstrated in a seminal study by Barerye *et al*[19]*.* With weeks after an incomplete SCI rat mid-thoracic dorsal hemisection model, Barerye *et al.* discovered that the injured hindlimb corticospinal tract (CST) collaterals had sprouted into the cervical grey matter 3 weeks after injury to contact long propriospinal neurons in spared tissue[19]. After 12 weeks, the synaptic contacts on parvalbumin^{+} long propriospinal neurons increase with

axons that connect with lumbar motor neurons region below the injury lesion[137]. The rewiring and formation of new circuits resulted in increases in hindlimb placing responses after 5 weeks and hindlimb flexor responses after 12 weeks[137]. The study suggests that neurons in the grey matter form connections in the lumbar locomotor circuits and increasing axon growth of gray matter neurons can be important.

Understanding the physiology of spinal interneuron connections can reveal potential factors that support circuit formation. These networks are essential for locomotor outputs and provide organized rhythmic inputs to motor neurons, facilitating repetitive movements such as walking and controlling flexor and extensor[141]. The key interneuron population focused on in this thesis is excitatory V2a interneurons, which are critical for right-left alternation in walking and diaphragm function[142]. Discovering cell type-specific factors that support V2a interneurons *in vitro* can aid in understanding ways to promote recovery post SCI *in vivo*.

1.5.2 V2a interneurons in spinal cord development

CPGs are intricate rhythm-generating networks of interneurons and motor neurons that drive critical motor functions, such as ipsilateral flexor-extensor activity, and are located primarily in the lumbar spinal cord[143–145]. The spinal interneurons that provide signals to motor neurons are V0, V1, V2, and V3 classes and are defined by their location in the ventral spinal cord. These interneurons are derived from the respective progenitor domain pools p0, p1, p2, and p3[143,146]. The dorsal-ventral orientation and differentiation of the neuroepithelial-derived progenitor cells are influenced by a sonic hedgehog (Shh) gradient in the floorplate for the ventral neural tube patterning. Whereas, the dorsal signals are generated from the bone morphogenic

proteins (BMPs) and wingless integrants (Wnts) gradients from the roof plate[145,147]. In addition, the ventral populations are organized along the rostral-caudal axis gradient with subsets of V2 interneurons being homogeneously distributed on the axis[143]. The V2a interneurons are positioned in medial and ventral sections within the brachial segment, making it important in the connectivity within CPGs[143].

The different progenitor populations in the ventral spinal cord are defined by expression of homeobox genes, specifically *Pax6* and *Nkx2.2*, with *Pax6* expression exhibiting low to high gradient in dorsal regions and *Nkx2.2* expression in progenitors that do not express *Pax6*[147,148]. V2 interneurons derive from Pax6-expressed progenitors in p2 domain. V2 interneuron subclasses are defined by expressions of Chx10, Lim3, and Gsh4 with being ventral to V1 interneurons and close to motor neuron subsets. Lhx3, a homeobox protein, is instrumental in defining the glutamatergic excitatory and inhibitory V2 interneurons[144]. This thesis focuses on identifying astrocyte-derived factors that can impact the axon growth of V2a interneurons. V2a interneurons are well-characterized excitatory neuron in locomotor circuits contributing to 30% of glutamatergic neurons in the ventral spinal cord with expression of vesicular glutamate transporter 2 (vGlut2) and identified mainly by Chx10 transcription factor expression[144]. Numerous studies demonstrated that V2a interneurons play a crucial role in generating rhythmic signals to motor neurons, facilitating respiratory breathing and right-left alternation. V2b and V2c interneurons are being studied to understand their inhibitory roles in the CPG-regulated locomotion[145,149]. The parameters in the connectivity can be modulated to determine changes in the motor outputs for potential functional outcomes. With V2a interneurons being a well-studied population for their plasticity in respiratory

functions post-SCI, it would be advantageous to promote the axon growth of these neurons, potentially leading to gains in functional outcomes.

Stem cells are a useful source of V2a interneurons to further explore their roles for SCI applications. Chx10 promotes V2a interneuron identity in developing spinal cord with repression of motor neuron pathways by competitive binding to gene regulatory elements of motor neuron[150]. There are differentiation protocols of V2a interneurons derived from mouse embryonic stem cells (mESCs) and human induced pluripotent stem cells (hiPSCs) that utilize concentrations of retinoic acid (RA), mild Shh agonist purmorphamine (Pur), and *N*-[*N*-(3,5-difluorophenacetyl-l-alanyl)]-(*S*)-phenylglycine t-butyl ester (DAPT) to mimic Shh gradient and inhibition of Notch signaling to generate cultures with around 20% $Chx10^{+}$ V2a interneurons[132,151,152]. This thesis utilized the enriched V2a interneuron population derived from Chx10-puro mESC cell line[132].

1.5.3 Important functions of V2a interneurons

Interneurons are activated post-SCI to facilitate plasticity in spared tissue. Ablation of V2a interneurons elucidates roles of these interneurons in CPG for controlling locomotion. CPG is a complex neural circuit in which excitatory glutamatergic neurons provide rhythmic drive to inhibitory glycinergic interneurons and motor neurons[153]. Crone *et al.* utilized a mouse model with Cre-activated diphtheria toxin (DTA) in *Chx10* locus to efficiently ablate V2a interneurons expressing *Chx10*[155]. The ablation demonstrated variability in cycle periods and burst amplitudes of motor outputs, suggesting V2a interneurons regulate locomotor rhythm[154,155]. The spinal cords from Chx10-DTA mice, under drug-induced locomotor activity, demonstrated altered left-right

alternation in raw traces of ventral root activity compared to spinal cord from wild mice[155]. Thus, V2a interneurons are critical for rhythmic motor outputs.

V2a interneurons are also important for the rhythmic motions required in respiratory muscle activity for breathing. Jensen *et al.* generated neonatal and adult mice that decreased excitability of the interneurons with inhibitory designer receptors exclusively by designer drugs (V2a-(G_i) DREADD) and injections of clozapine-N-oxide (CNO) to understand the roles of V2a interneurons in respiratory muscle activity[156]. Using whole body plethysmography, CNO injection in V2a-(G_i)DREADD neonatal mice caused reduction of respiratory rate and disrupted regularity of breathing with increase in breathing frequency[156]. Also, diaphragm activity increased with higher excitability of V2a interneurons[157]. With V2a interneurons playing a significant role in respiratory muscle activity, it has become a population of interest for transplantation post cervical SCI and increasing axon growth of these neurons in an injury microenvironment can aid in potentially regaining critical respiratory functions.

1.5.4 Effects of injured microenvironment on V2a interneurons

SCI demonstrates that interplay between multiple cell types contributes to secretion of factors in the microenvironment, causing rapid cell death in the acute phase and inhibition of axon growth in chronic phase. The inflammatory cytokines and chemokines are key contributors to signaling apoptotic pathways for neuron populations, including V2a interneurons in especially cervical SCI. The loss of V2a interneurons by protein misfolding at the lesion site leads to loss of motor neurons and thus contributes to the functional deficits[158,159]. This degeneration of V2a interneurons interrupts excitatory drive for motor neurons to increase inspiratory parameters of

accessory respiratory muscles as a breathing compensatory mechanism post injury[159]. Thus, it is crucial to promote axon growth and viability of V2a interneurons in a permissive microenvironment to engage in the plasticity potential post injury and potentially regain respiratory functions.

1.6 Role of ECM in healthy and injured spinal cord

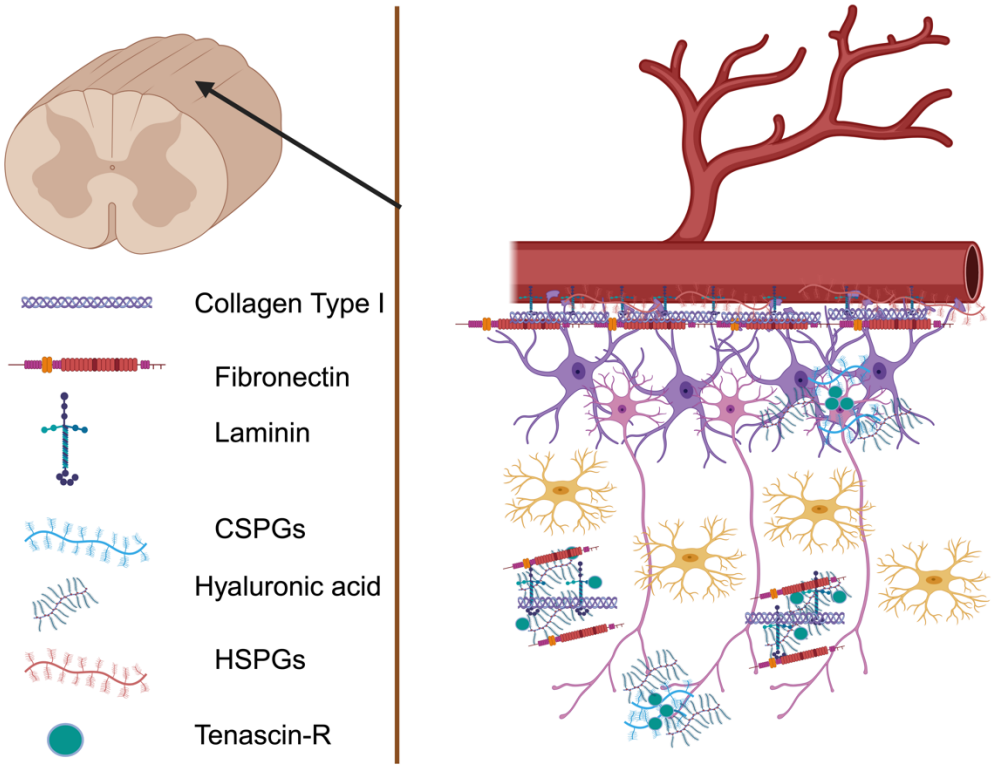

Figure 1.4[160] **Extracellular matrix can shape the microenvironment in the spinal cord** Astrocytes are main contributors to a variety of ECM molecules that compose the healthy CNS for neuron support and maintenance of blood vessel function and BBB. These ECM molecules are key in neural development with some promoting growth and others pruning excessive synapse formation.

The ECM is a critical component of the spinal cord microenvironment and consists of structural proteins that contribute to metabolic and functional support to the CNS. ECM from glia consists of key proteins necessary for synapse formation, development, and axon growth (Fig. 1.4). The ECM can also provide a feedback loop in maintaining glial function. However, the ECM composition changes detrimentally with higher axon-

growth inhibitory proteins during SCI with reactive glia contributing to cell death. A therapeutic strategy for SCI is to increase axon-growth permissive ECM proteins in the microenvironment to promote connections between neuron populations for potential functional recovery. Understanding ECM composition differences between healthy and injured spinal cord cell types is important in developing SCI treatments. This section details the effects of ECM changes and composition on axon growth and neuron support and some explored ECM-based treatments for axon regeneration. In addition, the section proposes the idea of ECM composition playing a potential role in astrocyte reactivity.

1.6.1 ECM contribution in healthy CNS

Proteins produced and secreted from different cell types throughout the developing CNS constitutes ECM, which makes up 10-20% of the adult brain volume, to support the CNS cellular morphology, progenitor proliferation, differentiation into specialized regional subtypes of glia and neurons, and migration of adult cells into different CNS compartments[160,161]. During development, the accumulation and changes of proteins secreted by variety of cell types makes the ECM a complex mixture to study. ECM protein-protein and ECM-receptor interactions at the cell membranes activate signaling pathways downstream that prompt cellular events[160,162]. The CNS ECM can be localized between 3 components: 1) basement membrane- collagen, fibronectin, perlecan, laminin, and nidogen 2) perineuronal nets (PNNs)- matrix consisting of mostly HA, tenascin-R, proteoglycans (core proteins with glycosaminoglycan chains), and linker proteins (stabilize interactions between hyaluronan and proteoglycans) surrounding neurons 3) neural interstitial matrix dispersed in CNS tissues[160,161,163,164].

With these compositions, the basement membrane is more regenerative than the other components. PNNs prevent aberrant axon growth and sprouting in regulating plasticity and thus also consist of various CSPGs, such as versican and neurocan in immature CNS and aggrecan, versican, and brevican in mature CNS[165,166].

1.6.2 ECM proteins affecting neural development and axon growth

The complex ECM composition involves a balance of different proteins that have varying impacts on axon growth of neuron populations in white and grey matter of the spinal cord. Research has shown certain ECM proteins, such as laminins, collagens, fibronectin, and heparan sulfate proteoglycans (perlecan), are more axon-growth permissive and chondroitin sulfate proteoglycans and tenascin are non-permissive[167]. The non-permissive proteins play roles in controlling aberrant axon growth[167]. This subsection discusses the important findings (mostly *in vitro*) of certain ECM components for axon growth and neural development and incorporation into biomaterial strategies for SCI applications *in vivo*.

Laminin

Laminin is a set of trimeric proteins consisting of α, β, and γ subunits and is present in various brain tissues and cell types in CNS[168]. There are numerous isoforms of laminin with the most common ones being laminin-1, 2, and 3 that have axon growth-promoting effects. Specially, laminin subtypes are present at synapse sites of neurons[169]. Most studies utilizes laminin-1 (consists of α, β, γ subunits) for studies of positive effects of laminin on neurite growth and for stimulating neural differentiation[170]. Integrin receptors on neurons are important in interacting with active domains of laminin isoforms to activate signaling pathways in supporting neural survival and axon length and branching[171,172]. The interactions between β1 integrin and laminin are involved in

forming neocortical layers and positioning of laminin that affects migrating neurons[173]. In addition, laminin secreted by astrocytes maintains blood-brain barrier (BBB) integrity and Aquaporin-4 (Aqp4) expression. Furthermore, myocilin^{+} glia limitans astrocytes is found bundled in laminin along blood vessels at the BBB during murine postnatal development, indicating laminin role for astrocyte development[174]. Astrocytes are a source of laminin that positively impacts axon growth post SCI.

Collagen

While collagen is a well-known ECM protein characterized by triple quaternary structure, it is less prevalent in CNS with its presence mainly in the basement membranes. Collagen type IV, and non-fibrillar XVII aid in axon guidance during neural development and growth cone migration[175–177]. Collagen type IV interacts with laminin to form tracts that interconnect the ventral horn and root in the feline spinal cord to become substrates for regenerating motor axons in both white and gray matter[178]. Varying concentrations of collagen type IV substrate with N1 domain as proteolytic fragment increases neurite extension of rat sympathetic neurons as demonstrated by application of anti-N1 serum inhibiting axon growth in short term cultures of less than 24 hours[179]. In long-term culture, collagen type IV substrates increase axon growth of sympathetic neurons but do not promote dendritic growth. Thus, certain collagen subtypes, such as collagen type IV, can be incorporated in hydrogels for potentially promoting axon regeneration[180–182].

Fibronectin

Fibronectin is a key glycoprotein secreted by cells throughout spinal cord neural development and differentiation[183]. Fibronectin plays roles in adhesion and migration of different neural cell types. Fibronectin substrates or recombinant fibronectin fragments

support axon growth of adult mice hippocampal and cortical neuron processes for 3 days of culture with $\alpha 5\beta 1$ integrin receptor mediating this effect[184]. During CNS injury progression with demyelination, astrocyte-derived fibronectin can increase proliferation and maturation of OPCs to combat myelin loss[185]. However, fibronectin is produced by fibroblasts forming the fibrotic core and increases inhibitory proteoglycan production[186]. The positive impacts of fibronectin on CNS cell types make it an ideal candidate to be incorporated into biomaterial strategies for axon regeneration *in vivo*.

Hyaluronan (HA)

HA is the critical backbone for the CNS ECM, surrounding cells. HA can attach tenascins and sulfate proteoglycans (chondroitin and heparan) through linker proteins for thermodynamic stability[18,187].It is a linear glycosaminoglycan that is part of the perineuronal nets in the cerebral cortex and gray matter with high molecular weight hyaluronan being produced by transmembrane synthetases[188,189]. Astrocytes expressing CD44 can play a role in interactions with HA for influencing the microenvironment. The binding of HA to HA-receptor for HA-mediated mobility (RHAMM) has been suggested to influence actin and microtubule dynamics for aiding migration of glia and neurons in neural tube development. The receptor is expressed by proliferating cells of ventricular zone for neural stem microenvironment and migrating neural crest cells[190,191]. The high molecular weight of HA is crucial for gelation, biocompatibility, and larger hydrogel pore size for axon regeneration and neural stem cell differentiation studies[191]. Upon SCI, inflammatory cascades begin to digest the HA to lower molecular weights and are damage-associated molecular patterns (DAMPs)[161]. Thus, high molecular weight HA can be an ideal candidate for supporting neuron viability and producing a permissive microenvironment.

Heparan sulfate proteoglycans (HSPGs)

HSPGs are present in almost all tissues with two forms in CNS tissues as perlecan in the ECM and syndecans on cell surface[192]. Perlecan aids in FGF-2 binding in fractones for rat, mice, and human neural development to regulate cell proliferation, differentiation, and survival[193,194]. Perlecan also plays critical role in motor axon guidance with its expression dominant in areas close to fasciclin^{+} motor axon pathways, motor neuronal cell bodies, and decision points in guidance using a *Drosophilia* embryo model[195]. This shows the potential use of HSPG in creating an axon-growth permissive environment.

CSPGs

This family of proteoglycans is instrumental in maintaining synaptic connections through mostly the GAG chains and is present in the perineuronal nets. Astrocytes, adult neural progenitor cells, and radial glia are all found to express CSPGs with particularly neurocan, brevican, phosphacan, and versican upregulated post CNS injury[34]. The most dominant effect researched about CSPGs is their role of inhibition in axon growth both in healthy and injured CNS. Reactive astrocytes in lesion borders are main contributors to these inhibitory CSPGs inhibiting axon-growth through PTPσ binding[34,196,197]. This axon repellent activity influences their role in proper CNS development with preventing axons from extending beyond the roof plate in spinal cord as an example[198]. Due to CSPG contribution to an axon-growth inhibitory microenvironment post CNS injury, numerous studies utilized ChABC to digest the CSPG deposits and demonstrated recovery with axon growth and modulation of macrophage phenotype to anti-inflammatory in different animal models[199–201]. Thus, a type of SCI treatment is to combat the CSPG effects.

1.6.3 ECM composition changes during spinal cord injury

Upon the physical insult initiating SCI cascades, neurons undergo severe apoptosis at injury site and astrocytes are activated to secrete more axon-growth inhibitory ECM molecules contributing to a microenvironment imbalance[18,202,203]. ECM remodeling is a key part of the secondary injury response for SCI, starting cascades that change cellular functions in the lesion. The key hallmark change is the upregulation of CSPGs (neurocan, brevican, phosphacan, and NG2), which are axon-growth inhibitory molecules and mainly produced by reactive astrocytes[34,167,202,204]. The increased CSPG production changes the potential for neural plasticity by PNNs and interstitial matrix and leads to aberrant LTP and synapse formations[205]. Specifically, after a dorsal column spinal cord lesion at C3, neurocan and brevican staining increased 24 hours after injury, peaked at 2 weeks near the lesion site, and persistent at 4 weeks post SCI, only returning to basal levels at 8 weeks[206]. Phosphacan staining increased steadily for 8 weeks post SCI in tissue surrounding lesion site[206]. *In vitro* studies of NG2, a proteoglycan, seem to inhibit neurite outgrowth by application of the main three domains of NG2 in fusion proteins in neural cell culture and treatments with NG2-antibody rescue the neurite outgrowth[207]. The CSPG method of action to inhibit axon growth is through binding to PTPσ. This indicates the complexity of ECM responses that impact axon growth post SCI.

A key ECM molecule in matrix of the fibrotic scar is elevated type I collagen genes (*Col1a1, Col1a2*) expressed 14 days after mouse thoracic contusion injury with border-forming astrocytes colocalizing with type I collagen staining[208]. Furthermore, the collagen elevation causes increases in N-cadherin and collagen-binding integrin receptor expression in reactive astrocytes when they switch to border-forming

astrocytes *in vitro*[208]*.* Type IV collagen is also present in the glial border with reactive astrocytes expressing the collagen isotype *in vitro* after 24-hour treatment of proinflammatory cytokines and *in vivo* within 1 month after rat SCI model[186,209]. Another major source of the collagen isoforms in the fibrotic scar is the proliferating perivascular fibroblasts that infiltrate the lesion site in response to inflammatory cascades[18,24,186]. The fibroblasts also secrete fibronectin composing the fibrotic scar[186]. Thus, these critical ECM components are instrumental in the inhibition of axon growth post SCI and are essential targets in ECM remodeling.

These reactive astrocytes seem to have a dual role in axon regeneration with their ECM secretion profiles. The disruption of blood flow causes reactive astrocytes to secrete high levels of nidogen, fibronectin, laminin, and collagen VI to repair the lost basal lamina into a restored glial limitans to separate peripheral and CNS and can aid in axons growing over this permissive matrix[18,203]. In addition, not all reactive astrocytes produce elevated levels of CSPGs as observed with rat thoracic crush and stab injury demonstrating $GFAP^-$ areas in spinal cord with increased CPSG staining and $GFAP^+$ areas in corpus callosum with no CSPG staining[204]. Furthermore, some of the CSPGs secreted by astrocytes might have some axon growth permissive role such as 6-sulfated CSPGs. 6-sulfated CSPGs are synthesized by chondroitin 6-sulfotransferases (C6ST-1) and C6ST-1 knockout mice demonstrated low number of dopaminergic axons crossing into lesion site with clear retraction in 35-day period compared to wild type mice[210]. This suggests astrocyte heterogeneity in reactivity and is a rationale for even reactive astrocyte subtypes being beneficial for axon regeneration[93]. Thus, there is a need to further understand astrocyte complexity to influence ECM strategies in SCI.

1.7 Current research strategies for spinal cord injury therapies

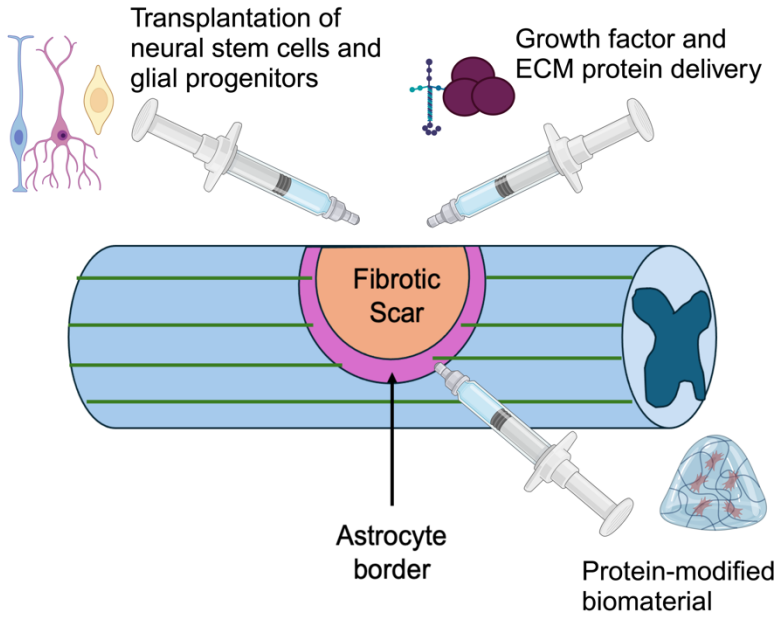

Figure 1.5 Current approaches for research in SCI treatments Combinatorial approaches of cellular transplantation, axon-growth permissive proteins in biomaterial, and drug delivery growth factor depots can aid overcome the inhibitory environment of the SCI fibrotic core to regenerate axon connections and bridge the lesion.

Since SCI involves complex molecular and cellular events detrimental to CNS cell types, it is important to utilize combinatorial approaches to address the different factors in the harsh spinal cord microenvironment. Key goals in SCI treatments are to decrease effects of the inhibitory microenvironment and increase axon growth through cell, neurotrophic factor, and biomaterial delivery (Fig 1.5). The delivery of permissive components to the injury site can improve neural plasticity, reorganize neural circuits, and ultimately lead to motor functional recovery. Furthermore, electrical stimulation at various spinal cord levels can provide excitatory drives for motor neurons in an injured spinal cord. To study the effects of these treatments for functional recovery from SCI,

compression and contusion SCI animal models can aid in understanding the mechanisms for promoting an axon growth permissive microenvironment.

1.7.1 Biomaterial treatment for spinal cord injury

Biomaterial strategies are widely researched for promoting a permissive microenvironment in injured spinal cord[211]. There are several design considerations in supporting neurons and axon guidance. Materials with soft, tunable properties favor neural differentiation and growth and thus are conduits for forming nerve guidance channels. Tailoring the material chemistry modulates the mechanical moduli to be similar to spinal cord tissue. Biomaterials with degradable components prevent the need for removal of the biomaterial implant and improve cellular viability in transplantation, depending on impacts of degradation rate and products. Furthermore, certain biomaterial crosslinking occurs at quick reaction times and room temperature with no need of a catalyst, such as materials based on hyaluronic acid (HA)-methylfuran (mF) crosslinking with polyethylene glycol (PEG)-dimaleimide in Diels-Alder click chemistry. All these properties make biomaterials an important consideration for clinical translation[212]. This section will highlight studies of a few important types of biomaterials and discuss the choices of biomaterial strategies employed in this thesis.

Natural biomaterials

Biomaterial scaffolds from components naturally present in human systems have been used in drug delivery platforms and for cellular transplantation due to their biocompatibility. Fibrin scaffolds have been researched for SCI treatments due to its role in wound repair. For example, controlled delivery of neurotrophin-3 (NT3) by fibrin scaffolds implants in the lesion site immediately after rat suction aspiration SCI injury

produced nerve fiber growth and reduced glial scar components in the white matter, but did not result in functional recovery[213]. In general, pre-polymerized fibrin scaffold implants in rat dorsal hemisection subacute SCI model also demonstrated significant decreases in $GFAP^+$ reactive astrocytes 2 and 4 weeks later, suggesting this could increase axon sprouting[214]. Overall, fibrin scaffolds can be neural supportive materials *in vitro* and *in vivo*, offering flexibility in delivering growth factors to SCI lesion site.

Collagen is utilized in natural biomaterials for SCI treatments. Three-dimensional gelatin sponge scaffolds implanted in monkey hemisection SCI model demonstrated no additional immunological responses after 8 weeks of implantation and interestingly showed decreased α-smooth muscle actin staining of activated fibroblasts at the injury site[215]. This suggests alleviation of the fibrotic scar formation and thus nerve tract regeneration into the lesion site[215]. The tissue remodeling further protected surrounding lesion tissue from deformation and myofibroblast-mediated compression during SCI and further increased laminin, collagen, and fibronectin deposition to support nerve fiber growth into the lesion[215]. This helped in mainly regaining motor function in ipsilateral hindlimb muscles[215]. Collagen scaffolds can facilitate cellular delivery in which porosity of the fabricated materials sustainably supports NSCs for delivery in SCI lesion site and promotes functional recovery[216]. Furthermore, porous, biodegradable collagen scaffolds support NSC viability and proliferation *in vitro* with fast calcium signals presented in networks of differentiated mostly gamma-aminobutyric acid (GABA) inhibitory neurons[216]. These NSC-loaded collagen porous scaffolds demonstrated substantial decreases in fault rate 11-12 weeks after mouse dorsal column crush SCI model to levels of uninjured mice, displaying the importance of natural biomaterials for SCI

recovery[216]. Overall, the use of natural biomaterials proves to be biocompatible and aid in axon regeneration.

Hydrogels

Due to its hydrophilic nature, hydrogels are powerful foundation for biomaterials to incorporate different chemistries and shear-thinning properties for easy injection into SCI lesion site and be biocompatibility[217–219]. Hydrogels can incorporate natural (collagen, cellulose, and silk fibroin) proteins or synthetic (PEG) base materials to house cells, growth factors, and exosomes for SCI treatments[218,220]. The material can be fine-tuned to have mechanical properties similar to the spinal cord tissue for integrating better in host environment[218,219]. There are different gelation strategies employed, such as photopolymerization and click-chemistry, as timesaving and easier chemical crosslinking methods without catalysts[212,217]. Click-crosslinked HA can be an injectable material for *in vitro* controlled release of growth factors, such as BDNF, to support neurons, making it an ideal chemistry for axon regeneration research[212,221]. Several studies used HA-based hydrogels to decrease glial scarring and inflammation after SCI[222,223]. Cell and growth factor delivery in HA-methylcellulose (HAMC) material are showing promise for retinal degeneration and SCI. Gupta *et al.* developed a fast-gelling, injectable material based on HAMC that reduced inflammatory response in a rat SCI model[222]. HAMC with platelet-derived growth factor (PDGF) promoted neural stem cell (NSC) differentiation into oligodendrocytes and reduced lesion size in rat SCI models[224]. HA-based hydrogels are commonly researched biomaterials for generating permissive spinal cord microenvironment. Thus, HA is used as the base material for our proposed combinatorial protein and astrocyte ECM containing biomaterial for promoting axon growth.

Tailoring hydrogel properties to incorporate ECM components for synthesis of ECM biomimetics in SCI treatments have become an important area of research. For example, protein- and peptide- containing hydrogels mimic properties of ECM promoting *in vitro* neurite extension and testing for therapeutic benefits in CNS injury models[225]. Laminin-derived peptides are immobilized on fibrin matrices through the enzymatic activity of coagulation Factor XIIIa and these peptide-containing fibrin gels produced significantly higher neurite outgrowth of dorsal root ganglion (DRGs) compared to native fibrin gels over 48 hours in culture[226]. These laminin-peptide modified fibrin matrices supported extensive neural regeneration in dorsal root bridging the gap from transected dorsal root nerve, demonstrating the *in vivo* applications of peptide-modified biomaterials[226]. In addition to impact on neurite growth, laminin peptide IKVAV amphiphile molecules that can self-assemble into polymers *in vivo* reduces apoptosis by caspase activity, increase oligodendrocyte formation for myelination potential, improvements in hindlimb functionality with 24 hours post SCI[227]. Furthermore, ECM-mimetic materials with protein-based composition can be biocompatible and mimic native cues and 3D architecture to support neuronal adhesion and survival[225,228]. In this thesis, we developed hydrogel that contained a mixture of selected protoplasmic astrocyte ECM proteins through Design of experiments (DoE) approach for axon growth. This protein-based hydrogel can eliminate the need of long astrocyte differentiation protocol to obtain the variable astrocyte phenotypic ECM for axon growth testing.

Synthetic biomaterials

Also, electrostatic positive and negative charged PLGA nanoparticles within HAMC help encapsulation of growth factors for more controlled delivery over 28 days to biological targets of neurons *in vitro*[229]. The pH levels and electrostatic interactions between the nanoparticles and growth factors can tune release over varying time periods for axon growth. The initial research in the synthetic polymers was focused more on fabrication of nerve guidance channels that align spare axons for regeneration to form axon bridges over SCI lesion sites[211]. This speared the work into polymer processing including electrospinning methods to generate topography found in healthy spinal cord. A few of the key aspects for using synthetic biomaterials as ECM mimetics are tunable mechanical properties through crosslinking, degradability, and biocompatibility[230]. Polymer processing adds fibrillar qualities to biomaterials and incorporation of bioactive peptides, such as IKAV, promotes cell adhesion and neurite outgrowth. These synthetic materials also can form in situ to maximize interactions with host tissue. This thesis work developed a protoplasmic astrocyte ECM mimetic with a foundation of HA crosslinked with PEG to have potential future *in vivo* capabilities in recapitulating signaling cues of astrocyte ECM for axon regeneration.

1.7.2 Decellularized ECM-based strategies for axon regeneration

With the ECM protein composition of glia and other neural cell types providing essential cues for neural development and SCI, it is important to harness axon growth permissive ECM signals to support axon regeneration post SCI. Initial ECM-based studies for SCI treatments were explored using decellularized tissue to harness structural, topographical cues in 3D scaffold environment to influence axon survival in SCI models[231]. Most decellularized tissues have been extensively researched for

skeletal muscle and cardiac applications[231,232]. Various methods are used for decellularization ranging from enzymatic with trypsin to chemical detergent treatment to perfusion of whole organs[232]. Decellularized scaffolds are produced using enzymatic and chemical approaches to remove the cellular components with retention of structural and biochemical properties.

Decellularized spinal cords are achieved by physical agitation, detergent usage, and enzyme treatment and showed no residual nuclei and preserved critical ECM proteins such as laminin, fibronectin, and collagen type IV[233]. It is important to note that decellularized tissues can also capture secreted growth factors such as fibroblast growth factor-2 (FGF-2) and fibroblast growth factor-1 (FGF-1). Furthermore, *in vitro* testing of decellularized porcine brain matrix at various concentrations in hydrogel showed increased M2 phenotype marker (Arginase1) in cultured rat macrophages and *in vivo* injection of this decellularized scaffold in rat thoracic spinal contusion model demonstrated reduced lesion size with increased M2 phenotype of macrophages[234]. This shows the promise of using decellularized nerves and spinal cords as treatment for enhancing pro-regenerative microenvironment.

1.7.3 Cellular transplantation

To promote a regenerative microenvironment post SCI, transplantation of glia, neural stem or progenitor cells, and neurons has become a research goal (Fig 1.2)[12]. Neural transplantation is researched to directly restore neuron loss in the injured spinal cord. In relation to this thesis focus on V2a interneurons, the transplantation of these interneurons is critical in enhancing and supporting respiratory plasticity. Neural progenitor cells (NPCs) and V2a interneuron aggregates delivered to cervical SCI lesion

led to NPC differentiation into neurons, increased axon growth, and increased diaphragm amplitude and activity[235]. Excitability of V2a interneurons is required for improving diaphragm function post cervical SCI through transplanted V2a interneurons having synaptic connections with injured neural circuits and functional innervations of V2a interneurons by host neurons in cervical SCI models[157,236]. Thus, it is important to understand biomaterial and delivery strategies to optimize survival and excitability of transplanted neurons for proper connectivity in SCI recovery.

NPC and neural stem cell (NSC) transplantations are popular researched therapies that promote axon-growth permissive microenvironment in injured spinal cord[237]. These cell types are mainly considered due to their presence in developing spinal cord as proliferative, multipotent states for generating neuron and glial populations[238]. Utilizing NPCs isolated from embryonic (E11.5, E12.5, and E13.5) mouse spinal cords in transplantation 4 weeks after cervical SCI resulted in V2a interneuron generation, serotonergic axon regeneration, and quick response to thermal changes in early-stage NPC grafts with V1 interneuron generation and dorsal fiber regeneration in later stage NPC grafts[239]. Protocols using CNTF and NT3 on iPSCs generated NSCs/NPCs with potential to differentiate into glia expressing Olig2 for oligodendrocyte progenitors and NFIA for gliogenic progenitors[240]. Transplantation of these NS/PCs 12 weeks after thoracic contusive SCI mouse model produced no teratoma, migrated away from transplantation site into host tissue, and differentiated into mature myelin basic protein $(MBP)^{+}$ oligodendrocytes for myelination of spared axons. This ultimately resulted in mice rotating on the rod and striding longer[240]. The

generation of glia and neurons from NPC and NSC transplantation aids in regaining loss of critical cells at the SCI lesion site.

1.7.4 Growth factor delivery

Delivery of neurotrophic factors promotes neuron survival and axon growth in the injured spinal cord. The delivery systems are fine-tuned with use of various biomaterial chemistries and release kinetics to present and retain growth factors at the lesion site. Neurotrophic factors were studied *in vitro* for promoting axon growth. Fabricated diblock co-polypeptide hydrogel depots released brain-derived neurotrophic factor (BDNF) and NT-3 over a prolonged period to the lesions formed by crush SCI at the thoracic levels in rats[26]. This facilitated robust growth of axons through the lesion core to the surrounding host tissue with laminin-blocking antibodies inhibiting these effects, suggesting that NT-3 and BDNF interact with laminin to stimulate axon growth[26].

1.7.5 Removal of inhibitory extracellular matrix (ECM) molecules

CSPGs are key ECM components that contribute to the inhibitory activity of the astrocyte border from SCI. A key research strategy of SCI treatments has been to remove CSPG mechanisms to regain axon connections. Chondroitinase ABC (ChABC), an enzyme that digests CSPGs, is often used to counteract the axon growth inhibition driven by CSPG[199,241]. Intrathecal administration of ChABC to lesioned dorsal columns of adult rats by cervical crush SCI demonstrated that within 2 weeks of treatment there was an increased presence of 2B6 (core protein of non-intact CSPGs) near the lesion site and surrounding white matter tracts. This corresponded with increased growth associated protein (GAP-43) in large-diameter neurons and bundles into the lesion, indicating CSPG degradation can play a role in axon growth[199]. The ChABC treatment

supported sprouting of CST axons into the gray matter, shown by injection of biotinylated dextran amine (BDA)-labeling in motor cortex, and these collaterals evoked strong postsynaptic potentials, indicating formation of functional synaptic connections[199]. This resulted in less errors made by treated rats on beam and grid walk tests[199]. ChABC treatments modify the axon growth inhibitory microenvironment in injured spinal cords and translate to functional improvements[242]. Furthermore, combinatorial treatment of ChABC injection and intermittent hypoxia 12 weeks post cervical rat SCI restored respiratory function by tonic firing of hemidiaphragm and increased serotonergic axon density[243]. Chronic degradation demonstrated synchronized ipsilateral diagram activity and increases in respiratory activity, suggesting functional recovery[243]. Overall, the removal of CSPGs can promote a regenerative microenvironment to support axon growth and connectivity.

1.8 Concluding Remarks

The roles of astrocyte phenotypes are complex with both beneficial and harmful aspects affecting the microenvironment for axon growth. Specifically, this thesis focused on investigating effects of astrocyte-derived proteins supporting V2a interneurons as a key neuron population involved in plasticity and functional rewiring with central pattern generators post SCI. However, the astrocyte field is still discovering the various non-reactive and reactive astrocyte-derived factors that can promote a regenerative microenvironment. Astrocyte differentiation protocols from stem cells have advanced the knowledge of gene and protein expressions of astrocyte phenotypes during development. Genetic technologies have been employed to engineer transgenic selectable cell lines for purifying stem cell-derived astrocyte phenotypic populations and

establishing *in vitro* cellular platforms to study astrocyte phenotypes. This thesis focuses on *in vitro* methods to characterize the puromycin selectable transgenic cell line as a platform to study astrocyte phenotypes for axon growth and how these astrocyte-derived factors can influence biomaterial design for potentially SCI. In Chapter 2, selected astrocyte phenotypes contain cells with high percentage of astrocyte markers and low percentages of other cell type markers, such as for neurons, oligodendrocytes, and undifferentiated stem cells. Chapter 3 details the process of identifying and testing a few selected protoplasmic astrocyte ECM proteins in a hydrogel platform as an ECM mimetic for axon growth applications. This thesis specifically focuses on studying the effects of selected astrocyte phenotypes and astrocyte-derived ECM proteins on axon growth of V2a interneurons. V2a interneurons were chosen as a target neuron population due to the loss of the interneurons in specifically cervical SCI. The defined mixtures of identified selected protoplasmic ECM proteins in HA-based hydrogel can be a scalable solution to bypass the 27-day astrocyte differentiation protocol for harvesting astrocyte-derived ECM. Furthermore, this ECM-mimic material can be a clinically translatable solution incorporating astrocyte-derived factors for generating permissive microenvironment for neurons after SCI. Overall, these chapters progress *in vitro* understanding of astrocyte phenotypes for axon growth of V2a interneurons. This work has also provided us with potential gene and protein targets in astrocytes that can be further studied for development of SCI therapies *in vivo*.

Chapter 2: Enrichment of astrocyte subtypes from mixed cultures using selectable transgenic mouse embryonic stem cell lines

2.1 Abstract

Astrocytes play multifaceted roles in both inflammation and axon regeneration following spinal cord injury (SCI), making them a key focus for identifying signals that promote axon growth. Previously, we developed protocols to differentiate mouse embryonic stem cells (mESCs) into the two main spinal cord astrocyte subtypes-protoplasmic and fibrous-but these methods yielded mixed cell populations. To address this, we engineered transgenic mESC lines expressing puromycin N-acetyltransferase (*PAC)* under astrocyte-specific promoters, enabling enrichment of protoplasmic and fibrous astrocytes via puromycin selection. The optimal timing for puromycin selection was determined using quantitative polymerase chain reaction (qPCR) analysis of *Aqp4, Olig2*, and *PAC* expression. The resulting enriched astrocyte cultures showed a reduced presence of non-astrocytic cells, including mature neurons, oligodendrocytes, and undifferentiated stem cells, while maintaining or increasing expression of general astrocyte markers as confirmed by immunostaining. Functionally, the selected astrocytes demonstrated calcium transients, glutamate uptake, and responsiveness to inflammatory stimuli. Additionally, bulk RNA-sequencing revealed significant upregulation of genes involved in extracellular matrix interactions and cell adhesion pathways in protoplasmic astrocytes, suggesting a role in promoting axon growth. these

enriched astrocyte subtypes offer valuable tools to dissecting astrocyte-neuron interactions and advancing therapeutic strategies for SCI.

2.2 Introduction

Spinal cord injury (SCI) is a severe, debilitating condition with complex pathophysiology that results in patients facing significant physical and financial burdens resulting from partial to complete loss of sensory and motor functions[1-4]. The loss of axon connections is a result of inhibitory microenvironment in injured spinal cord. Reactive astrocytes are key in contributing to the axon-growth inhibitory microenvironment by secretion of chondroitin sulfate proteoglycans (CSPGs) at the glial border[244–247]. Thus, research is leading into understanding the role of astrocyte in SCI.

Although astrocytes were once primarily viewed as detrimental following SCI, emerging evidence highlights their contributions to neural repair and limitation of inflammation[24–26,248,249]. In a healthy central nervous system (CNS), astrocytes help to maintain blood-brain barrier, supply neurotrophic factors, and regulate synapse health[25,68,244,250,251]. The two primary astrocyte phenotypes - protoplasmic in grey matter and fibrous in white matter – exhibit distinct morphologies and contribute to the support of ascending and descending axonal pathways[25,251]. Following injury, astrocytes can adopt distinct phenotypes, neurotoxic (A1) or neuroprotective (A2), which differentially influence axon growth[21,27,68,252]. Given the multifaceted roles astrocytes play in both healthy and injured spinal cord, it is essential to study their molecular, biochemical, and functional characteristics *in vitro* to better understand their response to injury and inform the development of effective SCI therapies. These studies are particularly valuable to

identify key astrocyte cues including extracellular matrix (ECM) proteins and signaling mechanisms that can support axon growth.

Our astrocyte differentiation protocol provides a quick, renewable, reproducible resource of nonreactive astrocyte phenotypes, which is contrasted to the reactive astrocytes generally isolated from primary cultures plagued by low viability during tissue extraction and enrichment methods. Specifically, our lab developed a protocol to generate fibrous and protoplasmic astrocytes from mouse embryonic stem cell lines (mESCs) utilizing glial-restricted progenitors with the addition of ciliary neurotrophic factor (CNTF) and bone morphogenic protein 4 (BMP4) to drive fibrous and protoplasmic astrocyte differentiation, respectively[44]. Studying non-reactive astrocytes allows us to determine phenotype-specific cues produced for neuron support and axon regeneration.

Most differentiation protocols (including the astrocyte differentiation protocol developed in our lab) produce heterogeneous cell populations[44,256]. The presence of other cell types can make astrocyte-specific effects on axon growth difficult to discern. Thus, it is crucial to enrich these stem cell-derived astrocyte cultures. Previous primary culture purification methods, such as immunopanning, cell sorting, and mechanical shaking, have the drawbacks of potentially negatively affecting cell viability and being expensive [118,122,123,129,254,255,257]. Thus, this study utilizes transgenic ESC lines with puromycin selection to enrich astrocyte subtypes[51,131–133]. We validated our approach using cell viability, qPCR, immunocytochemistry and flow cytometry to assess enrichment. Astrocyte function was assessed by measuring glutamate uptake, reactivity

to inflammatory stimuli, and calcium transients. Lastly, bulk-RNA sequencing of selected astrocyte subtypes confirmed expression of key astrocyte markers and revealed differential gene expression profiles associated with axon growth and neuronal support. These selected astrocyte subtypes can be useful *in vitro* cellular platforms for investigating interactions between astrocytes and various neuron populations for promoting axon-growth permissive microenvironment.

2.3 Materials and Methods

2.3.1 Cell lines

Table 2.1 Cell lines used to generate renewable sources of enriched astrocyte phenotypes.

Cell line name	Description
RW4 (ATCC, SRC,1018)	The parental wild type mouse embryonic stem cell line[51,131,132]
Aquaporin-4 (*Aqp4)-PAC*	Cell line with *puromycin-N-acetyl transferase (PAC)* under the control of the *Aqp4* gene regulatory element[258]
Olig2-PAC	Cell line with *puromycin-N-acetyl transferase (PAC)* under the control of the *Olig2* gene regulatory element[51]

2.3.2 mESC culture maintenance

All mESC lines were maintained in T-25 flasks coated with 0.1% gelatin (MilliporeSigma, G1393; in water) in complete media (CM) consisting of Dulbecco's modified Eagle's Medium (DMEM; Thermo Fisher Scientific, Carlsbad, CA) supplemented with 10% newborn calf serum (Thermo Fisher Scientific), 10% fetal bovine serum (Thermo Fisher Scientific), and 30 μM of each of the following nucleosides: adenosine, cytosine, guanosine, and uridine (Sigma) with 1000 U/mL leukemia inhibitory factor (LIF; MilliporeSigma, ESG1106) and 100 μM β-mercaptoethanol (BME; Thermo Fisher Scientific, 21985023) in 5% CO_2 at 37°C. For

passaging (usually every 2 days), mESCs were dissociated with 0.25% trypsin ethylenediaminetetraacetic acid (trypsin–EDTA; Thermo Fisher Scientific, 25200072) for 5 min, followed by quenching with CM and trituration to ensure single-cell suspension. Single cells were plated in a new flask containing CM +LIF +BME at a typical 1:5 ratio and grown for two days or until ~ 60-80% confluent.

2.3.3 Design of vector for selection cassette to generate Aqp4-PAC TG ESC line[258]

All cloning steps were carried out in *DH5α E. coli*. The targeting cassette was constructed in a Gateway compatible plasmid (pStart-K; Addgene #20346, Cambridge, MA) using a 718 bp SalI-AscI fragment of the 3' end of the 2nd intron of the *Aqp4* gene and a piece the 5' untranslated region of the 3rd exon of *Aqp4* (5' arm) and a 618 bp AscI-NotI fragment containing the genomic sequence of the 3' end of the 3rd exon of *Aqp4* (3' arm). A *PAC/Pgk-neo* dual resistance cassette was inserted in between the homology arms. From 5' to 3' order, it contains: an Asc1 site, Kozak sequence, the coding region of *PAC* with bGH polyA signal (PKO-Select Puro; Agilent Genomics, Santa Clara, CA), floxed phosphoglycerate kinase I (Pgk) promoter driving *neomycin phosphotransferase II* (*Neo*) expression with a bGH polyA signal, and another AscI site. Gateway recombination with the LR Clonase II Kit (Life Technologies #11791) was used to insert the entire region between the attL1 and attL2 sites into a pWS-TK3 vector, which contains *thymidine kinase* for negative selection of the electroporated ESCs[51].

2.3.4 Generation of Aqp4-PAC TG ESC line[258]

RW4 mESCs were electroporated as described in Iyer *et al* [132] with Cas9 expression vectors (Addgene plasmid #43945), Aqp4-PAC targeting vector (described above), and

guide RNAs (gRNA), inserted into a derivative of Addgene plasmid #43860, were generated by Genome Engineering Core at Washington University in St Louis. Two gRNAs were used for generating selectable cell lines (Table 2). These gRNAs contained no polymorphisms and had at least 3 bp (base pairs) mismatch with targeting sequence of the vector and other sites in mouse genome, leading to less probability of off-target. 1 x 10^7 RW4 ESCs were suspended in electroporation buffer (20 mM HEPES pH 7.5, 137 mM NaCl, 5 mM KCl, 0.7 mM Na_2HPO_4, and 6 mM dextrose) with 8 µg Aqp4-PAC targeting vector, 1 µg Cas9 expression vector and 1 µg of the gRNA vector. The electroporation was performed in a cold 0.4 cm cuvette (Bio-Rad, 1652081, Hercules, CA) at settings of voltage parameter 0.23 kV and capacitance parameter 960 µF on Gene Pulser Xcell Eukaryotic System (Bio-Rad, 1652661).

The electroporated cells were seeded in CM with BME and LIF on a gelatin-coated 10-cm dish overnight to recover followed by 10 days of CM with 150 nM fialuridine (FIAU, Moravek #M251, Brea, CA) for negative selection and 40 µg/mL geneticin (G418, Life Technologies #10131) for positive selection, replaced with fresh media every 2 days. After selection, 48 visible single colonies were picked, and these colonies were dissociated with trypsin-EDTA into 0.1% gelatin-coated 96-well plates and quenched with CM and maintained in CM with BME and LIF. Once confluent, the cells were passaged and seeded in two wells of 96 well plate. One of these wells was used to perform junction PCR with the forward and reverse primers (Table 2) to validate successful insertion of *PAC* in *Aqp4* locus. The resulting positive clones were also tested with copy number assay to ensure 1 copy of PAC was inserted. The copy number assay involved quantitative real-time PCR with mouse telomerase reverse

transcriptase (Tert; Thermo Fisher Scientific, 4458368) as the endogenous control, Rw4 ESCs as negative control, and previously established selectable cell line ESCs, Hb9-PAC ESCs. In addition, the copy number assay was performed for glyceraldehyde 3-phosphate dehydrogenase (GAPDH) copies in all the samples to ensure the cell lines all had 2 copies of GAPDH [131,132]. The chosen clones that contained 1 copy of PAC successfully inserted in Aqp4 locus were expanded to 80% confluency in T-75 flasks for cryopreservation.

Table 2.2 Oligonucleotides sequences used for generation and validation of Aqp4-PAC cell line[258]

Oligonucleotide name	**Sequence**
Aqp4 gRNA 1	GTGACAGAGCTGCGGCAAG
Aqp4 gRNA 2	ACAGAGCTGCGGCAAGGCGG
jPCR Forward	ACCCCGATGCCAAGTGGCTG
jPCR Reverse	GCGCCAGGAGGCCTTCCATCTGTTGCT
5' gibson aqp4 Forward	CTTTGTACAAAAAAGCAGGCTTTAAAGGAACCAATTCACTCTGGTGGGACTTGCAACTAT
5' gibson aqp4 Reverse	TGGCGAGGCGCACCGTGGGCTTGTACTCGGTCATATTGGCGGAGTCAGATTACGGGCACT
3' gibson aqp4 Forward	GGGATCCACTAGTTCTAGAGCGGCCGCCACCGCGGAGATGCCTTCAGGAAACAATGCTCA
3' gibson aqp4 Reverse	CCAACTTTGTACAAGAAAGCTGGGTCTAGATATCTCGAGTCAAAGCATCCAAACCCGTGA
5’ homology arm Forward	CAGTGTCGACCTCTGGTGGGACTTGCAACTAT
5’ homology arm Reverse	CAGTAGCAGCGGCCGCGGCGCGCCGGAGTCAGATTACGGGCACT
3’ homology arm Forward	CAGTGGCGCGCCACTCTTTCATTGCGGGTATCCAT
3’ homology arm Reverse	CAGTGCGGCCGCTCAATAGCAGAGCACCCAGG
PAC cassette Forward	TCTGGATTCATCGACTGTGG
PAC cassette Reverse	GCGCCAGGAGGCCTTCCATCTGTTGCT

2.3.4 Glial differentiation from mESCs and puromycin selection (Fig. 2.1)[258]

Astrocytes were differentiated from *Aqp4-PAC* mESCs as previously described to generate protoplasmic astrocytes and from *Olig2-PAC* mESCs to generate fibrous astrocytes[44]. Briefly: 1-1.5 x 10^6 ESCs were cultured in suspension on agar-coated 10 cm dishes in 10 mL DFK5 medium- DMEM/F12 (Life Technologies) plus 5% Knockout Serum Replacement (Life Technologies), 50 μM nonessential amino acids (Life Technologies), 1x Insulin Transferrin Selenium (Life Technologies), 100 μM BME (Sigma), 5 μM thymidine, and 15 μM of the following nucleosides: adenosine, cytosine, guanosine, and uridine (Life Technologies) for two days to form embryoid bodies (EBs). They were then cultured with media changed every 2 days for the next 4 days in 10 mL DFK5 with 2 μM retinoic acid (RA) and 600 nM Smoothened agonist (SAG) to generate ventral spinal cord progenitors. On day 6, the EBs were dissociated and seeded at density of 50,000-100,000 cells/cm^2 onto a gelatin-coated tissue culture treated 6-well plates (ThermoFisher) in Astro1 media (DFK5 with 20 μg/mL epithelial growth factor (EGF) (Peprotech), 10 μg/mL fibroblast growth factor 1 (FGF-1) (Peprotech), and 1 μg/mL laminin) for 5 days. On day 11 of differentiation, cultures were switched into astrocyte phenotypic media for an additional 4 days in the same plates (*Protoplasmic (astrocyte) media*- DFK5 with 10 μg/mL FGF-1, 10 μg/mL bone morphogenic protein 4 (BMP-4) (Peprotech) and *Fibrous (astrocyte) media*- DMEM/F12 plus 1 × G5 supplement (Thermo Fisher Scientific), 10 μg/mL ciliary neurotrophic factor (CNTF) (Peprotech)). On day 15, the protoplasmic astrocytes were reseeded onto gelatin-coated plates at a density of 50,000 or 100,000 cells/cm^2 and maintained in lineage specific media for additional 2 days. On day 17, protoplasmic astrocytes were selected

with 2 or 4 µg/mL puromycin in protoplasmic astrocyte media for 1 day. On day 18, the protoplasmic astrocytes were washed with phosphate buffered saline (PBS) and maintained in astrocyte phenotypic media in same culture plates until day 21 for reseeding. On day 21, the protoplasmic astrocytes were reseeded at 25,000 cells/cm^2 in 0.1% gelatin-coated 6-well tissue culture plates for further analysis until day 27[44].

On day 17, the fibrous astrocytes were reseeded onto gelatin-coated plates at a density of 10,000 or 20,000 cells/cm^2 and maintained in lineage specific media for additional 2 days. On day 19, fibrous astrocytes were selected with 4 µg/mL puromycin in fibrous astrocyte media for 2 days. On day 21, the fibrous astrocytes were washed with PBS and maintained fibrous media in same culture plates until day 23 for reseeding. On day 23, the fibrous astrocytes were reseeded at 20,000 cells/cm^2 in 0.1% gelatin-coated 6-well tissue culture plates for further analysis until day 27[44].

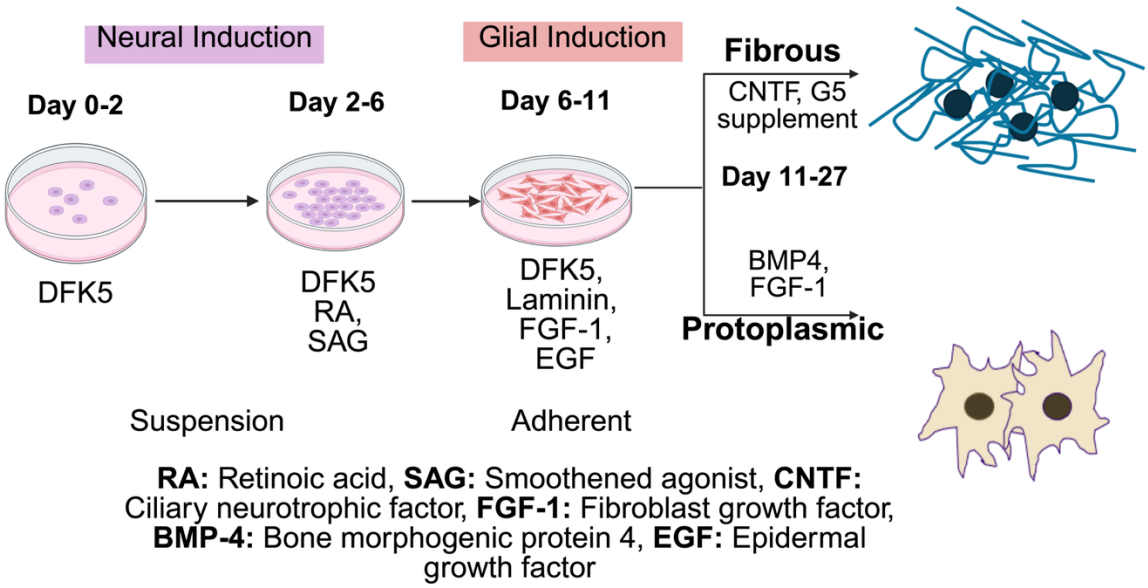

Figure 2.1 Differentiation protocol for protoplasmic and fibrous astrocyte phenotypes.

2.3.5 V2a interneuron differentiation

V2a interneurons were generated from Chx10-puro-TdTomato or Chx10-puro-eGFP mESCs and were induced using a $2^{-}/4^{+}$ protocol using 10 nM RA and 1 μM purmorphamine (Pur; EMD Millipore #540223) from days 2 to 6 and 5 μM N-{N- (3,5-difluorophenacetyl-L-alanyl))-(S)-phenylglycine-t-butyl-ester (DAPT; Sigma #D5942) for days 4 to 6. On day 6, 4μg/mL puromycin was added to the 10-cm dish containing V2a interneuron EBs for 24 hours. On day 7, selected V2a IN EBs were dissociated with 0.25% trypsin followed by quenching with CM and seeded at 50,000 cells/cm^2 on laminin-coated plates. Day 9 V2a interneurons were used for the glutamate assay.

2.3.6 Cytotoxicity assay

Astrocyte phenotypic cultures were grown in 48-well plates for viability assays and image analysis by viability staining. To test various selection conditions, 2 or 4 μg/mL puromycin for 1 day was added on day 17 for protoplasmic astrocytes, followed by a rinse with PBS before culture in protoplasmic astrocyte media and the viability assay was conducted on the same day. To test various selection conditions, 4 μg/mL puromycin for 1 day or 2 days was added on day 19, followed by a rinse with PBS before culture in fibrous astrocyte media and the viability assay was conducted on the same day. The viability assay was conducted with unselected astrocyte phenotypes as well on the same day. The assay followed the manufacturer instructions provided by LIVE/DEAD Viability/Cytotoxicity Kit for mammalian cells (Thermo Fisher Scientific, L3224). The images obtained by the assay were analyzed by counting the number of cells stained by calcein-AM and Ethidium homodimer using Fiji software[132,133].

2.3.7 Gene expression analysis[44,132]

To collect astrocyte mRNA for analysis, medium was aspirated, and cells were detached by using 0.25% trypsin–EDTA, followed by quenching in CM. Cells were pelleted at 300 × *g*. The cell pellets were resuspended in RLT buffer as provided from the RNeasy Mini Kit (Qiagen, 74106). Pellets were either frozen at −80°C or immediately used with the RNeasy kit using on-column DNase (Qiagen, 79254) to isolate RNA extracted from cell pellets per manufacturer protocols. 500 ng of RNA was reverse transcribed into cDNA using the High-Capacity cDNA Reverse Transcription Kit (Thermo Fisher Scientific, 4368813) per manufacturer protocols [44,132].

For quantitative polymerase chain reaction (qPCR), a master solution of ultrapure water, TaqMan Fast Advanced Master Mix (Thermo Fisher Scientific, 4444963), the TaqMan probe against the target gene using FAM-MGB dye, and TaqMan probe against mouse *β-actin,* a reference gene, using VIC-MGB_PL dye (Thermo Fisher Scientific, Mm02619580_g1), was prepared and loaded into appropriate wells of MicroAmp Fast Optical 96-Well Reaction Plate (Thermo Fisher Scientific, 4346906) in triplicate fashion. The plates were analyzed with QuantStudio 3 and 5 instruments (Thermo Fisher Scientific). The fold changes in mRNA expression levels were calculated using $2^{-\Delta\Delta CT}$ values with *β-actin* as the reference gene and comparison of samples relative to mESCs or certain reference point in the astrocyte differentiation protocol for respective experiments.

Table 2.3 qPCR probes for determining gene expression level of various markers in astrocyte phenotypic cultures

Gene	Primer ID
PAC	Custom-made: forward sequence-GGTGCCCGCCTTCCT Reverse sequence-CGGCGGTGACGGTGAA
Aqp4	Mm00802131_m1
Olig2	Mm01210556_m1
GDNF	Mm00599849_m1
GLT-1	Mm01275814_m1
GLAST	Mm00600697_m1
GFAP	Mm01253033_m1
Aldh1L1	Mm03048957_m1
C3	Mm01232779_m1
Serping1	Mm00437835_m1
Gpb2	Mm00494576_g1
Psmb8	Mm00440207_m1
Interleukin-6	Mm00446190_m1

2.3.8 Immunocytochemistry

Cells were rinsed with PBS and then fixed in 4% paraformaldehyde (Sigma) for 20 mins at 4^{o}C. The cells were then rinsed with PBS and then permeabilized in 0.1% Triton-X (Sigma) for 10 mins at 4^{o}C for nuclear and cytoplasmic stains or no permeabilization step was done for surface markers. Cells were blocked with 5% of an appropriate serum (Goat (Sigma) or Donkey (Sigma)) in PBS for 1 hr at 4^{o}C. Primary antibodies were used at the following dilutions: GFAP 1:500 (Thermo Fisher), A2B5 1:25 (DSHB), Aqp4 1:100 (Millipore), Olig2 1:500 (Proteintech), S100ß 1:500 (Proteintech), Glutamate transporter (GLT-1) 1:250 (Millipore), Glutamine synthetase (GS) 1:100 (Proteintech), Aldehyde dehydrogenase L1 1:100 (Millipore), Neurofilament Medium chain 1:25 (DSHB), RIP/CNPase 1:25 (DSHB), O4 1:100 (Millipore), SSEA-1 1:25 (DSHB), CD44 1:250 (Proteintech), Sox2 1:100 (Santa Cruz Biotechnology), Nestin 1:10 (DSHB), Fgfr3 1:100

(Sigma-Aldrich), C3 1:100 (Thermo Fisher), Col1a1 1:100 (Thermo Fisher), Wnt7a 1:100 (Proteintech). Primary antibody incubation was carried out overnight in 2% of appropriate serum in PBS at 4^{o}C. After 24 hr incubation, the cells were rinsed 3 times with PBS. Appropriate Alexa Fluor secondary antibodies (Life Technologies) were all used at a 1:1000 dilution (final concentration of 4 µg/mL) and incubated in 2% of appropriate serum in PBS for 1 hr at 4^{o}C. After the incubation, the cells are rinsed with PBS three times. 1:1000 Hoechst (Thermo Fisher Scientific) in PBS was incubated with the cells for 10 min at 4^{o}C prior to imaging on a Leica DMi8 and Nikon wide-field fluorescence microscope. The image analysis was performed by using Fiji software to count the number of nuclei by DAPI stain and the number of cells stained positive for the above chosen markers[259].

2.3.9 Flow cytometry

Protoplasmic and fibrous astrocytes were removed from the plate surface with 0.25% trypsin-EDTA and fixed using 4% paraformaldehyde for 20 min followed by 10 min incubation at room temperature with 0.1% saponin for nuclear markers. Then, the samples were blocked in 5% normal goat serum (NGS) in PBS for 30 min at room temperature. Primary antibody incubation was performed for 45 min in 2% NGS using the same dilutions as for immunocytochemistry (ICC) for the chosen markers in characterization. Cells were washed twice with PBS and secondary incubation was performed for 45 min prior to washing two times with PBS and cells were resuspended in PBS for runs on Attune NxT cytometer (Thermo Fisher Scientific). For analysis, cell gates were drawn based on forward scatter and side scatter. The gates were drawn based on secondary only and unstained controls to exclude around 99% of control

events from the gates to minimize the false positive rate. Quadrant gates for double stained samples were drawn based on secondary and unstained controls.

2.3.10 Calcium imaging of astrocyte cultures

On day 27 astrocytes, the media was aspirated, and fresh astrocyte subtype media was added with 10 μM Fluo4-AM for 1hour at 37^0C. The astrocyte cultures were then changed to calcium imaging buffer (250 mL water with 2.1 g NaCl, 20 mg $MgSO_4$, 95 mg KCl, 0.45 g sucrose, 90 mg $CaCl_2$, and 0.6 g HEPES at pH 7.4) with addition of 100μM Adenosine triphosphate (ATP) for 30 min incubation. Then, the astrocyte cultures were imaged at 488 nm excitation for 30 seconds at 4Hz using a Leica wide-field microscope. For analyzing the intensity over time, regions of interest (ROIs) were drawn and analyzed with Nikon elements analysis. These fluorescence transients were plotted as $\Delta F/F$ curves for the ROIs with F being the average fluorescence intensity during the 30-second baseline with no ATP[55,260,261]. There are control experiments in which the imaging series were conducted for the same duration without any addition of ATP.

2.3.11 Glutamate uptake assay

Day 27 unselected and selected astrocytes, day 9 V2a interneurons, and mESCs were washed with Hank's balanced salt solution (HBSS) with no calcium and magnesium and then replaced with 200 μM glutamate in HBSS with calcium and magnesium and no phenol red (Thermo Fisher) for incubation of 3 hours at 37^0C. The no cell control was defined as 0.1% gelatin-coated plastic wells containing only 200 μM glutamate solution and no cells. After 3 hours, 20 μl of each sample was added to a new well in a 96-well

plate and the glutamate assay was conducted as per manufacturer's instructions (Sigma-Aldrich MAK004-1KT; Abcam ab83389)[55].

2.3.12 Inflammatory response characterization

Day 27 unselected and selected astrocytes were treated with 30 ng/mL mouse recombinant TNF-α (Peprotech) in the astrocyte phenotypic media for 24 hrs[55]. Untreated and treated astrocyte mRNA were collected by using 0.25% trypsin–EDTA to detach cells, followed by quenching in CM. Cells were pelleted at 300 × *g* and isolated by aspirating medium. The cell pellets were resuspended in RLT buffer as provided from the RNeasy Mini Kit (Qiagen, 74106). Pellets were either frozen at −80°C or immediately used with the RNeasy kit using on-column DNase (Qiagen, 79254) to isolate RNA extracted from cell pellets per manufacturer protocols. The RNA was analyzed with qPCR for common astrocyte reactivity genes: *C3* (Complement C3)*, Serping1* (*S*erpin family G member 1)*, Gbp2* (Guanine nucleotide-binding protein subunit beta-2), and *interleukin-6* (IL-6)[262].

2.3.13 Bulk mRNA-sequencing

Bulk mRNA sequencing was performed on 6 total samples from two replicate experiments for each phenotype before and after selection (four conditions giving 24 total samples). Day 27 unselected and selected astrocytes were trypsinized for 5 min and quenched with CM. The cell suspensions were centrifuged at 300xg for 5 minutes and the supernatant was removed. Cells were lysed in Qiagen RNA Lysis buffer and RNA was extracted using RNeasy Mini Kit (Qiagen, 74106) with concentration calculated by Tecan plate reader instrument. The quality of RNA was assessed by Bioanalyzer or 4200 TapeStation System (High Sensitivity RNA – Agilent, 5067-

5579/5067-5580/5067-5581). Samples with integrity number at 7 or higher and 400-500 ng of samples were used in the Illumina Stranded mRNA Prep, Ligation (Illumina, 20040532) protocol. According to the manufacturer instructions (Illumina), the steps were mRNA isolation, cDNA first and second strand synthesis, adaptor ligation, and 12-13 cycles of library amplification with index adapters (Index adapters (Illumina RNA UD Indexes Set A, Ligation, Illumina, 20091655). Libraries were quantified using the Qubit High Sensitivity dsDNA assay (Thermo Fisher Scientific, Q32851) and quality control (QC) was performed using a 4200 TapeStation High Sensitivity D5000 assay (Agilent, 5067-5592/5067-5593). Libraries were pooled at equal concentration and sequenced on an Illumina NextSeq2000 (75bp paired-end sequencing) with at least 30 million reads per sample.

2.3.14 Bulk mRNA sequencing data analysis of unselected and selected astrocyte phenotypes

Base calls were converted to fastq files using Illumina's BaseSpace DRAGEN Analysis v1.3.0. Data was then imported as fastq files into the Partek Software platform. HISAT2 was the alignment tool used to align the sequencing reads to the *Mus musculu*s mm10 reference genome. The unaligned reads were filtered out with the reads having minimum intron length of 20 bases and maximum of 500,000. Mismatched readings were allowed between 2 and 6 mismatch readings as the penalty range. The aligned reads went through post- quality control demonstrating all samples containing 70-80% of the reads that aligned to the genome with total of 30-50 million reads and close to 2 alignments for each read amongst every sample. The average quality score of the aligned reads was high with an average Phred quality score close to 70. Then, these aligned reads were processed using HTSeq with strand specificity and union overlap

mode parameters to generate gene counts. Batch correction was performed using Partek's general linear model to harmonize the data from the two replicate experiments (performed on different days). Principal component analysis was performed on the normalized data set to demonstrate potential variance between unselected and selected astrocyte phenotypic roles. Differential gene expression analysis was performed using analysis of variance (ANOVA) to produces the list of genes in comparison between the various conditions with false discovery rate (FDR) step-up being <0.05 as the main criteria. A gene enrichment between selected phenotypes was done with the reference database Genetology biological processes (GObp using the enrichplot R package) and Kyoto encyclopedia of genes and genomes (KEGG) pathways.

2.3.15 Statistics

Statistical analysis was performed in GraphPad Prism9. Multiple comparisons statistics were accomplished using Scheffe's post hoc test for one-way ANOVA with a 95% confidence level. Values are reported as the mean plus or minus standard error.

2.4 Results

2.4.1 Generation of selectable cell lines for potential astrocyte phenotypic enrichment[258]

To generate enriched astrocyte cultures, transgenic *Aqp4-PAC* and Olig2-PAC mESC cell lines were used for protoplasmic and fibrous astrocytes respectively. The Aqp4-PAC transgenic mESC cell line was generated using a targeting cassette to insert puromycin N-acetyltransferase (PAC, an enzyme conferring puromycin resistance) into one allele of *aquaporin-4*, an astrocyte-specific gene[258]. The gene regulatory element for *aquaporin-4* (a critical water channel protein for maintaining water homeostasis) was

used to drive PAC expression. Enrichment of protoplasmic astrocytes was possible due to the higher expression of *Aqp4* in protoplasmic versus to fibrous astrocytes[44]. The *Aqp4-PAC* cell line was generated using clustered regularly interspaced short palindromic repeats (CRISPR) with Cas9 endonuclease (CRISPR/Cas9) mediated homology repair to insert the resistance cassette into one of the two *Aqp4* alleles in mESCs (Figure 2.2B)[258]. For purification of fibrous astrocytes, a previously generated transgenic cell line, *Olig2-PAC*, was used in which the puromycin resistance cassette was inserted in the *Olig2* gene locus[51,263]. These cell lines utilize different gene promoters to drive *PAC* expression for enrichment of astrocyte phenotypes.

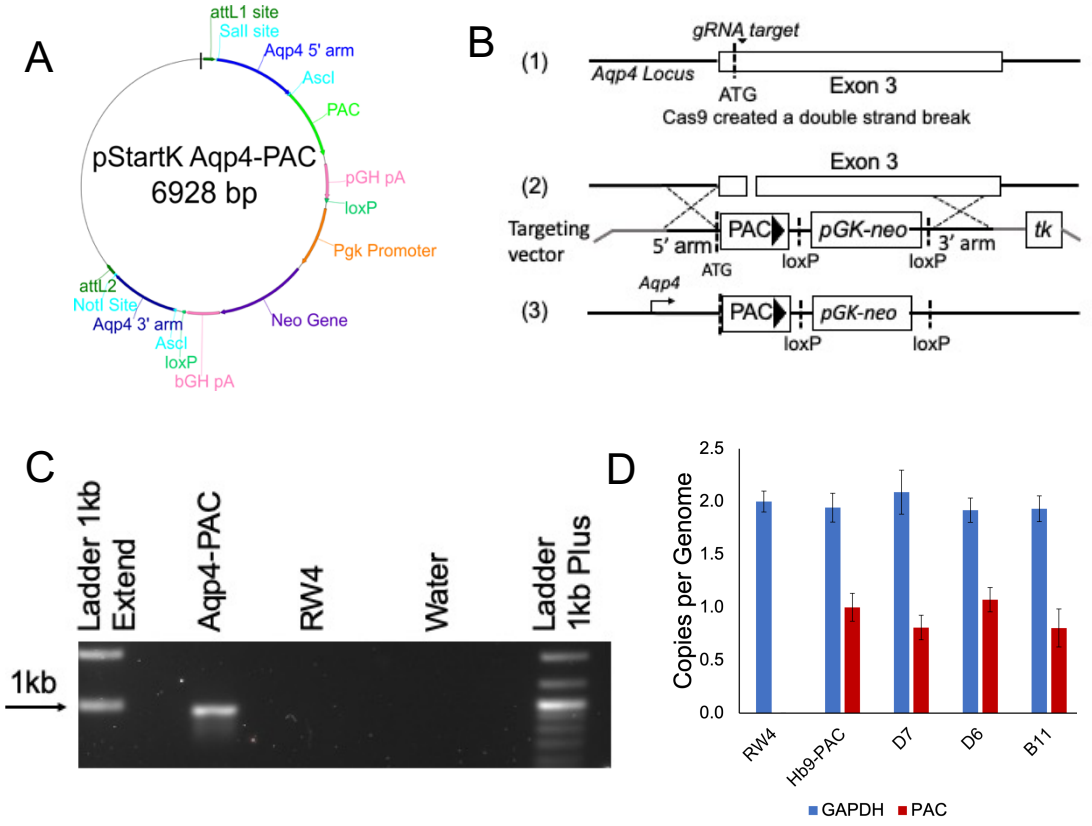

Figure 2.2[258] Generation of Aqp4-PAC mESC line using CRISPR/Cas9 genome engineering A) Plasmid diagram showing the Aqp4-PAC targeting cassette in pStartK plasmid. The plasmid contains PAC/Pgk-neo dual resistance cassette placed in between 2 homology arms for Aqp4 gene[258]. PAC is flanked by homology arms to allow for homologous recombination to occur at the Aqp4 start codon. **B)** Schematic showing PAC insertion in one of two Aqp4 alleles using CRISPR/Cas9 (1) gRNA target Cas9

to the exon 3 of Aqp4 locus and Cas9 creates double-stranded break, (2) Selection cassette in targeting vector aligns near the location of the double-stranded break, (3) Homologous recombination results in the insertion of selection cassette at the appropriate location in the Aqp4 locus **C)** Successful PAC insertion in the Aqp4 locus was confirmed through junction PCR with Aqp4-PAC DNA producing a 920bp band that is absent in the RW4 parental line. **D)** Copy number assay confirms that 1 copy of PAC was inserted in D7, D6 and B11 clones with comparison to a previously generated transgenic cell line, Hb9-PAC. RW4 parental line does not show any PAC inserted and contains 2 copies of GAPDH as an internal reference. Error bars are not S.E.M., but a range of possible copies[258].

The Aqp4-PAC cell line was generated using CRISPR/Cas9 strategy to insert the resistance cassette[258]. The resistance cassette includes the *PAC/Pgk-neo* for positive selection and the vector backbone contains the negative selection marker, thymidine kinase 3, for removing mESC colonies with random non-homology mediated repairs (Fig. 2.2A)[258]. The *PAC* insertion is targeted to the third exon of the Aqp4 gene (Fig. 2.2B)[258]. Surviving colonies from positive (neomycin) and negative (ganciclovir) selection were screened using junction PCR (jPCR) to confirm successful *PAC* insertion in the *Aqp4* locus (Fig. 2.2C). A copy number assay of these two colonies demonstrated that only one *Aqp4* locus was modified with the insertion of the cassette as indicated by one copy of *PAC*[258]. A previously generated Hb9-Puro cell line was used as the positive control for *PAC* insertion in one allele (Fig. 2.2D)[130]. Thus, the Aqp4-PAC cell line was successfully generated with one copy of *PAC* inserted in one *Aqp4* locus[258].

2.4.2 Determination of selection conditions for protoplasmic and fibrous astrocytes

To determine the timepoint for puromycin selection, *Aqp4*, *Olig2*, and *PAC* expression was assessed throughout the phenotypic astrocyte differentiation protocols. Protoplasmic astrocytes demonstrated increased *Aqp4* expression over time with consistent higher *Aqp4* expression in later stages of the differentiation with no significant differences (day 13 and later; Fig. 2.3A)[44,70,264]. However, PAC expression

peaked around day 17, and thus it was chosen as the selection timepoint for protoplasmic astrocyte enrichment. For fibrous astrocytes, *Olig2* and *PAC* expression were consistently high throughout the differentiation (Fig. 2.3B). *Olig2* is expressed in multiple cell types during neural development, thus the timing of selection is critical to enrichment of fibrous astrocytes (Fig. 2.3C). We observed *Olig2* expression in different cell types during the fibrous astrocyte differentiation protocol based on observation of morphology of cells expressing GFP derived from a transgenic Olig2-GFP cell line. Based on morphological observation, we hypothesized that while *Olig2* is expressed in many different CNS cell types during development, fibrous astrocytes were the main cell type contributing to the high *Olig2* expression after day 15 (Fig. 2.3C)[44,54,263,265]. Day 19 was chosen as the timepoint for fibrous astrocyte enrichment due to it being a time that fibrous astrocytes should dominate *Olig2* expression and is before the reseeding step utilized previously[30]. The timing of *Aqp4*, *Olig2*, and *PAC* expressions during astrocyte differentiation led to hypothesized timepoints for puromycin selection.

Next, the concentration and duration of selection was assessed at the timepoints chosen for protoplasmic and fibrous astrocytes derived from Aqp4-PAC and Olig2-PAC respectively. As a starting point, selection with 2 or 4 μg/mL puromycin for 1 day was tested for protoplasmic astrocyte enrichment and 4μg/mL puromycin for 1 or 2 days for fibrous astrocytes. The viability was assessed using live/dead cytotoxicity assay with calcein-AM (live cell stain) and ethidium homodimer (dead cell stain). 4μg/mL was only tested for fibrous astrocytes due to being qualitatively proliferative, leading to potentially higher puromycin concentration and longer exposure being necessary to reduce cells. It was observed that 2 μg/mL and 4μg/mL puromycin 1 day significantly reduced the

number of live cells in the selected protoplasmic cultures (123 ± 9) compared to unselected (379 ±19) (Fig. 2.3D). However, very few cells in selected protoplasmic astrocyte cultures were left after 4µg/mL and the morphology was affected, making the cells (protoplasmic astrocytes) potentially hard to proliferate after (Supplemental Fig. 2.1). Furthermore, puromycin concentrations were added for 2 days to protoplasmic astrocytes and resulted in cell death with remaining viable cells having no protoplasmic morphology (Supplemental Fig. 2.1B). Thus, 2µg/mL for 1 day was chosen as the criteria for protoplasmic enrichment. For fibrous astrocytes, the 4 µg/mL puromycin for 2 days significantly reduced the number of live cells (unselected 1054 ± 269 to selected 352 ± 76), indicating this to be a potential condition for fibrous astrocyte selection (Fig. 2.3E**)**. The selection criteria decided produced significant decreases in the number of live cells after puromycin exposure.

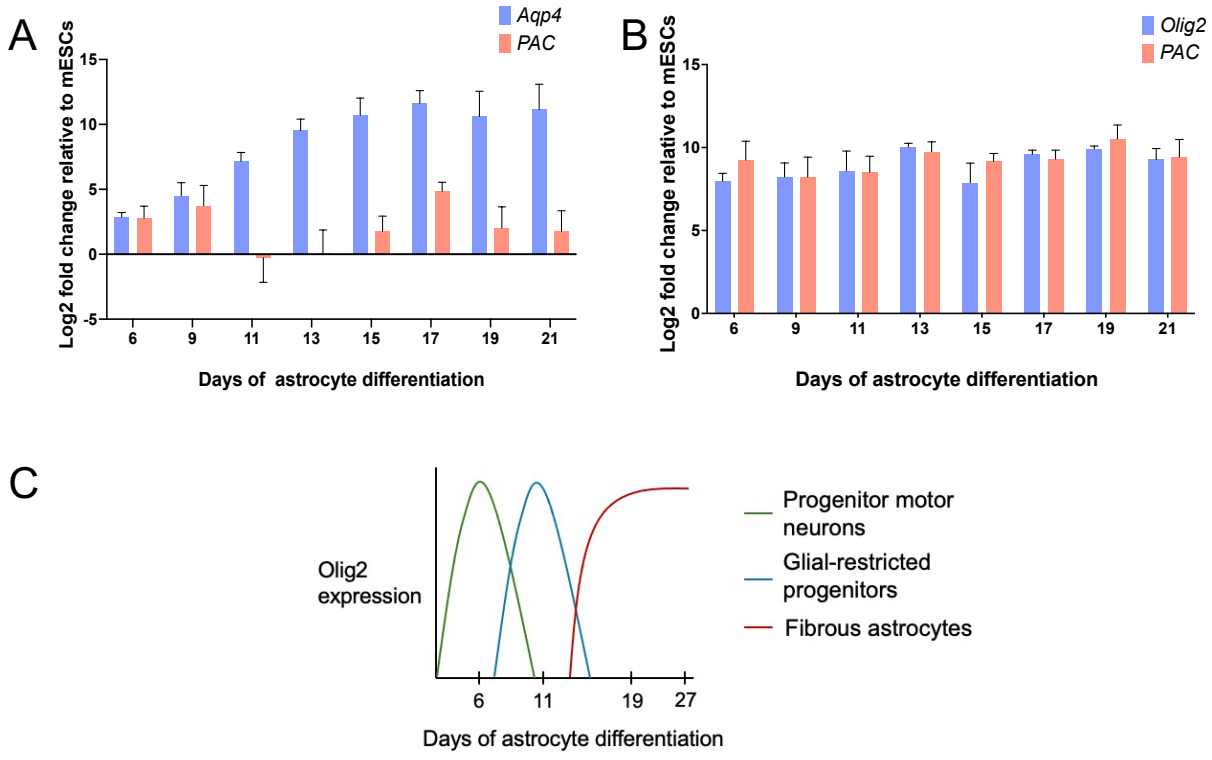

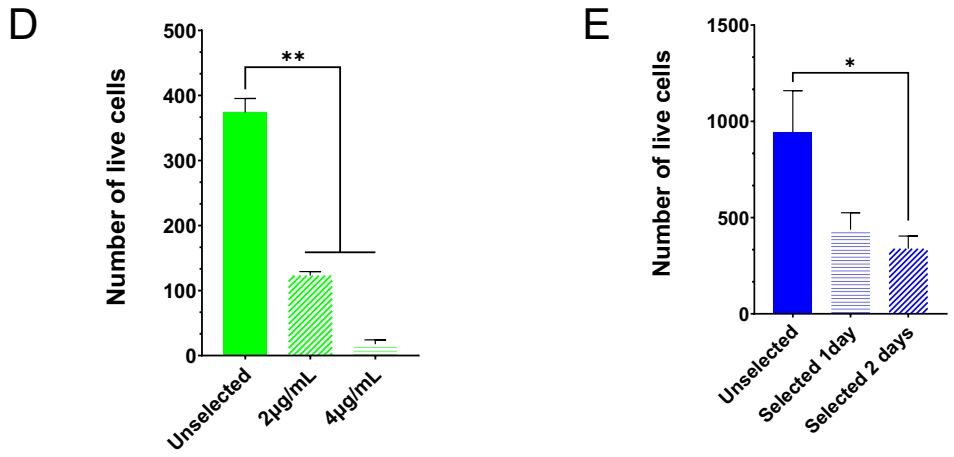

Figure 2.3 Puromycin addition to protoplasmic and fibrous astrocytes for reduction of cells was dependent on Aqp4, Olig2, and PAC levels throughout differentiation A) Expression of Aqp4 and PAC in Aqp4-PAC cell line during protoplasmic differentiation protocol (N=3, error bars= S.E.M.). **B)** Expression of Olig2 and PAC in Olig2-PAC cell line during the fibrous differentiation protocol (N=3, error bars= S.E.M.). **C)** Schematic diagram that demonstrates our hypothesis that Olig2 is expressed by different cell types during the astrocyte differentiation protocol. **D)** Selection of protoplasmic astrocytes with 2 and 4µg/mL puromycin for 1 day **(**N=2-6, error bars= S.E.M, ** p<0.01.)**. E)** Selection of fibrous astrocytes with 4µg/mL puromycin for 1 or 2 days **(**N=2-6, error bars= S.E.M, ** p<0.01.).

2.4.3 Evaluating enrichment of astrocyte phenotypes cultures post selection

To determine the effects of puromycin selection on astrocyte morphology and cellular composition post reduction of cells, ICC was utilized. The varied broad-star shape morphology of protoplasmic astrocytes and thin, elongated fibrillar structures of fibrous astrocytes was not drastically affected by puromycin selection (Fig. 2.4A-D). Protoplasmic astrocytes are characterized as $Aqp4^{+}/A2B5^{-}$ and fibrous astrocytes as $Aqp4^{+}/A2B5^{+}$. Aqp4 is a water channel membrane protein common in mature astrocytes with protoplasmic astrocytes more positive for Aqp4 than fibrous astrocytes[44,266]. The protoplasmic and fibrous astrocytes post selection demonstrated significant increases in the fraction of cells staining positive for Aqp4 (0.77 ± 0.02 and 0.66± 0.03 respectively) compared to unselected cultures (0.43 ± 0.03 and 0.50 ± 0.04) by ICC (Supplemental Fig. 2.2). Selected fibrous astrocytes also had a significantly increased fraction of cells

staining positive for A2B5, a cell surface ganglioside marker, (0.62 ± 0.05) compared to unselected fibrous cultures (0.79 ± 0.04) (Supplemental Fig. 2.2)[267]. A2B5 is present in glial precursors as well as developing white matter astrocytes and thus is used as a defining marker for fibrous astrocytes[268,269]. Furthermore, flow cytometry demonstrated a significant increase in fraction positive for Aqp4 post-selection in both astrocyte subtypes and significant higher fraction of cells positive for A2B5 significantly higher in $Olig2^+$ fibrous compared to protoplasmic astrocytes (Fig. 2.4E). In addition, significant fractions of cells positive for Olig2 and S100β (a calcium binding protein) in fibrous compared to protoplasmic astrocytes (Fig. 2.4E)[270,271]. S100β is a complex marker being expressed by Schwann cells, oligodendrocytes, and astrocytes[87,88]. With the low fraction of cells positive for RIP, a mature oligodendrocyte marker, in astrocyte cultures, $S100\beta^+$ cells characterize astrocytes. ICC also demonstrated that fraction of cells positive for Olig2 was significantly increased in selected fibrous astrocytes (0.74 ± 0.04) compared to unselected fibrous astrocytes (0.54 ± 0.06) and low number of Olig2-positive cells in protoplasmic astrocytes (0.08 ±0.03 and 0.06 ±0.02 respectively) (Supplemental Fig. 2.2)[44,54,265]. Furthermore, there were low fractions of cells positive for mature neurons (NFM), oligodendrocytes (RIP), and undifferentiated stem cells (SSEA-1) in selected astrocyte phenotypic cultures (Supplemental Fig. 2.2; Fig. 2.4E)[270–273]. ICC demonstrated significant decreases in fraction of undifferentiated stem cells in selected astrocyte phenotypic cultures as stained by SSEA-1 (Supplemental Fig. 2.2; 0.16 ± 0.03 to 0.05 ± 0.01 for fibrous and 0.08 ± 0.02 to 0.02 ± 0.01 for protoplasmic)[271]. Overall, selection maintains low fraction of other cell types, but does

not eliminate, in selected astrocyte cultures and enriches defining fibrous and protoplasmic astrocyte markers.

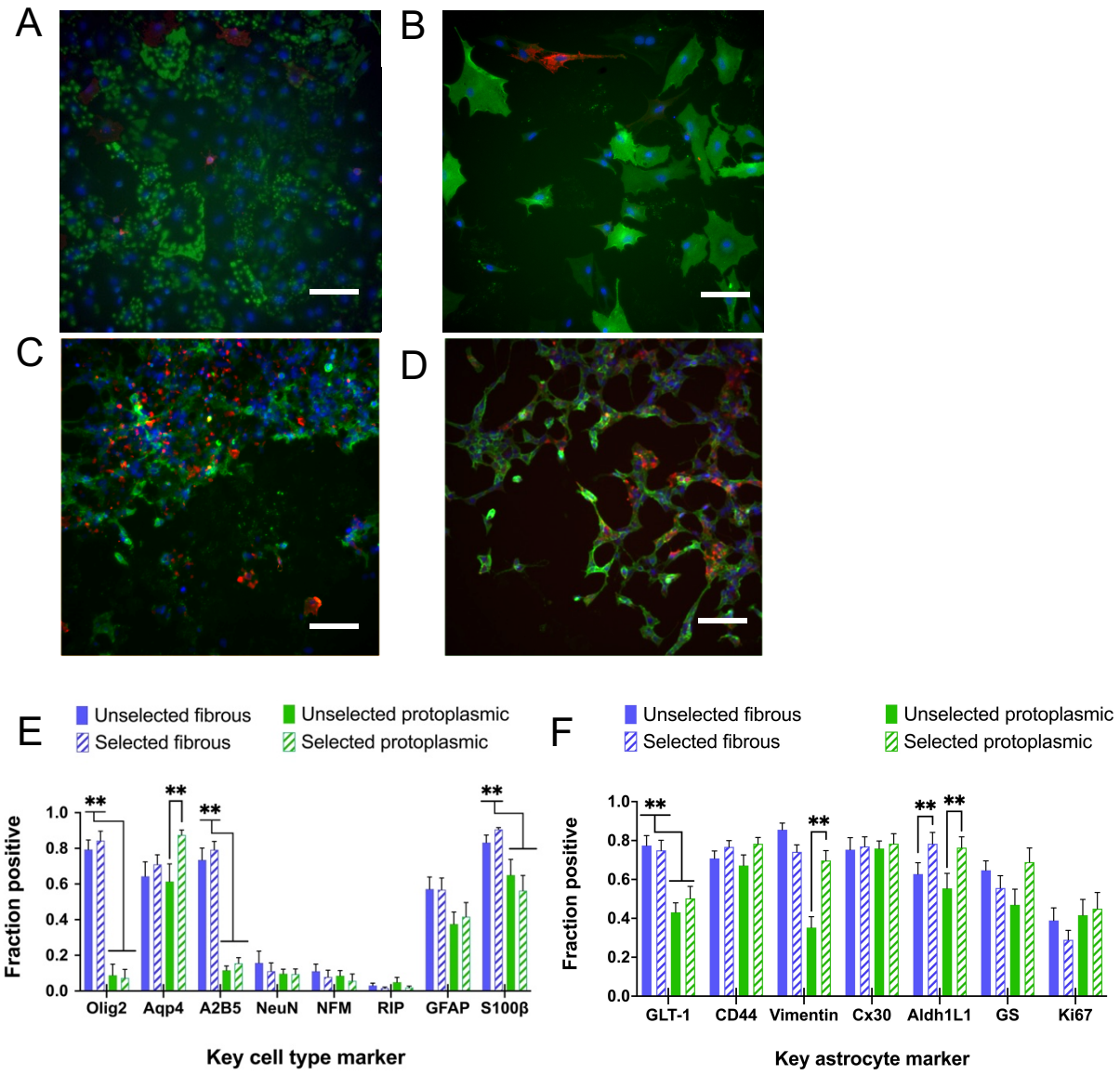

Figure 2.4 Puromycin selection enriches the fraction of cells positive for astrocytic markers and results in a low fraction of cells positive for other cell types A, B) Aqp4, A2B5 ICC staining for day 21 unselected and selected protoplasmic astrocytes with showing characteristic high Aqp4 (green) and low A2B5 (red) staining for protoplasmic astrocytes (Scale bar= 100μm). Hoechst stain (blue) is for nuclei. **C, D)** Aqp4, A2B5 phenotypic ICC staining for day 23 unselected and selected fibrous astrocytes with showing characteristic high Aqp4 (green) and A2B5 (red) staining for fibrous astrocytes (Scale bar= 100μm). **E)** Flow cytometry analysis for fractions positive of astrocyte subtype, mature neuron, and mature oligodendrocyte markers in unselected and selected astrocyte cultures 4 days after puromycin addition; **p<0.01 (N=3-10; Error bars= S.E.M.). **F)** ICC imaging analysis of astrocytic markers in

unselected and selected astrocyte cultures with staining 4 days after puromycin addition. *p<0.05, **p<0.01 compared to respective unselected astrocyte phenotypes (N=4, Error bars= S.E.M.).

Furthermore, ICC was performed with astrocyte general markers to characterize maturity states of astrocyte phenotypic cultures. High fraction of cells in unselected and selected astrocyte cultures are positive for glial fibrillary acidic protein (GFAP), a common astrocyte marker, and S100β with being >0.6 fraction positive in fibrous astrocytes (Fig. 2.4F)[28,249,274]. S100β$^+$ and GFAP$^+$ cells in Olig2$^+$ fibrous astrocytes support the characterization of white matter astrocytes[85,268]. Specifically, there were significantly higher fractions of cells positive for glutamate transporter-1 (GLT-1) in fibrous astrocytes compared to protoplasmic, supporting GLT-1 positivity higher in white matter astrocytes and suggesting increased glutamate activity in the fibrous astrocytes (Fig. 2.4F)[263]. Selected astrocyte cultures showed a significantly increased fraction positive for astrocyte marker aldehyde dehydrogenase-L1 (Aldh1L1), demonstrating astrocyte enrichment (0.60 ± 0.05 to 0.78 ± 0.06 for fibrous and 0.55±0.08 to 0.76±0.06 for protoplasmic) (Fig. 2.4F)[275]. Lastly, high fractions of cells in astrocyte cultures were positive for connexin-30 (Cx30; an astrocytic gap junction protein), CD44 (a surface receptor commonly found on astrocyte precursor cells) and vimentin (an intermediate filament found more in immature white matter astrocytes)[58-60]. This indicates that unselected and selected astrocyte cultures are a mixture of mature and immature astrocytes present in culture. were all present at high levels in unselected and selected astrocyte cultures.

2.4.5 Assessing the functionality of selected astrocyte phenotypes

Previously, our lab investigated the effects of day 27 astrocyte subtypes on axon growth. Thus, we wanted to determine astrocyte functionality for neuron support using

unselected and selected day 27 astrocyte subtypes. For basic characterization, qPCR confirmed that the day 27 fibrous astrocytes had a significantly higher *Olig2* mRNA expression level compared to protoplasmic and protoplasmic astrocytes had a significantly higher *Aqp4* mRNA expression level compared to fibrous (Supplemental Fig. 2.3). The mRNA expressions of neuronal and oligodendrocyte genes *Nefm* and *Cnp* respectively were low (Supplemental Fig. 2.3). This indicates that the selected astrocyte phenotypes highly express astrocyte phenotypic genes with low levels of genes indicative of other cell types at later time point of day 27.

A key function of astrocytes is their ability to respond to pro-inflammatory cues and demonstrate activation. The unselected and selected astrocytes phenotypic cultures were exposed to 30µg/mL TNFα in phenotypic media at day 27 for 24 hrs. The pro-inflammatory state was characterized by using qPCR to measure *Complement 3 (C3), proteasome subunit β type-8 (Psbm8), guanylate-binding protein (Gpb2), C1 inhibitor (Serping1),* and *interleukin-6* (*IL-6)* mRNA expression levels*.* Fibrous astrocytes respond to TNF-α stimulation with significantly increased *C3, Il-6, Psbm8*, and *Gbp2* mRNA levels, indicating these astrocytes are pro-inflammatory and reactive post stimulation (Fig. 2.5 A, B). Furthermore, the TNFα stimulation was able to significantly increase *Psbm8* and *IL-6* mRNA levels in protoplasmic astrocytes *in vitro* (Fig. 2.5A, B). The activation of astrocytes by pro-inflammatory cytokines can be useful for studying the effects of reactive astrocytes on axon growth with potentially elucidating characteristics of neurorepair and neurotoxic reactive astrocytes.

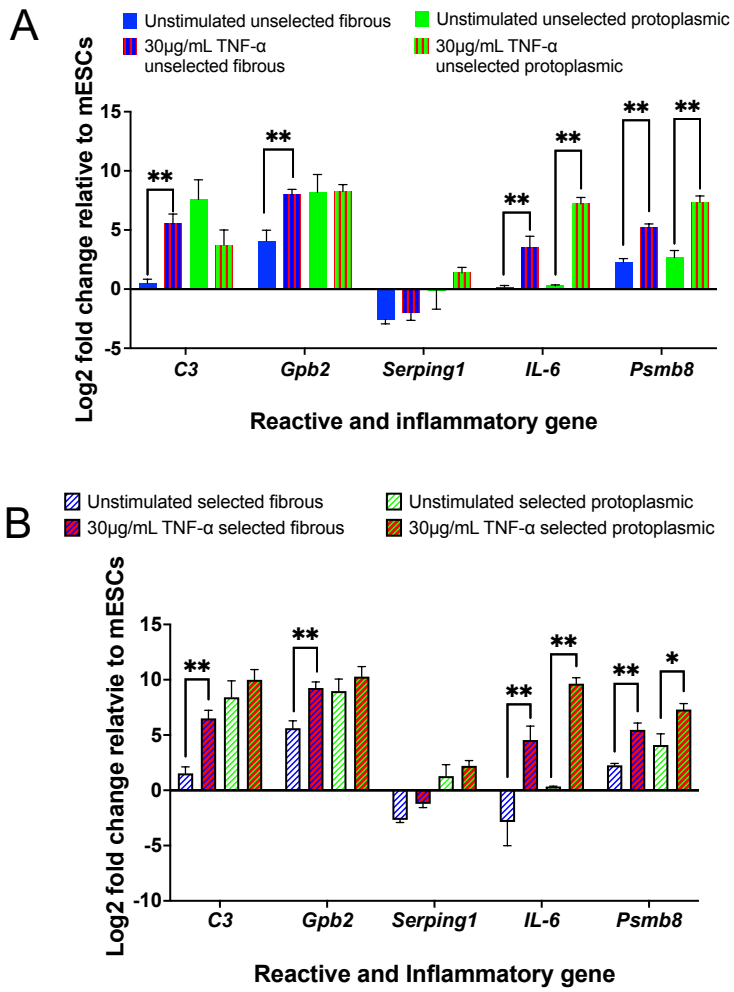

Figure 2.5 Astrocyte subtype cultures respond to inflammatory stimulus post puromycin selection **A)** qPCR analysis of astrocyte reactivity (C3, Psbm8, Gbp2, and Serping1) and pro-inflammatory (Il-6) gene markers in unselected astrocyte phenotypes with and without 30 ng/mL TNF-α stimulation and shows that certain reactivity genes are upregulated post inflammatory stimulation (N=3-6; * $p<0.05$, ** $p<0.01$; Error bars =SEM). **B)** qPCR analysis of astrocyte reactivity (C3, Psbm8, Gbp2, and Serping1) and pro-inflammatory (Il-6) gene markers in selected astrocyte phenotypes with and without 30 ng/mL TNF-α stimulation and shows that certain reactivity genes are upregulated post inflammatory stimulation (N=3-6; * $p<0.05$, ** $p<0.01$; Error bars =SEM).

A glutamate uptake assay was conducted for unselected and selected astrocyte cultures as a measure of astrocyte functionality. Glutamate uptake by astrocytes occurs through glutamate transporters (such as GLT-1) and aids in preventing excitotoxicity[276]. The glutamate uptake fraction in the astrocyte groups were calculated with comparison to the initial concentration 200µM glutamate (Supplemental Figure 2.4). For the ongoing glutamate assay studies, two kits were utilized based on the same exact reaction due to

the previously used Sigma-Aldrich kit being recently discontinued. Thus, only few replicates have been conducted with the Abcam kit and future studies of more replicates of astrocyte subtypes will need to be conducted using the Abcam kit. With the Sigma-Aldrich kit, it can be observed that astrocytes post selection demonstrate glutamate uptake similar to unselected astrocytes, indicating selected astrocytes are not affected in this function by puromycin exposure (Supplemental Figure 2.4A). This could be attributed to the presence of GLT-1 positive cells found in the unselected and selected astrocyte cultures. However, day 9 V2a interneurons (2 days on laminin) did not seem to have glutamate uptake activity as well as Olig2-PAC mESCs (seems to release more glutamate than uptake). Similar trends of glutamate uptake were noticed with the Abcam kit (Supplemental Figure 2.4B). An exception is the selected protoplasmic astrocytes have a lower glutamate uptake similar to that of the day 9 V2a interneurons, compared to the fibrous and unselected protoplasmic astrocytes. This could be due to only one biological replicate of astrocytes being conducted with the Abcam kit, while three biological replicates were completed for the day 9 V2a interneurons and mESCs. It is also important to note that the no cell control demonstrates some amount of glutamate uptake and thus was accounted in the uptake fraction for astrocytes, neurons, and stem cells.

Calcium flux, visualized with Fluo4-AM, by astrocytes has been one of general mechanisms in supporting neuron and synaptic transmission and astrocytes demonstrating calcium transients are thus considered functional[65,66]. Unselected and selected astrocyte phenotypes at day 27 demonstrate calcium transients as shown by $\Delta F/F$ (changes in fluorescence intensity normalized to average fluorescence intensity for

the time period) over time, indicating astrocyte functionality (Supplemental Fig. 2.5). These could be characterized as global calcium waves traveling through the ROI (entire astrocyte including soma) with identified increases and decreases in fluorescence intensity (Supplemental Fig. 2.5C)[278,279]. The increases and peaks occur at different times most likely due to the various morphology differences between astrocyte subtypes[260]. With average calcium transients calculated in various astrocyte groups, selected astrocyte phenotypes have peaks in calcium transients later in the duration of time than unselected (Supplemental Fig. 2.5D). In addition, change of fluorescence intensity decreased over time with no ATP stimulation to astrocytes with fibrous demonstrating more clear transients, indicating presence of baseline calcium transients that might not be sustained without ATP addition (Supplemental Fig. 2.5E). Overall, the selected astrocyte phenotypes are functional with generating calcium transients.

2.4.6 Characterizing the global gene expression of selected astrocyte cultures

We wanted to understand the effects of puromycin selection on differences in gene target expressions between selected astrocyte subtypes for neuron support and axon growth using bulk RNA sequencing. Unselected and selected astrocyte cultures were assessed by bulk RNA sequencing at a later time point post puromycin exposure, day 27, to characterize patterns of gene expressions across conditions. Dimension reduction by principal component analysis demonstrated that condition-to-condition differences in the overall gene expression patterns were a primary source of variation in the data (Fig. 2.6A). The two phenotypes before and after selection were largely separated by a combination of the first two PCs, which captured >45% of variation in the

data combined (Fig. 2.6A). Unselected and selected fibrous astrocytes were clustered close to each other due to *Olig2*, the selection marker for fibrous astrocytes, being highly expressed. However, unselected and selected protoplasmic astrocytes were separated more by PC2 and this could be attributed to Aqp4 being the selection marker for this subtype. Thus, the PCA analysis is important in demonstrating variance between unselected and selected astrocyte subtypes.

Significantly different gene expressions between selected astrocyte phenotypes were identified by ANOVA with a false discovery rate (FDR) <0.05. 1105 genes were upregulated in selected protoplasmic astrocytes and 253 upregulated genes in selected fibrous astrocytes (Fig. 2.6B; Supplemental Table 2.2). Critical genes upregulated in selected protoplasmic astrocytes were extracellular matrix protein genes, *Col6a1* and *Col6a2,* immune-regulation, neuroprotective genes, *Ccn3* and *Cxcl10,* and axon growth-related genes, *Ngf* (encodes for nerve growth factor) and *Snai2* (Fig. 2.6B)[280,281–283]. Also, there are 3 main reactive astrocyte genes upregulated in selected protoplasmic astrocytes, *C3, Igfbp5,* and *Tagln*[281,282]*.* Critical genes upregulated in selected fibrous astrocytes are *Neto1* and *Slc6a11*, genes involved in synaptic scaffolding and astrocyte metabolism studies[284,285]. These differential gene markers can be potential targets for characterizing functions between selected protoplasmic and fibrous astrocytes.

Additionally, we constructed a bubble heatmap to visualize the presence of astrocyte genes and decreases of other cell type genes with comparison between unselected and selected astrocyte phenotypes (Fig. 2.6C). *Vim, Aqp4,* and *Cd44* were upregulated in Z-score for selected protoplasmic astrocytes compared to unselected

protoplasmic astrocyte and fibrous astrocytes, supporting *Aqp4* being the selection marker to enrich protoplasmic astrocytes. *Fut4* (gene encoding for undifferentiated stem cells), *Gfap*, and *S100b* were decreased in Z-score for selected protoplasmic astrocytes from unselected protoplasmic astrocytes with these genes having low presence in fibrous astrocytes. *Nefm* was not present in selected astrocytes with high Z-score in unselected fibrous astrocytes only. *Olig2, Slc1a3, Slc1a2, Glul,* and *Ki67* were highly present in fibrous astrocytes compared to protoplasmic. Overall, the changes in astrocyte subtype and other cell type genes support astrocyte enrichment.

To identify gene targets for axon regeneration, genes with fold change above 1 that are differentially expressed between selected protoplasmic to selected fibrous astrocytes (upregulated in selected protoplasmic) and genes with fold change below 1 differentially expressed (upregulated in selected fibrous astrocytes) were analyzed through pathway enrichment analysis with *Mus musculus* database as reference. The Gene Ontology biological process (GObp) database was utilized to determine what gene pathways were significantly enriched in astrocyte phenotypic cultures. Using the enrich plot visualization tool, the selected protoplasmic astrocytes express 40-50 genes that are significantly enriched ($p=1^{-10}$ to 2^{-10}) in cell-substrate adhesion, cell-cell adhesion, regulation of inflammatory responses, extracellular matrix (ECM) organization, and collagen metabolic process that could affect interactions with neurons (Fig. 2.6D). The selected fibrous astrocytes expressed 20-30 genes that are significantly enriched (p-value= 1^{-56}) in regulation of gliogenesis, regulation of Wnt signaling, synaptic vesicle mediated transport, and synapse organization (Fig. 2.6E). These gene

expressions could drive differentiation and synapse formation support by fibrous astrocytes. There are identified key genes that might have an impact on axon growth of neuron populations by astrocyte subtypes.

A

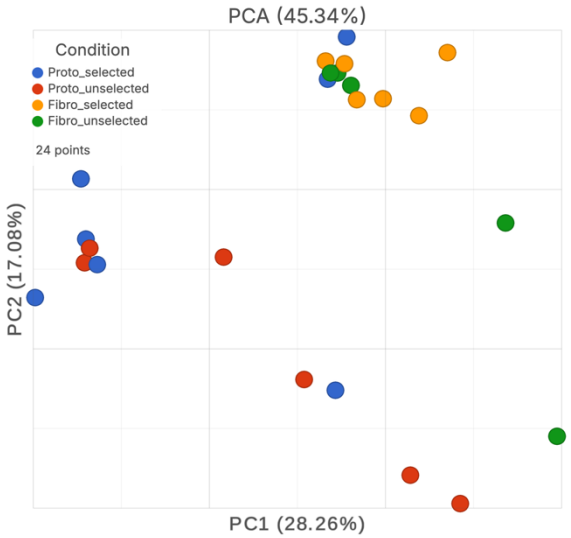

B

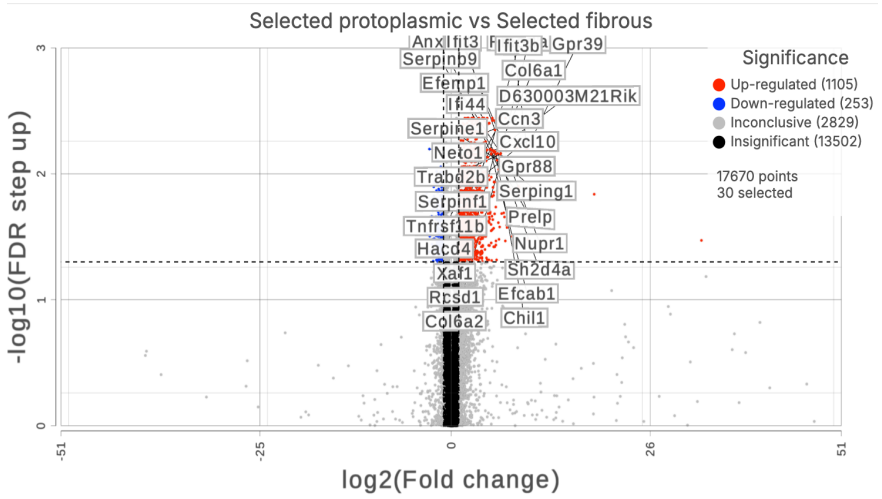

C

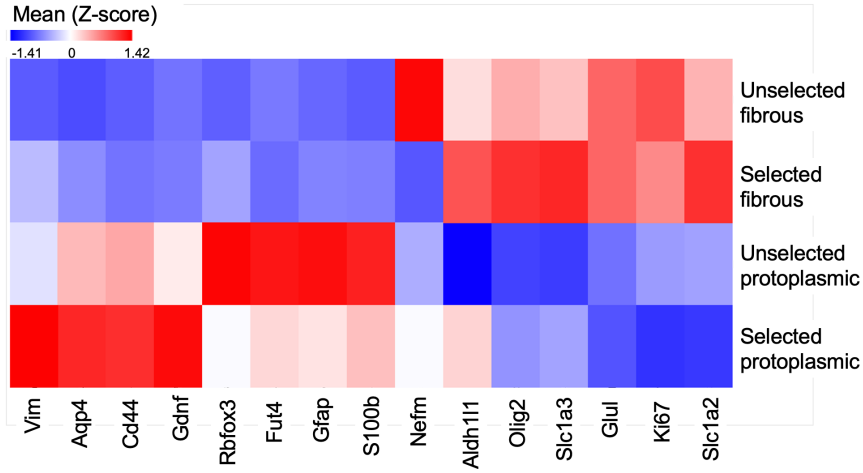

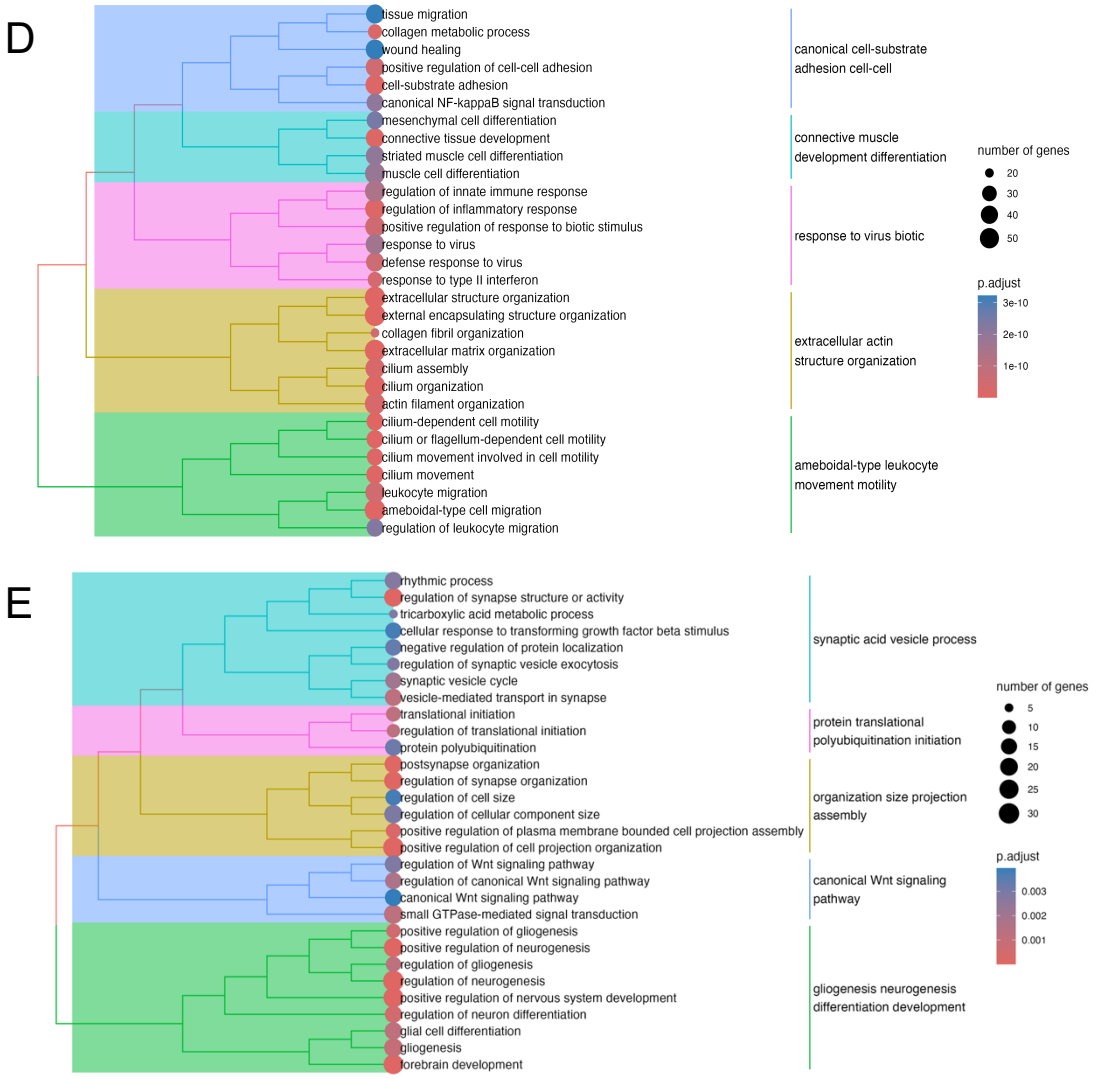

Figure 2.6 Bulk RNA-sequencing of unselected and selected astrocyte phenotypes demonstrate key differential genes and pathways that can be potential targets for future studies of understanding astrocyte phenotypic functions. A) Principal component analysis of all the astrocyte samples demonstrating the variance mostly separates the unselected and selected for protoplasmic astrocytes and less variance existed between unselected and selected fibrous astrocytes. **B)** The volcano plot of differential genes in selected protoplasmic astrocytes compared to selected fibrous astrocytes shows certain genes are upregulated and downregulated in selected and protoplasmic astrocytes with an FDR step-up below significance level of 0.05 with a few genes highlighted in each phenotype. **C)** Heatmap of the specific genes of astrocyte phenotype and other cell type markers used in ICC observed at Figure 3 demonstrated that there were low Z-scores (indicated by blue) for other cell type markers in the selected astrocyte phenotypes with different key astrocyte genes present at high Z-scores (indicated by red) in each selected astrocyte phenotype. **D)** Gobp analysis of upregulated genes expressed at fold change greater than 1 in selected protoplasmic astrocytes compared to selected fibrous astrocytes demonstrated that pathways related to cell-substrate adhesion, collagen metabolic process, and ECM organization are significantly upregulated by the color for p-value and the size of the bubble representing a few genes. **E)** Gobp analysis of upregulated genes expressed at fold change greater than 1 in selected fibrous astrocytes compared to selected protoplasmic astrocytes demonstrated that pathways related to positive regulation for cell cycle, translation at synapses, and spindle organization are upregulated.

2.5 Discussion

Our goal was to reduce other cell types and enrich astrocyte phenotypes in mixed cultures derived from mESCs by using puromycin selectable transgenic cell lines. ICC and flow cytometry demonstrated a low level of undifferentiated stem cells, mature neurons, and mature oligodendrocytes in the selected astrocyte cultures. There are observed cells positive for mature and immature astrocyte markers present in the selected astrocyte cultures, indicating that the astrocytes are on a spectrum of maturity states[21,286]. Aldh1L1 is expressed in both $GFAP^+$ and $GFAP^-$ astrocytes in grey and white matter and was found in both selected fibrous and protoplasmic astrocyte cultures[287]. Both astrocyte subtypes were positive for Cx30 and GLT-1, indicating maturity[288,289]. More cells in selected fibrous astrocyte cultures were positive for S100β compared to protoplasmic astrocytes, which aligns with S100β expression being higher in white matter glia[290]. This effect could be further attributed to Olig2 being the selection marker for fibrous astrocyte enrichment. The high fraction of cells in both unselected and selected astrocyte subtypes positive for CD44 and vimentin demonstrates presence of immature astrocytes[291]. Specifically, high fraction of cells positive for Olig2, A2B5, CD44, and S100β can indicate presence of immature astrocytes in the O-2A lineage for fibrous astrocyte cultures pre- and post-selection[54]. While the selected astrocyte cultures contain a mixture of immature and mature astrocytes, the puromycin selection can aid in astrocyte enrichment based on Aqp4 and A2B5 staining[44]. Furthermore, it is crucial to highlight that the puromycin selection did not eliminate other cell types even though there are high fractions of cells positive for astrocyte markers. Overall, we have enriched protoplasmic and fibrous astrocytes from Aqp4-PAC and Olig2-PAC cell lines, respectively.

The inflammatory and reactivity response of selected astrocyte cultures suggests that these astrocytes can be used with *in vitro* studies of neuroinflammation. Selected astrocyte subtypes are activated with TNF-α stimulation as observed with increases in mostly with *Psbm8 and Il-6*. Protoplasmic astrocytes contained higher *C3* presence compared to fibrous astrocytes, and this was corroborated by the RNA-sequencing data. The increases of *C3* might be properties of beneficial reactive astrocytes that might impact axon growth[72,73,292]. Furthermore, bulk RNA-sequencing of selected protoplasmic astrocytes demonstrated significant presence of both general neurotoxic (*Igfbp5, Tagln, C3*) genes and neuroprotective genes *(S100a6, Ccn3, Cxcl10, Igfbp7)* when compared to fibrous astrocyte cultures (Supplemental Table 2.1). This indicates selected protoplasmic astrocytes potentially having neurorepair properties of beneficial reactive astros. In addition, immune regulatory genes, *H2ax, Serpine1,* toll-like receptors *Tlr2* and *3*, *Casp1* and *8,* cytokine *Ccl2,* and *H2-Dmb1,* were present in selected protoplasmic astrocytes. Furthermore, different inflammatory factors apart from TNFα could be used to stimulate varied inflammatory responses and reactivity for each subtype[40]. Thus, these selected astrocyte subtypes can be an *in vitro* cellular platform for mimicking the neuroprotective roles of reactive astrocytes involving inflammatory and immune pathways post SCI.

The selected astrocyte cultures demonstrate glutamate uptake as a potential function for neuron support. The importance of glutamate uptake by astrocytes is to prevent excitotoxicity for neurons. The high fraction of cells positive for GLT-1 in the astrocyte cultures can potentially play a role in glutamate uptake. Altering the GLT-1 positivity in selected astrocyte cultures might affect neuron survival and be an *in vitro*

cell culture platform for studying neuron-astrocyte interactions. Furthermore, it would be useful to conduct further studies of glutamate uptake on different time points of V2a interneurons from day 9 to more mature time points with help of astrocyte conditioned medium to culture the neurons to 1-week and 2-week time points. It is potentially possible that V2a interneurons at later time points could have increased glutamate uptake. In addition, other coatings of plastic wells could be tested to determine potential reduction of glutamate uptake as close to zero in the no cell control. Also, due to the complication of the discontinued Sigma Aldrich kit, more glutamate uptake studies of astrocytes with the Abcam kit will need to be conducted for better and complete understanding of the glutamate uptake of selected astrocyte subtypes.

It was observed that the astrocyte calcium transients are slower during the 30-second duration compared to more active transients in neurons *in vivo*[293]. Calcium transients in neurons demonstrate sharp increase and decrease for calcium peaks compared steady increase and decrease for calcium transients in astrocytes[294,295]. This indicates our observed calcium transients are similar to that observed in astrocytes *in vivo* and *in vitro* with selected astrocytes potentially having low presence of neurons[296]. In addition, based on the waveforms, it seems that these astrocyte ROIs can be considered as either attached or isolated as types of potential contact with neighboring astrocytes[279,297,298]. While calcium transients were observed in selected astrocyte phenotypes, the changes as $\Delta F/F$ are quite low in percentage and could be characterized as noise. This is most likely due to collecting calcium imaging videos 30 minutes after ATP addition for only a short time interval of 30 seconds compared to immediately upon ATP exposure for longer times as in some previous studies[55,96].

Furthermore, the low ΔF/F values could be due to the 1hr incubation of Fluo-4 AM and thus different incubation times of 5 min and 15 minutes should be tested with imaging series obtained for duration of 3 minutes to verify the use of 1 hour incubation. There would be higher fluorescence signal with the application of GCaMP (genetically encoded calcium indicator) under GFAP promoter as the calcium indicator in transfection of astrocytes and specifically target to observe calcium transients in astrocytes. This could be another approach for achieving a higher ΔF/F in astrocytes. In addition, these waveforms for calcium transients in the astrocytes could be due to the ROI used being around a whole single astrocyte rather than focusing on smaller ROIs around the soma as observed with global transients[295,299]. Thus, there is more to study about the calcium transients displayed by unselected and selected astrocytes.

A key type of potential astrocyte-specific axon-growth permissive cue identified from bulk RNA-sequencing is ECM. There were numerous genes related to ECM-receptor interactions, cell adhesion and ECM remodeling upregulated in selected protoplasmic astrocytes. Specifically, *Col1a1, Col4a1,* and *Col6a1* were upregulated in selected protoplasmic astrocytes while the low number of cells were positive for Col1a1 and significantly higher number of cells were positive for Col4a1 in selected protoplasmic astrocytes (Supplemental Fig. 2.5)[300]. Furthermore, *MMP2* was more significantly present in selected protoplasmic astrocytes than selected fibrous[78]. This indicates that selected protoplasmic astrocytes could be a more neurorepair subtype and the ECM should be investigated for effects on axon growth of different neuron populations. The interactions between selected protoplasmic astrocyte ECM proteins and neural receptors can be important for supporting axon growth. Interestingly, genes

related to various key signaling pathways, such as Wnt, and synaptic vesicle exocytosis, were upregulated in selected fibrous astrocytes, suggesting potential implications in supporting astrocyte-neuron communication. *Wnt7a,* a critical gene in mTOR, Wnt, and Hippo signaling pathways that helps in blood-brain barrier maintenance, was upregulated in selected fibrous astrocytes with significant protein expression as well (Supplemental Fig. 2.5)[294,301]. These selected fibrous astrocytes can be a cellular platform for studying support of white matter neuron interactions *in vitro.* Overall, the selected astrocyte phenotypes post- puromycin selection proves to be instrumental *in vitro* cellular platforms for studying astrocyte specific function and gene and protein targets important for axon regeneration.

2.6 Conclusions

The study has shown successful generation of a selectable transgenic mESC cell line to enrich protoplasmic astrocytes *in vitro*[258]. This work has characterized the effects of puromycin selection on astrocyte phenotypes. The selection criteria reduced other cell types with a high fraction of cells positive for astrocyte marker expression in enriched astrocyte cultures. In addition, the selected astrocyte phenotypes demonstrate calcium transient activity, glutamate uptake, and response to inflammatory stimuli, indicating functionality post selection. However, it is important to recognize the limitations of the cell lines in astrocyte enrichment. Selection of fibrous astrocytes with Olig2-PAC cell line can result in low numbers of oligodendrocytes and neurons due to *Olig2* expression in these other cell types. The selectable cell lines and puromycin addition does not eliminate other cell types but reduces the levels to a very low amount. This can allow for astrocyte enrichment with functional attributes.

The sequencing data can serve as an important resource for identifying genes in axon guidance and ECM-receptor pathways with astrocyte phenotypic differences. This can influence future studies for investigating the potentially important cues of selected protoplasmic astrocytes that support axon regeneration. Finally, these enriched astrocyte phenotypes are not designed for clinical, translational and ideally would serve as an investigative platform for examining astrocyte phenotypic differences supporting neuron populations. These neuron protective astrocyte cues, such as ECM proteins, can be incorporated in biomaterial scaffolds as potential SCI therapies *in vitro* and *in vivo*[60].

Chapter 3: Investigation of astrocyte phenotypic components and extracellular matrix proteins on supporting axon growth of V2a interneurons *in vitro*

3.1 Abstract

Astrocytes are essential regulators of the extracellular matrix (ECM) and secrete growth factors that contribute to a regenerative microenvironment conducive for axon growth. Following spinal cord injury (SCI), axon connectivity is disrupted within a predominantly inhibitory milieu. Understanding between glia and neurons is therefore critical for elucidating mechanisms of axon regeneration. In this study, we investigated the influence of enriched astrocyte subtypes-fibrous and protoplasmic-derived from mouse embryonic stem cells (mESCs). on axon growth from V2a interneurons *in vitro.* V2a interneurons were used due to their pivotal role as an excitatory neuron population in the spinal cord. In both 2D co-culture systems and 3D hyaluronic acid (HA)- based hydrogels, protoplasmic astrocyte-derived components significantly enhanced V2a axon growth compared to fibrous astrocytes. Proteomic analysis of astrocyte-derived ECM revealed elevated expression of key axon growth -associated proteins by protoplasmic astrocytes, including collagen XVIII (Col18a1), perlecan, laminin-1, anti-thrombin-III, and fibronectin. Defined ECM protein mixtures were formulated and into HA hydrogels to assess their capacity to mimic the proregenerative effects of native protoplasmic ECM. These engineered hydrogels successfully recapitulated the axon grow promoting properties of protoplasmic ECM, offering a scalable, cell free platform for supporting

V2a interneuron growth *in vitro*. This work highlights the potential of astrocyte subtype-specific ECM mimetics in developing regenerative strategies for SCI.

3.2 Introduction

Spinal cord injury (SCI) is a debilitating condition that disrupts network connectivity between motor neurons and interneuron populations resulting in loss of sensory and motor functions[302]. One strategy to restore synaptic connectivity after injury involves leveraging the plasticity of spinal interneuron heterogeneity in gray matter of spinal cord[140,148,303]. This study utilizes the model of increasing axon growth of one specific interneuron type, V2a interneurons, with potential application towards affecting axon growth of other interneurons, such as V0, V1, and V3[140]. V2a interneurons are an excitatory ventral neuron population involved in diaphragm function and respiratory breathing patterns in specifically cervical SCI models[140,148,154,155,157,303,304]. Protocols have been established to derive V2a interneurons from human pluripotent cells and mouse embryonic stem cells (mESCs), enabling the study of their synaptic integration with other classes of interneurons and motor neurons[132,152]. These approaches have facilitated targeted transplant studies aimed at enhancing respiratory plasticity and improving diaphragm function post-SCI[7]. However, when V2a interneurons are transplanted into the hostile microenvironment of the injured spinal cord, alterations in cell phenotype and low survival rate of the transplanted neurons has been observed[140,148,303].Therefore, identifying microenvironment cues from other spinal cord cell types that can increase axon growth of V2a interneurons is crucial.

Astrocytes play a vital role in synapse formation and neuron support. Both protoplasmic astrocytes in the grey matter and fibrous astrocytes in the white matter

extend complex processes to ensheath axons and support neuronal homeostasis[297,305]. Glutamate transporters in astrocyte membranes aid in glutamate uptake and prevent excitotoxicty[306]. Furthermore, astrocyte calcium signaling acts as internal communication that regulates potassium and neurotransmitter uptake contributing to a balance environment[297,307]. Through these functions, astrocyte help to sustain excitatory and inhibitory synaptic networks and support regenerative responses[308]. Thus, astrocytes may play an important role in promoting axon growth after SCI.

Astrocyte-secreted cues, including extracellular matrix (ECM) proteins and growth factors, have the potential to promote axon growth. Incorporating these glial-derived cues into biomaterial-based therapies may enhance axon growth after SCI. Notable astrocyte-derived ECM proteins that support synaptogenesis and axon growth include Hevin and SPARC (secreted protein in acidic and rich in cysteine), which regulate presynaptic input and promote glutamatergic synapse formation. Additional candidates, such as thrombospondin, glypicans, as well as ECM glycoproteins, laminin and fibronectin, are also known to influence axon growth[17,308]. Conversely, border-forming astrocytes secrete inhibitory molecules, such as chondroitin sulfate proteoglycans (CSPGs), which can hinder axon regeneration. Therefore, investigating the specific effects of astrocyte-derived cues on axon growth is essential for understanding the diverse roles of astrocyte subtypes and for informing the development of future SCI therapies.

In our previous work, we demonstrated that ECM derived from protoplasmic astrocytes differentiated from mouse embryonic stem cells supported greater axon growth than ECM from fibrous astrocytes, both *in vitro* and *in vivo*[44]. However, the

mESC-derived astrocyte cultures contained other cell types (neurons, oligodendrocytes, and undifferentiated stem cells) that may have included the observed ECM effects. To address this issue, we generated transgenic puromycin selectable cell lines to enrich specific astrocyte subtypes and minimize contributions from other cell types. Using these enriched cell populations, we investigated the effects of astrocytes subtype on V2a interneurons axon growth. ECM from selected protoplasmic astrocytes significantly increased axon extension of V2a interneurons compared to ECM from selected fibrous or unselected astrocytes, suggesting that differences in ECM protein compositions underlie these effects. We identified several key proteins highly upregulated in selected protoplasmic astrocyte ECM that could be incorporated in hydrogels. We used a HA-based hydrogel platform with defined protoplasmic astrocyte ECM proteins to generate a simplified, defined astrocyte ECM mimetic support axon growth from V2a interneurons *in vitro*. This biomaterial platform offers a promising alternative to the labor-intensive 27 day- astrocyte differentiation protocol, while ensuring consistent protein composition.

3.3 Materials and Methods

3.3.1 Cell culture media formulations[44,132]

Complete Media (CM)- consisting of Dulbecco's modified Eagle's Medium (DMEM; Life Technologies #11965-092, Carlsbad, CA) supplemented with 10% newborn calf serum (Life Technologies #16010-159), 10% fetal bovine serum (Life Technologies #26140-079), and 1x Embryomax Nucleosides (Millipore #ES-008-D, San Francisco, CA).

DFK5- **D**MEM/**F**12 (Life Technologies) plus **5**% **K**nockout Serum Replacement (Life Technologies #10828-028), 50 µM nonessential amino acids (Life Technologies #11140-050), 1x Insulin-Transferrin-Selenium (Life Technologies #41400-045), 100 µM

β-mercaptoethanol (BME; Thermo Fisher Scientific, 21985023), 5 μM thymidine, and 1x Embryomax Nucleosides.

Astro1 media- DFK5 with 20 μg/mL epithelial growth factor (EGF) (Peprotech, #315-09), 10 μg/mL fibroblast growth factor 1 (FGF-1) (Peprotech, 450-33A), and 1 μg/mL laminin (Life Technologies #23017-015)

Protoplasmic (astrocyte) media- DFK5 with 10 μg/mL FGF-1, 10 μg/mL bone morphogenic protein (BMP-4; Peprotech, #315-27)

Fibrous (astrocyte) media- DMEM/F12 plus 1 × G5 supplement (Life Technologies, #17503012), 10 μg/mL ciliary neurotrophic factor (CNTF; Peprotech, #450-13)

Neuronal media- 50% Neural basal media (Life Technologies) and 50% DFK5 media with 1 × GlutaMAX (Life Technologies #35050-061), 1 × B27 (Life Technologies #17504-044), and 10 ng/mL of the following growth factors for 24 h: glial-derived neurotrophic factor (GDNF; Peprotech #450-10, Rocky Hill, NJ), neurotrophin-3 (NT-3; Peprotech #450- 03, Rocky Hill, NJ), and brain-derived neurotrophic factor (BDNF; Peprotech #450-02, Rocky Hill, NJ).

3.3.2 mESC culture maintenance[258]

Aqp4-puro, Olig2-puro, Chx10-puro TdTomato or Chx10-puro eGFP, and RW4 (ATCC, SCRC-1018) mESC lines were maintained in T-25 flasks coated with 0.1% gelatin (MilliporeSigma, G1393; in water) in CM with 1000 U/mL leukemia inhibitory factor (LIF; MilliporeSigma, ESG1106) and 100 μM β-mercaptoethanol (BME; Thermo Fisher Scientific, 21985023) in 5% CO_2 at 37 °C. For passaging approximately every 2 days, mESC colonies were dissociated with 0.25% trypsin ethylenediaminetetraacetic acid (trypsin–EDTA; Thermo Fisher Scientific, 25200072) for 5 min, followed by quenching

with CM and trituration to ensure single-cell suspension. Single cells were plated in a new gelatin-coated flask containing CM + LIF + BME at a typical 1:5 ratio and grown for two days or until ~ 60-80% confluent.

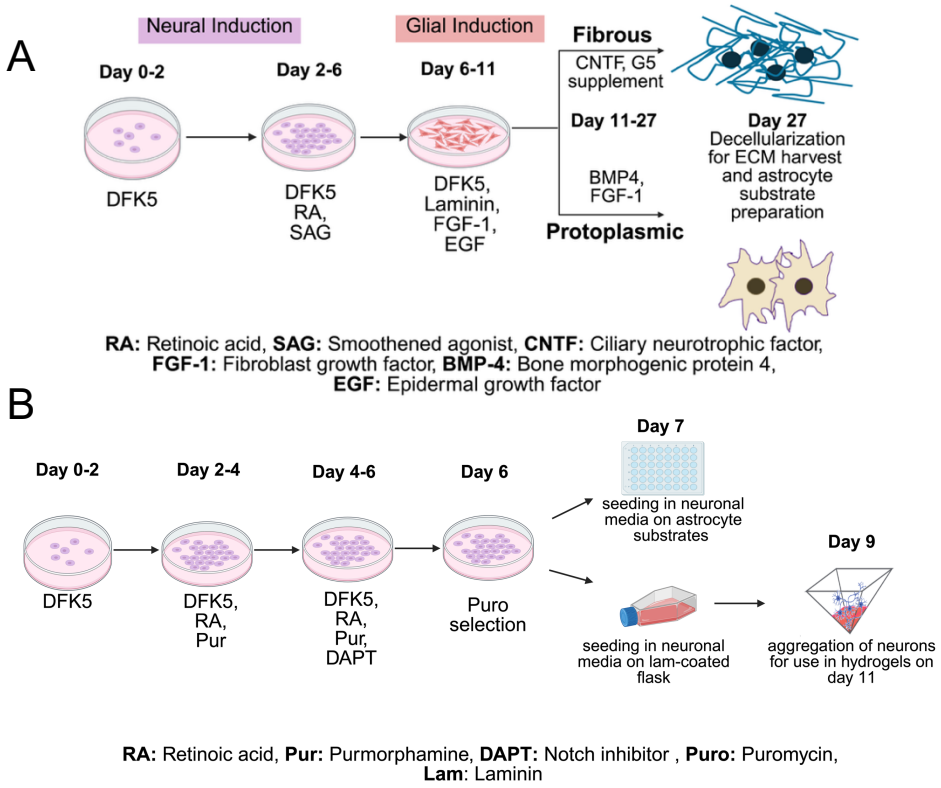

Figure 3.1 Astrocyte and V2a interneuron differentiation protocols for experimental design of investigating effects of astrocyte subtypes on axon growth A) Timed differentiation for generating and collecting astrocyte substrates and ECM collection **B)** Timed steps of V2a interneuron differentiation for seeding of V2a interneurons on astrocyte substrate types and V2a aggregates in astrocyte ECM and protein hydrogels

3.3.3 Glial Differentiation from mESCs and puromycin selection of astrocyte phenotypes (Fig. 3.1A)[258]

Astrocytes were derived from Aqp4-PAC mESCs as previously described to generate protoplasmic astrocytes and from Olig2-PAC mESCs to generate fibrous astrocytes. On day 0, 1-1.5 x 10^6 ESCs were cultured in suspension on agar-coated 10 cm dishes in 10 mL DFK5 for two days to form embryoid bodies (EBs). On days 2 and 4, the media was changed with 10 mL DFK5, 2 μM retinoic acid (RA; Sigma #R2625), and 600nM Smoothened Agonist (SAG; Fisher Scientific, #566661) to generate ventral

progenitors of the spinal cord. On day 6, the EBs were dissociated and seeded at density of 50,000-100,000 cells/cm^2 onto a gelatin-coated tissue culture treated 6-well plates (ThermoFisher; #3516) in Astro1 media for 5 days. On day 11, cultures were switched into astrocyte phenotypic media (protoplasmic or fibrous) for an additional 4 days in the same plates[51].

On day 15, the protoplasmic astrocytes were reseeded onto gelatin-coated plates at a density of 50,000 or 100,000 cells/cm^2 and maintained in lineage specific media for additional 2 days. On day 17, protoplasmic astrocytes were selected with 2 µg/mL puromycin (Sigma #P8833) in protoplasmic astrocyte media for 1 day. On day 18, the protoplasmic astrocytes were washed with phosphate buffered saline (PBS) and maintained in astrocyte phenotypic media in same culture plates until Day 21 for reseeding. On day 21, the protoplasmic astrocytes were reseeded at 25,000 cells/cm^2 in 0.1% gelatin-coated 6-well tissue culture plates for ECM deposition that was harvested through modified Hudson decellularization protocol.

On day 17, the fibrous astrocytes were reseeded onto gelatin-coated plates at a density of 10,000 or 20,000 cells/cm^2 and maintained in lineage specific media for additional 2 days. On day 19, fibrous astrocytes were selected with 4 µg/mL puromycin in fibrous astrocyte media for 2 days. On day 21, the fibrous astrocytes were washed with PBS and maintained in astrocyte phenotypic media in same culture plates until Day 23 for reseeding. On day 23, the fibrous astrocytes were reseeded at 20,000 cells/cm^2 in 0.1% gelatin-coated 6-well tissue culture plates for ECM deposition that was harvested through detergent-based decellularization[44,60]. For ECM use in hydrogel experiments and proteomic analysis, 1mL 50mM Trehalose was added to culture plates

and proteins were scraped using a cell-scraper. The resulting ECM protein suspension was lyophilized overnight and stored in -20^{o}C[60].

3.3.4 Astrocyte substrate preparation

Day 21 astrocyte phenotypic cultures were seeded onto the wells of gelatin-coated 48-well plates at density of 20,000- 25,000 cell/cm^2 and cultured in phenotypic media for 6 days to be used at day 27 for V2a interneuron seeding (Fig. 3.1). For frozen astrocytes, the astrocytes were kept in the freezer overnight at day 27. On day 27, a modified Hudson decellularization protocol was conducted for the unselected and selected astrocyte subtypes. On day 1 of decellularization, the astrocytes are washed in sterile water for 15 minutes and then exposed to a solution of 10mM phosphate (composed of equal amounts of 100mM sodium phosphate monobasic-Sigma Aldrich S3139 and dibasic-Sigma Aldrich S5136 with water to adjust to final concentration), 50mM NaCl (Fisher Scientific AC424290250), 125mM sulfo-betaine-10 (Fisher Scientific AC459680250) for 2 hours on a rocker for more even spread of solution over the astrocytes. Then, the astrocytes were washed with solution of 50mM phosphate and 100mM NaCl and placed on the rocker overnight in a solution of 10mM phosphate, 50mM NaCl, and 0.6mM sulfo-betaine 16 (Sigma Aldrich H6883). On day 2 of decellularization, the astrocytes were rinsed 3 times at 5 minutes each with a solution of 10mM phosphate and 50mM NaCl. Then, the astrocytes are placed in the solution of 10mM phosphate, 50mM NaCl, and 125mM sulfo-betaine- 10 for 1 hour. After, the astrocytes are placed in the solution of 10mM phosphate, 50mM NaCl, and 0.6mM sulfo-betaine 16 for 2 hours. Finally, the astrocytes are washed 3 times at 5 minutes

each with a solution of 10mM phosphate and 50mM NaCl to produce the decellularized astrocyte substrates for neuron seeding.

3.3.5 V2a interneuron culture (Fig. 3.1B)[132]

V2a interneurons were generated from Chx10-puro-TdTomato or Chx10-puro-eGFP mESCs and were induced using a $2^{-}/4^{+}$ protocol using 10 nM RA and 1 μM purmorphamine (Pur; EMD Millipore #540223) from days 2 to 6 and 5 μM N-{N- (3,5-difluorophenacetyl-L-alanyl))-(S)-phenylglycine-t-butyl-ester (DAPT; Sigma #D5942) for days 4 to 6. On day 6, 4μg/mL puromycin was added to the 10-cm dish containing V2a interneuron EBs for 24 hours. On day 7, selected V2a IN EBs were dissociated with 0.25% trypsin followed by quenching with CM and seeded at 10,000- 20,000 cells/cm^2 on day 27 astrocyte substrates in 48-well plate with neuronal media. Average neurite extension was measured using ImageJ for analysis[132].

3.3.6 Preparation of V2a interneuron aggregates (Fig. 3.1B)

Two days after selection, V2a interneurons seeded in laminin-coated flask were lifted using Accutase (Sigma, A6964) treatment for 30 min and 800,000-1 million cells were transferred into a single well in a Aggrewell 400 (Stemcell Technologies, #34415) plate with 1200 microwells per well to get approximately aggregates of 500–600 cells. The well had been previously treated with anti-adherence rinsing solution (Stem Cell Technologies, #07010) to reduce surface tension and cell adhesion to aid in promotion of aggregate formation. The interneurons were cultured for 2 days in neuronal media in the aggrewell for neuro-aggregate formation. At this time, neuro-aggregates were lifted and collected for counting before seeding into hydrogels with astrocyte extracellular matrix (ECM) and individual proteins[309].

3.3.7 Hyaluronic acid (HA)-methylfuran (mF) synthesis[212]

400 mg HA (Creative PEGWorks, MW 250 kDa, #HA-103) was dissolved in 40 mL 2-(N-morpholino) ethanesulfonic acid (MES) buffer (pH 5.5) within a round bottom flask. 750 mg of 4- (4,6- dimethoxy-1,3,5-triazin-2-yl)-4- methylmorpholinium (DMTMM) (TCI America, #D2919) was added to the solution and stirred for 10 min. 124.5 µL of 5-methylfurfurylamine (TCI, #M1311) was then added dropwise, with the reaction carried out for 72 hours under constant agitation by magnetic stir bar. The solution in the flask was dialyzed in tubing (Thermo Scientific, #88243) against DI water for two days with water replaced every 24 hours. The solution was lyophilized for two days to ensure removal of all water. The final product was collected as a white fibrous material and stored at -20^{o}C until further use for hydrogel solution preparation.

3.3.8 Determination of functionality of HA-mF using nuclear magnetic resonance (NMR) spectroscopy[309]

10 mg/mL of HAmF was dissolved in deuterium oxide (Thermo Fisher Scientific) for 24 hours and H^1 NMR was used to characterize the product to calculate the degree of methylfuran substitution.

3.3.9 Hydrogel synthesis[309]

Lyophilized HAmF was dissolved in phosphate buffer saline (PBS) buffer at pH 7.4 overnight at 11 mg/mL and crosslinked with PEG-diMal (MW 3150, Rapp Polymere, #113000) in PBS at 156 mg/mL and combined in a 20:1 volume ratio of HAmF to PEG-diMal for a final molar ratio of 3:1 methylfuran to maleimide.

3.3.10 Preparation of HAmF-PEGdiMal hydrogels with V2a interneuron aggregates and proteins

Hydrogel format was conducted in 96-well plates with a gel volume of 30-35 µL in each well with 3 wells for each experimental and control group. This resulted in a total gel volume of 120 µL for each protein/astrocyte phenotypic ECM tested in the hydrogel with V2a interneuron aggregates with negative control being hydrogel alone with no proteins and positive control with 10 µg/mL generic laminin. Additional hydrogel testing was conducted with protein concentrations at 5, 10, and 25µg/mL for laminin-1 and fibronectin to demonstrate the use of protein testing on axon growth in the hydrogel system. The astrocyte ECM concentrations used were all at 50 µg/mL. These proteins/astrocyte ECM were added to measured amounts of HA solution in microcentrifuge tubes for each hydrogel condition for 120 µL. Then, 45-50 V2a interneuron aggregates were added in DFK5/NB media to the solution. Finally, the PEG-dimaleimide amount was added to the hydrogel in a ratio of 20:1 volume ratio of HAmF to PEGdiMal for a final molar ratio of 3:1 methylfuran to maleimide. The final contents were mixed and added at 30-35µL to each well in the 96-well plate. Lastly, 100µL of neuronal media was added on top of the thin hydrogels for culture of 2 days in incubator at 37C. After incubation, the V2a interneuron aggregates were imaged at 488 or 555nm excitation fluorescence to observe the neurite extensions from the aggregates. The images were analyzed with ImageJ software to quantify the average neurite growth, which was calculated as the average radius of an annulus between the aggregated body area and the outer ring of neurite extension[309].

For the chosen 7 selected protoplasmic astrocyte ECM proteins, low and high concentrations were considered as K_d and $5xK_d$ for each protein, respectively.

Table 3.1 The specific low (K_d) and high concentrations tested for each protein in HAmF-PEGdiMal hydrogel for testing effects on axon growth of V2a interneurons

Protein name	K_d	High concentration	Manufacturer
Perlecan	2.06 µg/mL[310]	10.3 µg/mL	Sigma Aldrich #H477
Collagen 4a1	0.15 µg/mL[311]	0.75 µg/mL	Biomatik RPU40899
Nidogen-2	0.85 µg/mL[312]	4.25 µg/mL	Biomatik RPU51609
Collagen18a1	0.4 µg/mL[313]	2 µg/mL	Abcam ab56290
Anti-thrombin III	1.49 µg/mL[314]	7.45 µg/mL	Abcam ab93233
Laminin-1	10 µg/mL	50 µg/mL	RD systems #3400-010-02
Fibronectin	11 µg/mL	55 µg/mL	Innovation Research IMSFBN1MG

3.3.11 Proteomic analysis of decellularized astrocyte ECM[44]

Day 21 selected protoplasmic astrocytes and Day 23 selected fibrous astrocytes were seeded at 25,000 cells/cm^2 onto gelatin-coated plates and allowed to grow until day 27 time point and decellularization. After decellularization, the residual proteins were scraped off the plate into 50mM Trehalose and lyophilized overnight. The resulting powder was dissolved in sterile water, and the protein concentration was quantified using Pierce's BCA assay (Thermo Fisher Scientific). 10µg from 4 biological replicates of decellularized selected astrocyte phenotypes was processed to obtain peptides through the EasyPep Mini MS sample prep kit instructions (Thermo Fisher Scientific), which reduces, alkylates, and digests the ECM proteins into peptides. The resulting peptide solutions were provided to the University of Washington Proteomics Resource Center (UWPR) for MS analysis. All samples were analyzed on an Exploris480 mass spectrometer (ThermoFisher Scientific) equipped with an EASYnLC 1200 Ultra-performance liquid chromatography UPLC system (ThermoFisher Scientific) and in house developed nano spray ionization source. Selected astrocyte ECM peptide samples (4 µL at 200-400 µg/µL at start of MS prep) were loaded from the autosampler

onto a 100 µm ID Integrafrit trap (NewObjective) packed with Reprosil-Pur C18-AQ 120 Å 5 µm material (Dr. Maisch) to a bed length of 3-cm with a volume of 18 µL at a flow rate of 2.5 µL/min. After loading and desalting with 0.1% formic acid in water (LCMS grade from Fisher), the trap was brought in-line with a pulled fused-silica capillary tip (75-µm i.d.) packed with 35 cm of Reprosil-Pur C18-AQ 120 Å 5 µm (Dr. Maisch). Peptides were separated using a linear gradient, from 6-35 % solvent B (LCMS grade 0.1 % formic acid, 80 % acetonitrile in water (Fisher) in 90 min at a flow rate of 300 nL/min. The raw files were pooled by selected astrocyte phenotype and converted to mzXML and searched against a mouse protein sequence database using Comet. The search results were then processed with PeptideProphet and ProteinProphet tools from the Trans-Proteomic Pipeline software suite. The results of identified protein groups were viewed through pepXML and protXML files.

3.3.12 Selection of proteins for axon growth testing in hydrogel platform with V2a interneuron aggregates and testing on V2a interneurons

Protein identifications and probabilities were assigned using the ProteinProphet algorithm. The Abacus software provided the quantitative results using the normalized spectral abundance factors for each identified protein based on peptide spectral counts[315]. The following settings were applied in the Abacus analysis: (i) a protein group must contain a peptide with a peptide probability of 0.99; (ii) minimum peptide probability of 0.5 for a peptide to be considered in the spectral counts; and (iii) minimum protein probability of 0.9. The results were tabulated into an Excel file. A ratio of normalized spectral abundance factor for selected protoplasmic astrocyte to selected fibrous astrocyte was calculated for each identified protein. These ratios were ranked

highest to lowest to determine the proteins found upregulated in selected protoplasmic astrocyte ECM (ratio higher than 1). 7 proteins upregulated in selected protoplasmic astrocyte ECM were chosen based on several criteria including the role of protein in extracellular space and matrix, commercial availability of human or mouse versions, potential axon growth evidence, and proteins available as a tag-free option to be used in cell culture applications.

3.3.13 Design of Experiments (DoE) analysis to determine combinations of chosen proteins added to hydrogel

Using JMP software, a custom design for DoE was conducted with the inputs of factors with 2 levels to represent the proteins at high and low concentrations ($5xK_d$ and the K_d concentration for each protein) of the proteins that produced axon growth at the high concentrations. The resulting table provides the concentrations and protein combinations to test in the HAmF-PEG maleimide hydrogel format *in vitro* with V2a interneuron aggregates (Supplemental Table 3.1).

3.3.14 Immunocytochemistry (ICC)

Cells were rinsed with PBS and then fixed in 4% paraformaldehyde (Sigma) for 20 mins at 4^{o}C. The cells were rinsed with PBS and permeabilized in 0.1% Triton-X (Sigma) for 10 mins at 4^{o}C if staining for nuclear or cytoplasmic markers. Cells were blocked with 5% of an appropriate serum (Goat (Sigma) or Donkey (Sigma)) in PBS for 1 hr at 4^{o}C. Primary antibodies were used at the following dilutions: Synaptic vesicle 2 (SV2) 1:100 (DSHB), Aquaporin-4 1:100 (Millipore), Perlecan 1:100 (Thermo Fisher Scientific), Decorin 1:100 (Santa Cruz Biotechnology), Endostatin Col18a1 antibody (Thermo Fisher Scientific), and Fibronectin antibody (Proteintech). Primary antibody incubation was carried out overnight in 2% of appropriate serum in PBS at 4^{o}C and were rinsed 3

times with PBS after incubation. Corresponding Alexa Fluor secondary antibodies (Life Technologies) were all used at a 1:1000 dilution (final concentration of 4 µg/mL) and incubated in 2% of appropriate serum in PBS for 1 hr at 4°C. After the incubation, the cells are rinsed with PBS three times. 1:1000 Hoechst (Invitrogen) in PBS was incubated with the cells for 10 min at 4°C prior to imaging on a Leica DMi8 or Nikon wide-field fluorescence microscope. The image analysis was performed by using Image J to count the number of nuclei by DAPI stain and the number of cells stained positive for the above chosen markers.

3.3.15 Statistics

Statistical analysis was performed in GraphPad Prism9 and Microsoft Excel. Multiple comparisons statistics were accomplished using Scheffe's post hoc test for one-way analysis of variance (ANOVA) with a 95% confidence level. Values are reported as the mean plus or minus standard error.

3.4 Results

3.4.1 Effects of astrocyte subtype substrates on V2a interneurons

To investigate how astrocyte subtypes influence axon growth of V2a interneurons, we utilized mature day 27 astrocyte cultures derived from transgenic puromycin-selectable mESC lines to ensure subtype enrichment and minimize cellular heterogeneity. These mature cultures exhibited a high fraction of cells positive for astrocyte subtype markers and low fraction of cells positive for markers of other cell types (Supplemental Fig. 3.1). V2a interneurons, enriched from a separate transgenic selectable cell line, were seeded onto various astrocyte-derived substrates - including live, frozen, and decellularized astrocyte ECM, as well as conditioned media, to

investigate the contributions of whole cells, membrane components, ECM proteins, and soluble factors, respectively[132]. Constitutively expressed TdTomato in the V2a interneurons enable clear visualization and quantification of the axon outgrowth. The results revealed significant differences in the average neurite length depending on the astrocyte subtype and substrate condition. Notably, components from selected protoplasmic astrocytes significantly enhanced neurite extension compared to those from selected fibrous, unselected fibrous, and unselected protoplasmic astrocyte components, except for conditioned media (Fig. 3.2A). Among all conditions, decellularized substrates from selected protoplasmic astrocytes produced the most robust axon growth, markedly outperforming those from selected fibrous decellularized astrocytes (182± 7.5 compared to 29.1±3.1). Furthermore, the V2a interneurons cultured on decellularized selected protoplasmic substrates exhibited extensive neurite outgrowth in contrast to the sparse and short extensions observed on decellularized selected fibrous astrocytes (Fig. 3.2B, C; Supplemental Fig. 3.2A, B). These findings indicate that selected protoplasmic astrocytes provide axon growth-permissive components likely through distinct ECM protein composition.

To better understand the mechanism underlying the observed axon growth differences, we characterized the composition of the various astrocyte-derived substrates. Immunocytochemistry (ICC) analysis of live astrocyte cultures on Day 27 revealed a high fraction of cells positive for astrocyte markers, such as GFAP, S100β, and Aqp4, and low fraction of cells positive for other cell types, including neurons, oligodendrocytes and undifferentiated stem cells (Supplemental Fig. 3.1). Additionally, cultures of V2a interneurons on live astrocyte substrates showed a high fraction of

neurons positive for synaptic vesicle protein 2 (SV2), a marker of synapse formation, suggesting astrocyte substrates support synaptogenesis (Supplemental Fig. 3.3A, B)[316]. Decellularized astrocyte substrates retained subtype specific ECM components, with thrombospondin enriched in selected fibrous ECM and perlecan in selected protoplasmic ECM, consistent with prior proteomics analyses of astrocyte cultures derived from non-transgenic mESC lines[44]. Together these findings suggest that selected protoplasmic astrocytes produce ECM and growth factor cues that are permissive to axon growth, potentially explaining their enhanced support for V2a interneuron neurite extension.

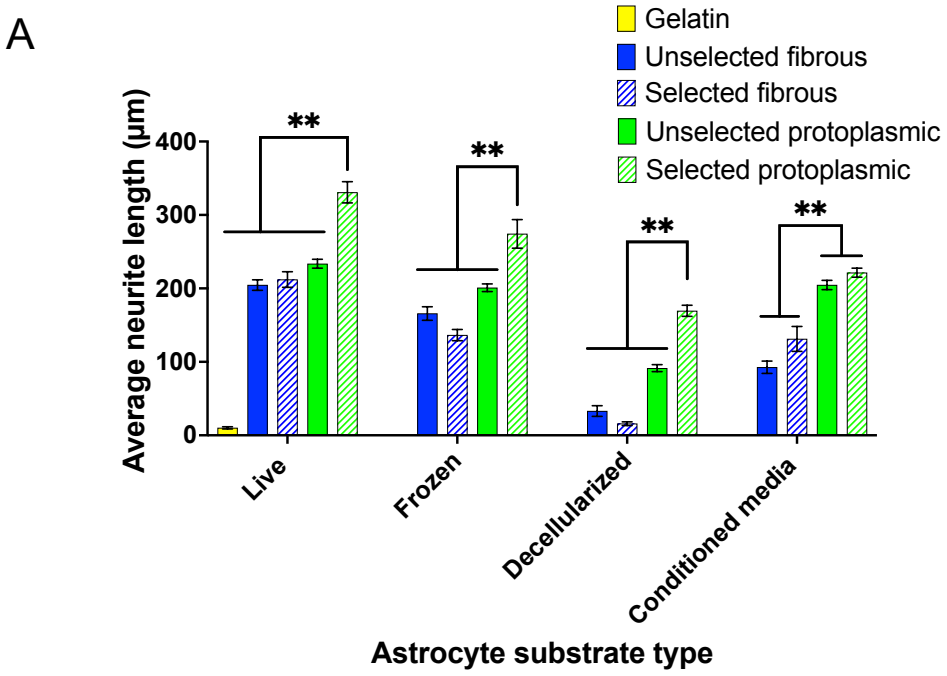

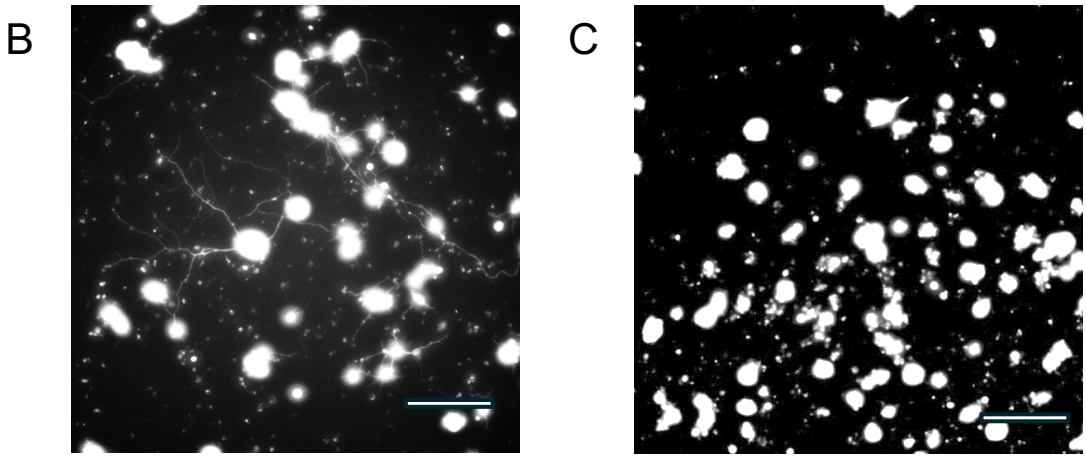

Figure 3.2 Selected protoplasmic astrocyte components significantly promote V2a interneuron neurite growth. A) Effects of live (whole cell), frozen (membrane), and decellularized (ECM) astrocyte phenotypes on axon growth of V2a interneurons n=50-100; * $p<0.05$ and ** $p<0.01$. **B)** Representative image of V2a interneurons seeded on decellularized selected protoplasmic astrocytes; Scale bar= 100μm. **C)** Representative image of V2a interneurons seeded on decellularized selected fibrous astrocytes; Scale bar= 100μm.

3.4.2 Effects of astrocyte subtype ECM in hydrogel on V2a interneuron aggregates

To evaluate whether axon growth-promoting effects of astrocyte-derived ECM observed in 2D cultures translate to a 3D environment, we incorporated phenotypic ECM into hyaluronic acid-based hydrogels and assessed their effect on V2a interneuron axon extension. This hydrogel platform allows for the incorporation of growth factors and ECM proteins by mixing them in the HA solution prior to cross-linking with PEG-dimaleimide, enabling controlled presentation of bioactive cues. To optimize ECM protein conditions, we tested varying concentrations of two control proteins, laminin and fibronectin in the hydrogel. Laminin at 25 μg/mL produced the greatest enhancement in axon growth (Supplemental Fig. 3.4). When comparing astrocyte subtype-derived ECM, hydrogels containing ECM from selected protoplasmic astrocytes showed significantly increased V2a interneuron axon growth compared to those containing ECM from selected fibrous astrocytes (Fig. 3.3A-C; 149.4 ± 9.1 compared to 52.4 ± 16.5). These results support the conclusion that specific axon-growth permissive proteins are

upregulated in the ECM from selected protoplasmic astrocytes, and that these components retain their bioactivity in a 3D hydrogel environment.

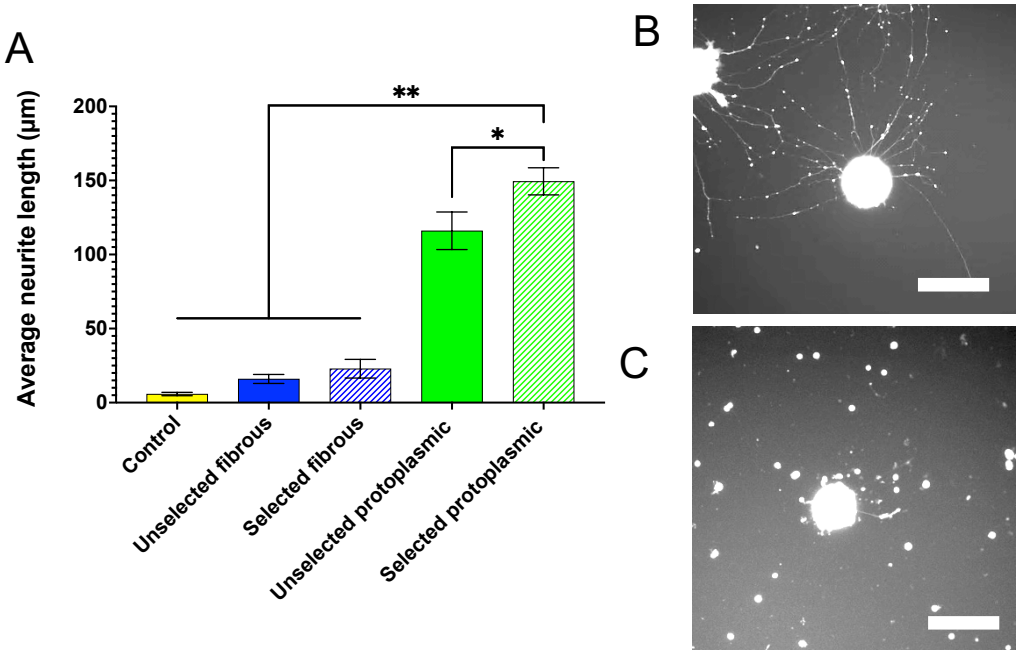

Figure 3.3 Selected protoplasmic ECM in HAmF-PEGdiMal hydrogels significantly increased axon growth of V2a interneurons A) Selected protoplasmic ECM significantly supported axon growth compared to other astrocyte groups tested with at least 50 neuroaggregates in 3 trials; * $p<0.05$ and **$p<0.01$ **B)** Representative image of V2a interneuron aggregates in selected protoplasmic ECM hydrogel; Scale bar =100µm C) Representative image of V2a interneuron aggregates in selected fibrous ECM hydrogel; Scale bar= 100µm

3.4.3 Proteomic analysis of astrocyte subtype ECM

To identify ECM proteins that may underlie the axon growth-promoting effects of astrocyte subtypes, we performed liquid chromatography- mass spectrometry (LC-MS/MS) proteomic analysis on day 27 decellularized ECM from selected protoplasmic and fibrous astrocyte cultures. These data provide insight into phenotype-specific ECM composition and highlight candidate proteins for biomaterial-based strategies to enhance axon growth. Proteomics data were process using Abacus, a computational tool that extracts spectral counts from label-free mass spectrometry datasets[315]. Protein identification was performed against the *Mus musculus* (mouse) protein database and abundance was estimated using adjusted normalized spectral abundance factors

(AdjNSAF), which accounts for peptide spectra and the protein length[315,317,318]. A total of 5792 proteins were identified across both astrocyte ECM types (Supplemental Fig. 3.6A). Abacus provided multiple protein abundance metrics including total, unique, and adjusted spectral counts, with AdjNSAF values used for downstream comparison.

Majority of proteins exhibited differential abundance between selected protoplasmic and fibrous ECM (Fig. 3.4A), with some proteins uniquely present in one phenotype (Fig. 3.4B). To identify proteins highly enriched in selected protoplasmic ECM, we calculated the ratio of AdjNSAF values between the two phenotypes (Fig. 3.4C). Proteins with ratios 30 or greater were considered uniquely present in selected protoplasmic ECM. Cross referencing with Matrix DB revealed that 351 of the 5792 proteins are found in the matricellular space (Supplemental Fig. 3.5A). Among these, 59 ECM proteins were found at higher abundance ratio (ratio >1) in selected protoplasmic ECM, with 28 proteins highly upregulated (ratio >5) and 16 exclusively present proteins in selected protoplasmic ECM. These proteins represent promising candidates for further investigation into their roles in promoting V2a interneuron axon growth.

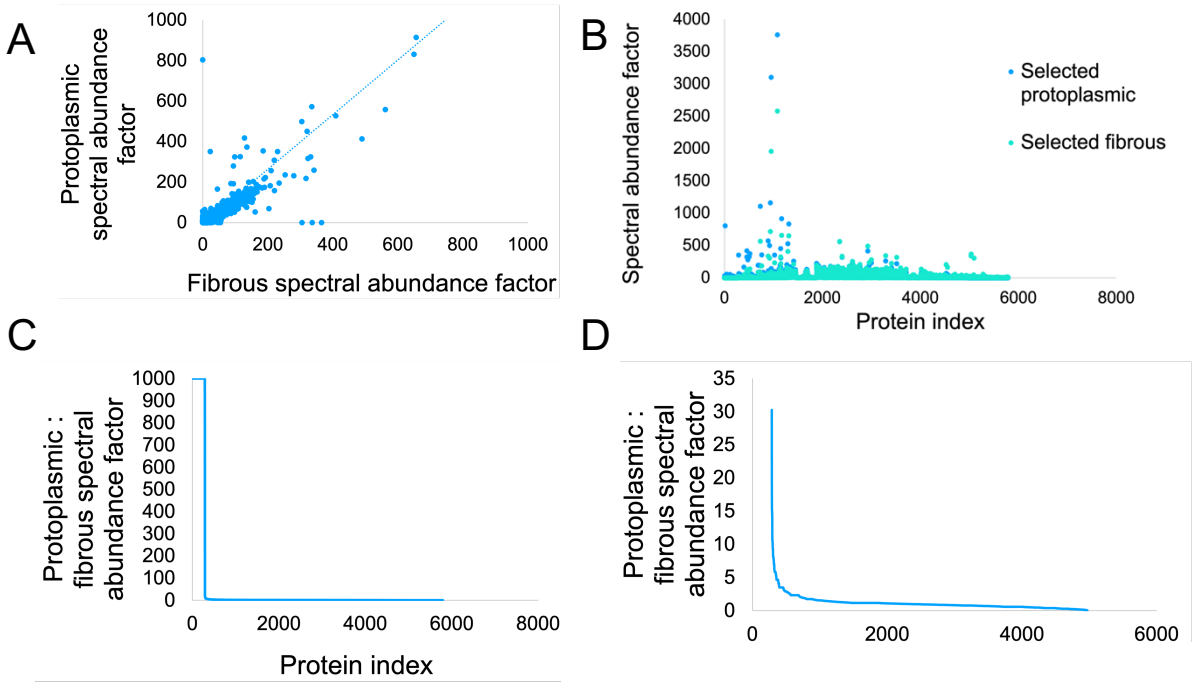

Figure 3.4 Proteomics analysis identified ECM proteins enriched in selected protoplasmic astrocyte culture that are candidates for promoting axon growth A) Plot of spectral abundance values for different proteins identified in both selected astrocyte phenotypes of 3 trials**. B)** Proteins identified have different spectral abundance values for each astrocyte phenotype. **C)** Proteins sorted by ratio of spectral abundance in selected protoplasmic to selected fibrous demonstrate proteins exclusively found in selected protoplasmic to proteins found in both phenotypes to proteins exclusively found in selected fibrous

Table 3.2 Ratio of ADJNSAF values for selected protoplasmic ECM to selected fibrous ECM for each protein chosen to test in hydrogel system

Protein	Ratio of ADJNSAF selected protoplasmic to selected fibrous
Perlecan	1000
Laminin-1	15.1
Fibronectin	15.1
Col18a1	5.58
Anti-thrombin III	2.72
Col4a1	2.68
Nidogen-2	2.08

3.4.4 Decision criteria for selected protoplasmic astrocyte ECM proteins for hydrogel

To translate the proteomic findings into a functional biomaterial platform, we aimed to identify and incorporate key ECM proteins upregulated in selected

protoplasmic astrocyte ECM into a hydrogel system for synthesis of an astrocyte ECM mimetic capable of promoting V2a interneuron axon growth. Protein selection was guided by four criteria: 1) an ADJNSAF ratio greater than 2 in selected protoplasmic versus fibrous ECM 2, 2) literature evidence supporting a role in axon growth or neural development, 3) availability of human and/or mouse isoforms, and 4) commercial availability from a reliable supplier. Using these criteria, we selected seven ECM protein candidates for testing in the HAmF-PEGdiMal hydrogel system at varying concentrations and in combination (Table 3.2). Laminin-1 and fibronectin, well characterized basement membrane proteins, are known to support neurite outgrowth and astrocyte migration, and play roles in central nervous system (CNS) patterning[172,184,319–323]. Perlecan, a heparan sulfate proteoglycan core protein, contributes to axonal and synaptic integrity[324,325]. Collagen XVIII (Col18a1) has been implicated in guiding axon regrowth of retinal ganglion cells during optic nerve regeneration[326,327]. Anti-thrombin III, a secreted plasma glycoprotein, may exert neuroprotective effects by modulating thrombin activity and immune responses[328,329]. Collagen IV alpha 1 (Col4a1), a component of the basement membrane, supports granule cell development and axonal projection[311]. Lastly, nidogen-2 is involved in neuromuscular junction maturation and synaptic organization[330]. Together, these proteins represent a diverse set of ECM components with established or potential roles in neural development and regeneration, making them strong candidates for inclusion in astrocyte ECM-mimetic hydrogels aimed at enhancing V2a interneuron axon growth.

To determine the individual contributions of candidate ECM proteins to V2a interneuron axon growth, we conducted an initial screening using high concentrations (5

times higher than the reported dissociation constant, K_d values from the literature) incorporated into the HAmF-PEGdiMal hydrogel[310–314]. V2a interneuron aggregates were cultured within these hydrogels to assess axonal outgrowth responses. Among the proteins tested, laminin-1, fibronectin, and anti-thrombin III individually significantly enhanced axon growth compared to the other candidates (Fig. 3.5A). In contrast, nidogen-2 and Col4a1 supported minimal axon growth (4.5 ± 3.1 and 6.6 ± 2.1 respectively), whereas Col18a1 and perlecan showed moderate effects (36.3 ± 4.2 and 44.3 ± 7.2 respectively). Notably, although laminin-1, fibronectin, and anti-thrombin III individually promoted axon growth relative to the negative control, their effects were still significantly lower than those observed with the fully selected protoplasmic ECM incorporated into the hydrogel. These findings suggest that no single protein fully recapitulates the axon growth-promoting effects of the native astrocyte ECM, indicating that combinations of ECM components are likely to contribute to the enhanced axon outgrowth observed with selected protoplasmic astrocyte ECM.

3.4.5 Design of Experiments (DoE) approach for testing effects of selected protoplasmic ECM proteins on V2a interneurons

To systematically evaluate the combinatorial effects of selected protoplasmic ECM proteins on V2a interneuron axon growth, we implemented a custom design of experiments (DoE) approach using five candidate proteins - laminin-1, fibronectin, perlecan, Col18a1, and anti-thrombin III – at defined high and low concentrations. Initial testing revealed that perlecan and Col18a1, when incorporated individually at high concentrations into the hydrogel, consistently resulted in minimal axon growth across all V2a interneuron aggregates. Based on these findings, we hypothesized that these

proteins are unlikely to promote axon growth at their K_d concentrations and thus adjusted their low concentration values to match their respective K_d levels (Table 3.1). The custom DoE included all second through fifth order interactions among the 5 proteins generating 36 unique protein combinations at the high and low concentrations for the hydrogel-based axon growth assays (Supplementary Table 3.1). From these, we designated a subset as “high priority combinations” defined by the inclusion of perlecan and col18a1 at the high concentrations (Table 3.3). These high priority combinations produced significantly different axon growth responses from V2a interneuron aggregates (Fig. 3.5B), with the most effective combinations containing at least 3 of the 5 proteins at high concentrations - mostly Col18a1, perlecan, and anti-thrombin III - suggesting potential synergistic interactions. However, even the most effective combinations did not fully recapitulate selected protoplasmic ECM effects on axon growth despite showing significant differences among themselves (Fig. 3.5B, D). This highlights the complexity of ECM-mediated signaling.

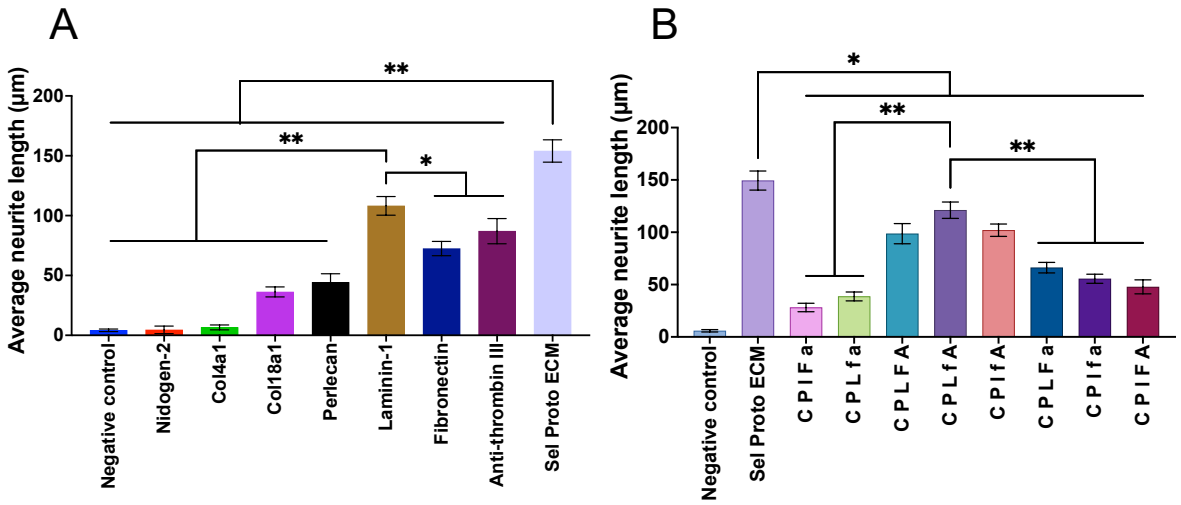

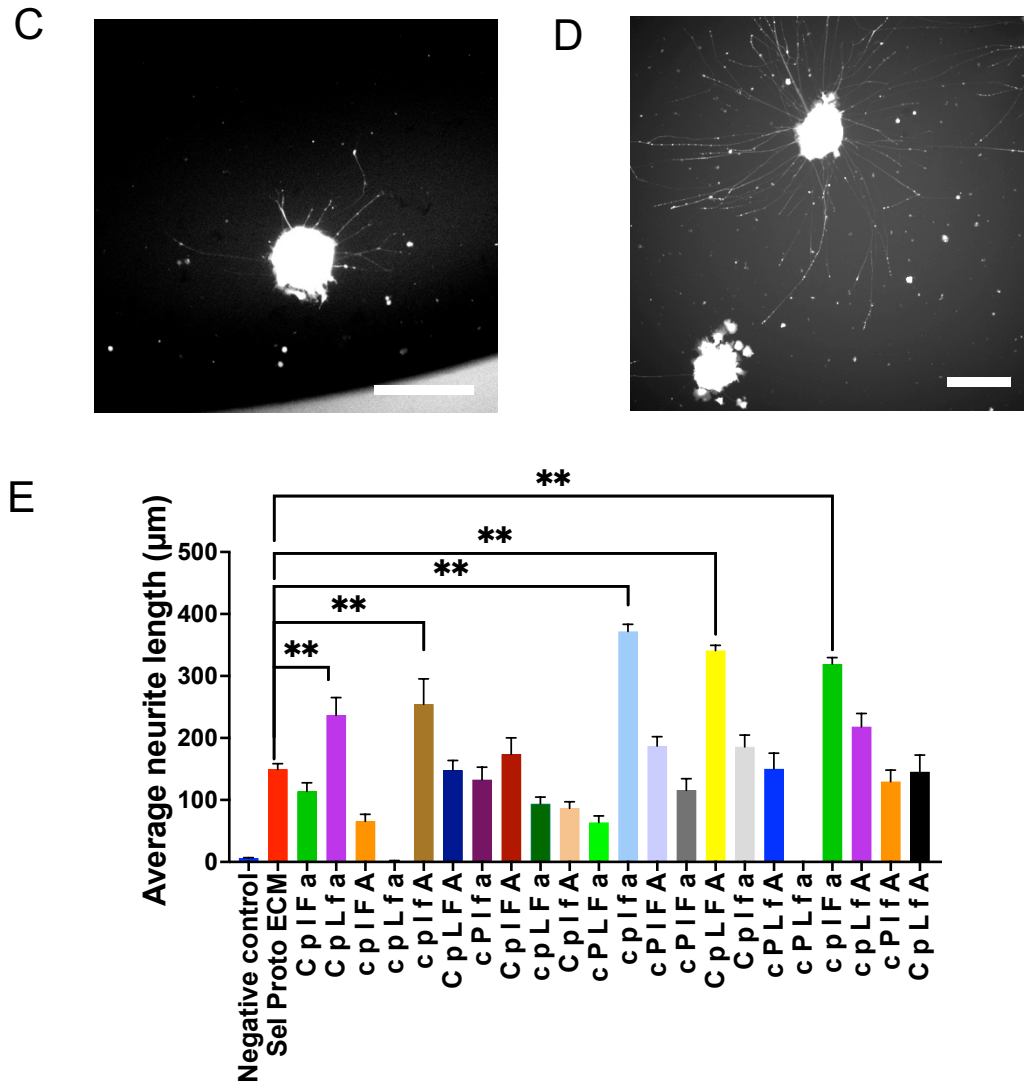

Figure 3.5 Effects of single proteins and combinations of 5 proteins at high and low concentrations on axon growth of V2a interneurons in comparison to selected protoplasmic ECM in hydrogel A) Individual proteins at high concentrations demonstrated that laminin-1, fibronectin, and anti-thrombin III significantly increased axon growth with at least 50 neuroaggregates; * $p<0.05$ and ** $p<0.01$ comparison to selected protoplasmic ECM (Sel Proto ECM) in hydrogel. **B)** Combinations with at least 3 proteins at high concentration increased axon growth significantly compared to other combinations tested with at least 50 neuroaggregates; * $p<0.05$ and ** $p<0.01$ in comparison to Sel Proto ECM in hydrogel. **C)** Representative image of V2a interneuron aggregates in HAmF-PEGdiMal hydrogel with 5 proteins in combination with 2 µg/mL col18a1 (C), 10.3 µg/mL perlecan (P), 10µg/mL laminin-1 (l), 55µg/mL fibronectin (F), 1.49µg/mL anti-thrombin III (a); Scale bar= 100µm **D)** Representative image of V2a interneuron aggregates in HAmF-PEGdiMal hydrogel with V2a interneuron aggregates in HAmF-PEGdiMal hydrogel with 5 proteins in combination with 2µg/mL col18a1 (C), 2.06 µg/mL perlecan (p), 50µg/mL laminin-1 (L), 55µg/mL fibronectin (F), 7.45 µg/mL anti-thrombin III (A); Scale bar= 100µm **E)** Additional combinations demonstrated the highest axon growth with at least 15 neuroaggregates; * $p<0.05$ and ** $p<0.01$ comparison to Sel Proto ECM in hydrogel

Table 3.3 The specific combinations from JMP custom design output (Supplementary Table 1) that contain only high concentrations (5* K_d) of perlecan and col18a1 with both low and high concentrations for laminin-1, fibronectin, and anti-thrombin III.

Combination	Col18a1 (µg/mL)	Perlecan (µg/mL)	Laminin-1 (µg/mL)	Fibronectin (µg/mL)	Anti-thrombin III (µg/mL)	Abbreviation
1 and 27	2	10.3	10	55	1.49	C P I F a
3	2	10.3	50	11	1.49	C P L f a
8 and 11	2	10.3	50	55	7.45	C P L F A
9	2	10.3	50	11	1.49	C P L f A
18 and 24	2	10.3	10	11	7.45	C P I f A
29	2	10.3	50	55	1.49	C P L F a
31	2	10.3	10	11	1.49	C P I f a
35	2	10.3	10	55	7.45	C P I F A

To further explore the impact of protein concentration on axon growth, we next tested the remaining combinations in which the perlecan and Col18a1 were included at the low concentrations, aiming to determine whether these conditions could match or exceed the axon growth supported by selected protoplasmic ECM containing hydrogels. Several of these combinations resulted in axon growth levels that were comparable to – or significantly greater than – those observed with fully selected protoplasmic ECM in the hydrogels (Fig. 3.5C, E). The most effective combinations either included all five proteins at low concentrations or featured high concentrations of laminin-1 and fibronectin in combination with Col18a1 (Supplementary Table 1). Additionally, some of the combinations that achieved axon growth responses similar to the selected protoplasmic ECM contained 2 or 3 of the 5 proteins at high concentration, suggesting that specific concentration-dependent interactions among these proteins can recapitulate the ECM's growth promoting effects. Overall, these findings demonstrate that modulating the concentrations of a defined set of five ECM proteins within a hydrogel platform can effectively mimic the growth supportive properties of protoplasmic ECM, offering a promising strategy for engineering biomaterial platforms.

Table 3.4 The high priority combinations from DoE in which the high concentrations for all the proteins are adjusted to 50µg/mL (Supplementary Table 2)

Combination	Col18a1 (µg/mL)	Perlecan (µg/mL)	Laminin-1 (µg/mL)	Fibronectin (µg/mL)	Anti-thrombin III (µg/mL)	Abbreviation
1 and 27	50	50	10	50	1.49	C P I F a
3	50	50	50	11	1.49	C P L f a
8 and 11	50	50	50	50	50	C P L F A
9	50	50	10	11	1.49	C P L f A
18 and 24	50	50	10	11	50	C P I f A
29	50	50	50	50	50	C P L F a
31	50	50	10	11	1.49	C P I f a
35	50	50	10	50	50	C P I F A

To minimize variability in axon growth outcomes due to differences in protein concentration, we standardized the high concentration of perlecan, Col18a1, and anti-thrombin III to 50 µg/mL and re-evaluated the original 36 protein combinations using this adjusted formulation. These combinations were tested in the HAmF-PEGdiMal hydrogel system, with a focus on the same nine high priority combinations (Supplemental Table 3.2, Table 3.4). Most of these high priority combinations supported axon growth levels that were comparable to or significantly higher than those observed with the selected protoplasmic ECM hydrogel (Fig. 3.6A-C). Notably, combinations containing at least four proteins at the 50µg/mL concentration yielded the most robust axon growth responses. In contrast, the repeated low priority combinations – also tested at 50µg/mL – largely failed to support axon extension (Supplemental Fig. 3.6A-C). Combinations with only one or two proteins at high concentrations were similarly ineffective while those with three proteins at high concentration showed moderate axon growth (Supplemental Fig. 6A-C). These findings underscore the importance of protein concentration and combinatorial effects in modulating axon growth within the hydrogel platform. They suggest that tuning the concentration of key ECM proteins can effectively

replicate the axon growth-promoting properties of selected protoplasmic astrocyte ECM, offering a promising strategy for engineering defined, reproducible ECM mimetics.

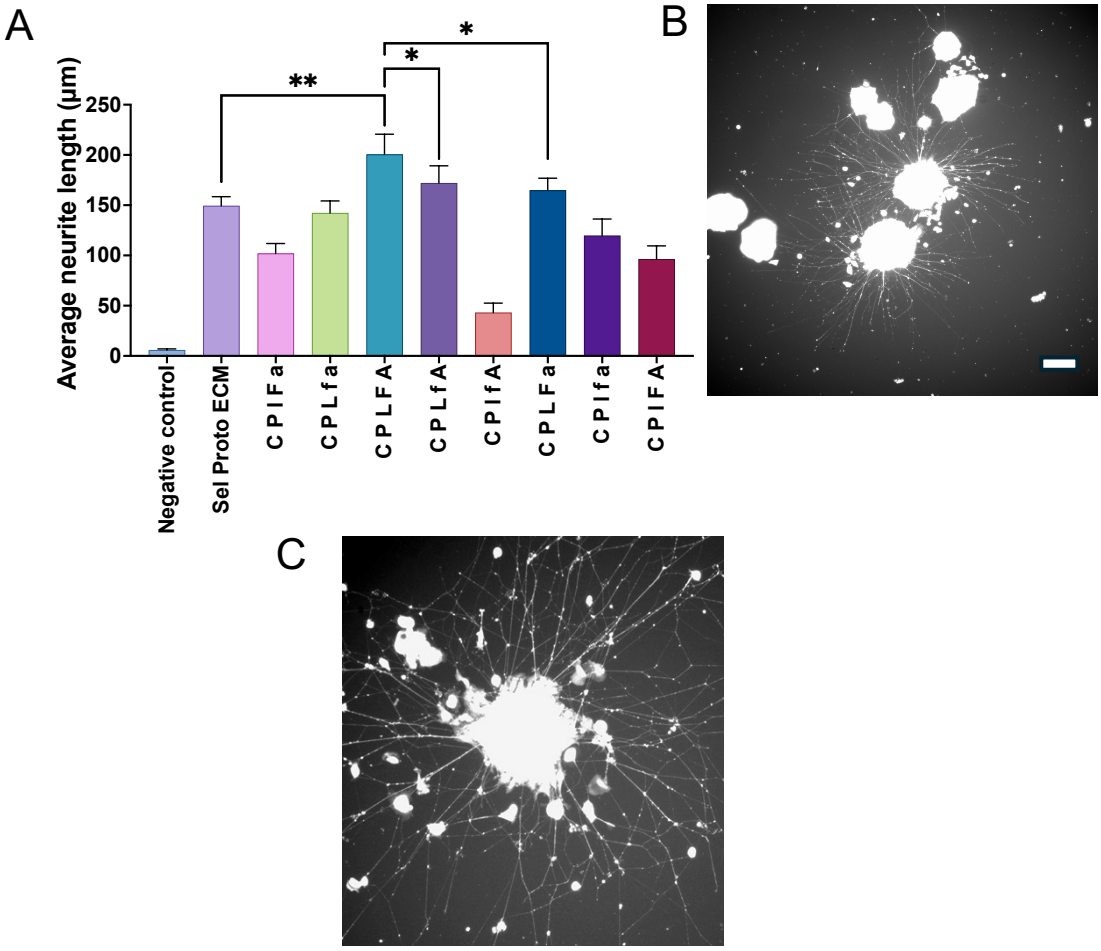

Figure 3.6 Effects of combinations with high concentration being 50µg/mL for each protein on axon growth of V2a interneurons in comparison to selected protoplasmic astrocyte ECM in hydrogel A) Certain combinations increased axon growth of V2a interneurons significantly compared to other combinations and selected protoplasmic ECM with at least 50 neuroaggregates in 3 trials; * $p<0.05$ and ** $p<0.01$ **B)** Representative image of V2a interneuron aggregates in HAmF-PEGdiMal hydrogel with 50µg/mL col18a1 (C), 50µg/mL perlecan (P), 50µg/mL laminin-1 (L), 50µg/mL fibronectin (F), and 50µg/mL anti-thrombin III (A)**. C)** Representative image of V2a interneuron aggregates in HAmF-PEGdiMal hydrogel with 50µg/mL col18a1 (C), 50µg/mL perlecan (P), 50µg/mL laminin-1 (L), 11µg/mL fibronectin (f), and 1.49µg/mL anti-thrombin III (a).

3.4.6 Least squares regression model for axon growth of V2a interneurons by selected protoplasmic ECM mimetic hydrogels

To identify key protein interactions influencing axon growth, we developed a least squares regression model based on the average axon growth values from the 36

protein combinations tested in the hydrogel system. The model produced a strong fit (R=0.98), revealing several statistically significant interactions (p=0.02) that contribute to axon growth outcomes (Fig. 3.7A). The effect summary highlighted perlecan as a major factor, with its concentration significantly impacting axon growth (Supplemental Fig. 3.7A). Additionally, interactions in Col18a1 and laminin-1, fibronectin, and anti-thrombin III were found to be significant, as were interactions between perlecan and anti-thrombin III or fibronectin and anti-thrombin III. The interaction profiler further illustrates how varying concentrations between two proteins influences axon growth (Fig. 3.7B). For example, increasing Col18a1 in the presence of low concentrations of laminin-1, is predicted to reduce axon growth, while pairing it with high laminin-1 concentrations is predicted to enhance axon growth (Fig. 3.7B). In contrast, increasing Col18a1 concentration is predicted to have little effect with either low or high concentrations of fibronectin. Given the complexity of the full model – which included all second through fifth order interactions – applied a stepwise regression approach to reduce overfitting and isolate the most impactful variables.

The refined model maintained a strong fit (p-value= 0.0001, R= 0.96 Fig. 3.7C) confirming that varying concentrations of perlecan and laminin-1 significantly influence axon growth (Supplemental Fig. 3.7B). It also identified key interactions among Col18a1 and laminin-1, fibronectin and anti-thrombin III, and 4 proteins of col18a1, perlecan, laminin-1, and anti-thrombin III as critical contributors to axon growth of V2a interneurons (Fig. 3.7B). These regression models provide a valuable framework for predicting protein interactions and optimizing ECM mimetic formulations to replicate the axon growth promoting effects of selected protoplasmic astrocyte ECM.

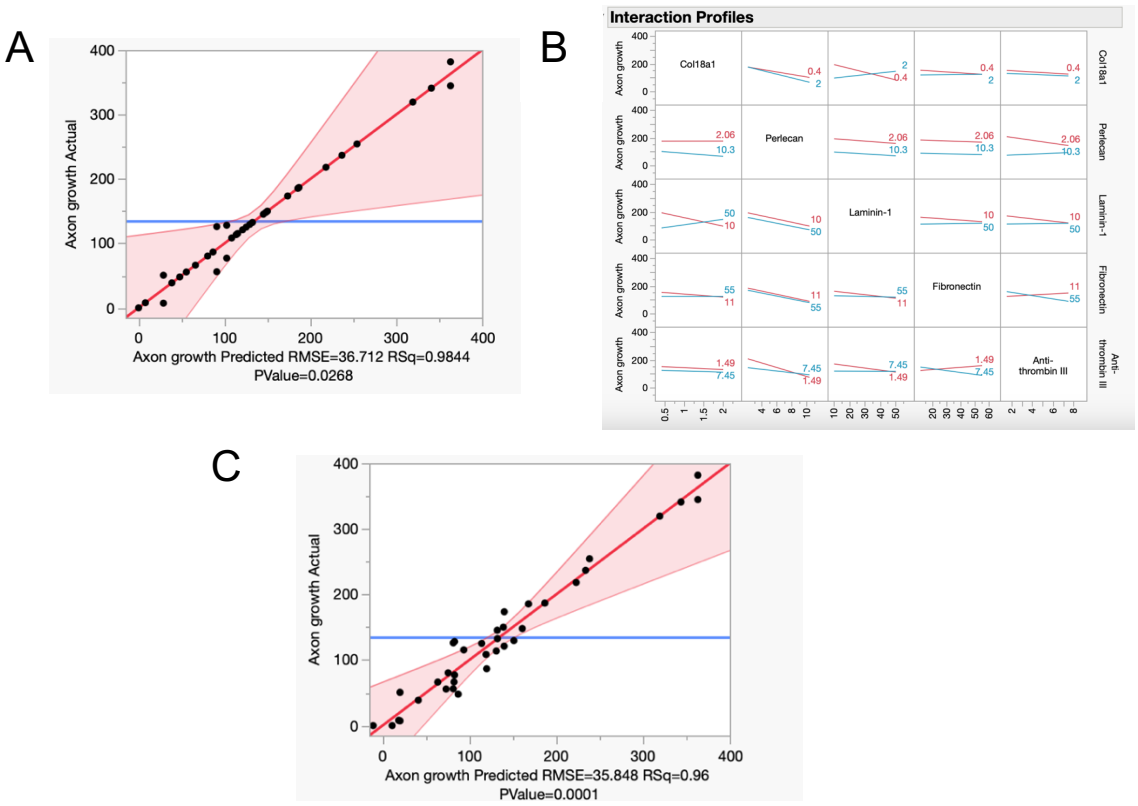

Figure 3.7 Standard least squares regression model from DoE observations demonstrates key potential interactions of the 5 proteins (tested at low concentration of K_d and high concentration of 5* K_d) that impact axon growth significantly A) Actual vs predicted plot that demonstrates a best fit line by least squares model with significant p-value and small error for the model based on the average axon growth values for each of the 36 combinations. **B)** Interaction profiler output that displays the predictions of axon growth based on two-way interactions at varying concentrations of specific protein pair. **C)** Actual vs predicted plot that demonstrates a best fit line by stepwise regression model reduction with significant p-value and small error for the model based on the average axon growth values for each of the 36 combinations.

Using axon growth data from runs where all proteins were tested at high concentrations (50µg/mL), we developed the least squares regression model that revealed enhanced predictive power and highlighted key protein interactions influencing V2a interneuron axon growth. The model demonstrated a strong fit (R= 0.985, p= 0.0006; Supplemental Fig. 7C) and the effect summary identified laminin-1, fibronectin, perlecan, and Col18a1 as significant contributors to axon growth (p-value <0.05; Supplemental Fig. 7D). Notably, the model revealed several critical interactions including those between Col18a1 and perlecan, laminin-1 and fibronectin, and a three-

way interaction among laminin-1, fibronectin, and anti-thrombin III. These interactions may serve as key targets for future studies aimed at optimizing axon growth responses. Interaction profiling showed that axon growth generally increased when one protein's concentration was raised while the other was maintained at a high level, except in the case of Col18a1 and anti-thrombin III, where this trend did not hold (Supplemental Fig. 7E). To reduce model complexity and overfitting, a stepwise regression approach was applied. The resulting reduced model retained the same interaction profiles and continued to highlight the importance of varying the concentrations of Col18a1, laminin-1, perlecan, and fibronectin in modulating axon growth of V2a interneurons (Supplemental Fig. 7G). Key interactions – such as those between Col18a1 and anti-thrombin III and between laminin-1 and fibronectin- can be further studied and optimized for increasing axon growth. Overall, this refined regression model offers a valuable predictive tool for guiding the design of ECM mimetic hydrogels and optimizing protein concentrations to enhance axon growth of V2a interneurons.

3.5 Discussion

It was observed that the selected protoplasmic astrocytes more effectively supported axon growth of V2a interneurons compared to selected fibrous astrocytes. We hypothesize that this is due to phenotypic match, where grey matter astrocytes support more growth of neurons that project in grey matter, while white matter astrocytes may better support more growth of neurons that project in white matter[331]. In the spinal cord, protoplasmic astrocytes are in close contact with both excitatory and inhibitory synapses in grey matter. In contrast, fibrous astrocytes interact with oligodendrocytes and neurons to facilitate myelination and provide metabolic support

essential for maintaining axon integrity. A variety of glial-derived cues influence synapse formation and neural signaling, which can, in turn, impact axon growth. Further investigation into fibrous astrocytes may reveal their potential to support axon growth from neurons that reside in or project through white matter[331]. There might be a potential to understand how to utilize the astrocyte subtype specific ECM to promote connectivity between white matter and gray matter neuron populations. This could be studied through application of pre- and post-synaptic marker staining with various neuron populations on the decellularized substrates and ECM hydrogels to demonstrate potential synaptic connectivity. It is also important to consider that

Spectral counting using AdjNSAF, a reliable semi-quantitative proteomic metric, informed our identification of key proteins that were upregulated in selected protoplasmic astrocyte decellularized ECM. We demonstrated that varying concentrations of the five specific proteins incorporated into the HAmF-PEGdiMal hydrogel promoted neurite outgrowth, suggesting these proteins may play a central role in recapitulating the ECM composition of protoplasmic astrocytes. Additionally, proteins present at lower ratios (1-2) in selected protoplasmic ECM may also contribute to axon growth and should be considered for inclusion in future protein formulations to explore more complex protein-protein interactions. Some proteins used in this study, such as for Col18a1, were human versions, which may have influenced axon growth outcomes given that the neuronal cells were of murine origin. The limited availability of species-specific protein isoforms from reliable commercial sources constrained our ability to include other candidates identified through proteomic analysis. Moving forward, incorporating known secreted growth factors identified in the ECM proteomics dataset

(Supplemental Table 1) could further refine the composition of the selected protoplasmic ECM mimic.

This study highlights the use of a HAmF-PEGdiMal hydrogel system combined with interneuron aggregates as a platform for evaluating axon growth with average neurite length. The modular nature of this hydrogel system allows for the incorporation of individual proteins to assess their specific effects on axon growth. Due to the nature of aggregates being composed of numerous neurons, it is hard to measure neurite growth per neuron. The tracing of the total neurite outgrowth area can account for potential differences in types of neurite outgrowth. However, it is important to acknowledge that there are observations of aggregates producing both short and long neurites that can be potentially due to interactions of certain neurons with the protein components in the hydrogel. There can be uses in post-injury microenvironment for hydrogel combinations to support longer extensions from aggregates and others to support more sprouting of shorter neurites around the aggregates. While the initial results with five selected proteins are promising, further investigation is needed to elucidate the molecular interactions among these proteins and their collective influence on axon growth. Further experiments should aim to determine binding affinities (K_d values) of each protein within the hydrogel, which would involve quantifying specific binding coefficients. Additionally, it will be important to study how these proteins interact with the hydrogel's individual components and to characterize their diffusion over time - potentially using enzyme-linked immunosorbent assays (ELISA). Protein size relative to the hydrogels' pores may influence accessibility for the V2a interneuron aggregates. A deeper understanding of these hydrogel-protein interactions will enable more precise

tuning of the hydrogel composition for both *in vitro* and *in vivo* applications. Moreover, sequencing mRNA from V2a interneurons could help identify key receptors that interact with the tested proteins. These insights would support more accurate determination of optimal protein concentrations to better mimic the native protoplasmic ECM environment. One limitation of hydrogel-based ECM models is the potential for heterogeneous distribution of proteins, which may lead to variability in protein-aggregate contact and axon growth responses. Overall, systematic exploration of the different parameters of the protein hydrogel platform interacting with V2a interneurons could further enhance its utility in promoting axon growth.

In this study, we employed the foundational principles of DoE to develop a predictive model assessing how combinations of proteins influence axon growth. DoE serves as a powerful framework for identifying optimal concentration ranges that can be tuned to engineer biomaterials mimicking the selected protoplasmic ECM. The outputs from our custom DoE model provide a valuable basis for generating future hypotheses regarding how specific protein-protein interactions and concentration dynamics affect axon growth. Our analysis highlighted key two-way interactions – specifically between fibronectin and anti-thrombin III, Col18a1 and laminin-1, and perlecan and anti-thrombin III- as promising targets for further investigation. These pairings offer insight into how modulating protein binding affinities and concentrations may enhance axon growth. Notably, the least squares regression model revealed that higher concentrations of the five tested proteins yielded more significant interaction effects, suggesting that protein concentration directly influences the molecular kinetics, as well as the capacity to engage with V2a interneurons. These findings underscore the importance of further

exploring hydrogel-protein dynamics to optimize the composition of selected protoplasmic ECM mimetics. Such optimization could lead to enhanced axon growth *in vitro* and *in vivo*.

3.6 Conclusion

The study demonstrated that ECM derived from selected protoplasmic astrocytes enhanced axon growth of V2a interneurons compared to ECM from selected fibrous astrocytes, in both 2D surface and 3D hydrogel environments. We hypothesized that this effect is due to a higher expression of axon growth promoting ECM proteins by selected protoplasmic astrocytes. However, clinical translation of hydrogels containing native protoplasmic astrocyte ECM is limited by challenges, such as quality control and lengthy differentiation timeline required to generate this ECM. To address this, the study aimed to develop a defined, protein-based mimic of protoplasmic ECM in the HAmF-PEGdiMal hydrogel system. Proteomic analysis identified candidate ECM proteins enriched in selected protoplasmic astrocytes, and five key proteins were selected based on criteria including commercial availability, human or mouse version, and relevance to neuronal function. These proteins were incorporated in the hydrogel system and tested using a DoE approach to evaluate their individual and combined effects on axon growth at varying concentration. The results revealed that specific combinations of these five proteins could replicate or even surpass the axon growth promoting effects of native protoplasmic ECM. These defined protein mixtures within the HAmF-PEGdiMal hydrogel represent a promising, tunable biomaterial platform for SCI therapy with potential for future *in vivo* validation in SCI models.

Chapter 4: Summary and future directions

4.1 Summary of findings

This thesis characterizes mESC-derived astrocyte phenotypes and their associated ECM proteins that can be instrumental in promoting axon growth from V2a interneurons *in vitro*. Astrocyte phenotypes have complex, often contradictory, roles *in vivo.* Certain secreted ECM molecules contribute to an inhibitory microenvironment, while others limit inflammation and protect remaining neuronal connections. It is important to study the astrocyte-specific cues that can promote a pro-regenerative microenvironment for axon growth. Our lab utilized mESCs as a scalable source of neural cell types and developed differentiation protocols resulting in heterogeneous cultures of fibrous and protoplasmic astrocyte cultures, which contain also other cell types, such as neurons, oligodendrocytes, and undifferentiated stem cells. This makes it difficult to elucidate astrocyte-specific cues.

To overcome the challenge of heterogeneity in mESC-derived astrocyte cultures, we utilized and characterized puromycin-selectable cell lines for astrocyte subtypes. In chapter 2, we determined an optimal time point of puromycin selection in the astrocyte differentiation protocol that generated enriched astrocyte subtype cultures that contained a lower percentage of other cell types (i.e. low levels of NFM and RIP expression) and a higher percentage of cells positive for astrocyte markers (i.e. high Aqp4 expression in protoplasmic and high Aqp4 and A2B5 expressions in fibrous). These selected astrocyte cultures did stain positive for both immature (CD44 and vimentin) and mature astrocyte markers (Aldh1L1 and S100β). Furthermore, the selected astrocyte cultures were able to uptake glutamate, respond to an inflammatory

stimulus, and produce calcium transients. Bulk RNA-sequencing of the selected astrocyte phenotypes demonstrated that selected protoplasmic astrocytes have upregulated genes in pathways related to ECM reorganization and cell adhesion. Selected fibrous astrocytes have upregulated genes in pathways related to cellular proliferation and localized protein synthesis at synapses. With ICC staining, selected protoplasmic astrocytes express Col4a1 and selected fibrous astrocytes express Wnt7a and integrin7a. Furthermore, both selected astrocyte substrate types supported SV2 expression in V2a interneurons. Overall, the selected astrocyte subtypes can be used as a cellular platform to study astrocyte-specific cues for promoting axon growth of different neuronal populations.

In chapter 3, we focused on observing the effects of unselected and selected astrocyte phenotypes on V2a interneurons, a critical excitatory neuronal population. We discovered that selected protoplasmic astrocytes and their membrane, ECM, and conditioned media components significantly increased axon growth of V2a interneurons compared to fibrous astrocyte components. Furthermore, we observed that selected protoplasmic ECM in HA-based hydrogels promotes higher levels of axon growth than selected fibrous ECM hydrogel, indicating there are differential proteins within the ECM compositions of the astrocyte subtypes that drive this axon growth difference. Through proteomics, we identified a list of ECM proteins that are upregulated in selected protoplasmic astrocytes to be further tested in the previously described hydrogel platform for their ability to promote axon growth of V2a interneurons.

The proteins were chosen based on a criterion including manufacturer availability, mouse or human origin, and untagged modality. 5 proteins (collagen18a1,

perlecan, laminin-1, fibronectin, and anti-thrombin III) were tested in HAmF-PEGdiMal hydrogels. DoE was used to identify various combinations of high and low concentrations of these proteins to test. It was found that there were defined mixtures of proteins that can promote greater levels of axon growth compared to selected protoplasmic ECM. Thus, these combinations in the hydrogel can be utilized as a selected protoplasmic astrocyte ECM mimetic for axon growth applications without the need for astrocyte differentiation to harvest ECM. The defined mixture in the hydrogel can be a scalable approach for improving axon growth of V2a interneurons post SCI.

4.2 Thoughts on future directions

Astrocyte phenotypic components can modulate axon growth to stimulate neuronal connectivity. In this section, I describe a few approaches that can utilize selected astrocyte phenotypes as a platform to study astrocyte-derived proteins and genes for informing SCI therapies. *In vitro* methods with electrophysiology can aid in probing astrocyte-regulated connectivity between interneurons and motor neurons. Furthermore, transgenic methods can modify selected astrocyte phenotypes to increase or decrease expression of certain axon-growth related genes. The selected protoplasmic ECM mimetic material has potential for understanding the interactions amongst the 5 proteins and proteins to V2a interneuron receptors to fine-tune the concentrations of proteins in the hydrogel. This material can be tested in SCI models to examine neuronal connectivity and potential functional recovery *in vivo*.

4.2.1 Astrocyte phenotype support of neuronal connections *in vitro*

This thesis demonstrated that protoplasmic astrocytes support axon growth from V2a interneurons more than fibrous astrocytes. The observation could be due to

protoplasmic astrocytes and V2a interneurons both residing in the gray matter of the spinal cord. It is possible to repeat the 2D and 3D studies in this thesis to investigate the potential of selected fibrous astrocytes to offer greater support of axon growth to white matter neurons, such as CST neurons. Understanding the astrocyte phenotypic support for different neuron populations that connect through both gray and white matter can help to rebuild CPG connectivity. The proteomics data has provided a list of proteins upregulated in selected fibrous ECM, such as spondin-1, Col2a1, and vitronectin, that can be used to build also defined protein hydrogel as a selected fibrous ECM mimetic to support white matter neurons. It would be interesting to utilize a combination of astrocyte phenotypic ECM proteins to support axon growth of gray and white matter neurons involved in CPG connectivity for motor neuron signals[332]. These *in vitro* neuron connections could be assessed by utilizing multielectrode array (MEA) or whole cell recordings to probe electrophysiological properties of different neurons that might indicate rhythmicity important for locomotor movements, such as left-right alternation, breathing, and swimming[333]. The amplitude and duration of bursting in co-culture of different neuron populations and mono-neural cultures with astrocyte phenotypic factors can help determine the key microenvironment to support neuronal connectivity. Applying selected protoplasmic and fibrous-derived ECM proteins to co-culture of interneurons, CST neurons, and motor neurons can be used as an *in vitro* model for circuit formation. This *in vitro* investigation could give potential ideas on how connectivity might be probed in a future in vivo study with the inclusion of both astrocyte subtype ECM proteins.

4.2.2 Probing glial crosstalk for effects on axon growth

As observed in spinal cord development and SCI, astrocytes, oligodendrocytes, and microglia are influenced and matured by different cues secreted from the cell types. Specifically, hiPSC-derived immature astrocytes secrete tissue inhibitor of metalloproteinase 1 (TIMP1), a protein that regulates OPC differentiation and oligodendrocyte maturation[92]. This crosstalk between astrocytes and oligodendrocytes can aid in improving recovery post brain injury by promoting both axon growth and myelination[92]. During spinal cord development, fibrous astrocytes and oligodendrocytes are derived from the same bipolar progenitor cells, suggesting that these populations can influence each other's glial fate and maturation. During reactive astrogliosis post SCI, it is observed that the secretion of pro-inflammatory cytokines by pro-inflammatory microglia M1 promotes an A1 reactive astrocyte state. This suggests the importance of generating *in vitro* tri-culture models of the main glial types to study triggers of certain cell type phenotypes and their effects on axon growth of neuronal populations. Currently, the multi-culture models consist of two types of glia and neurons. However, it would be interesting to expand the model to include three types of glia with neurons[334,335]. This model can utilize protoplasmic and fibrous astrocytes derived from the selectable transgenic cell lines as described in this thesis to further understand the effects of astrocyte phenotypic differences on maturation of oligodendrocytes and regulation of microglia phenotypes in neuroinflammatory settings.

Specifically, it would be important to understand the ECM composition from stem cell-derived oligodendrocytes and other neuron populations in healthy and injured spinal cords to compare to the astrocyte ECM composition. This can provide understanding of

how different cellular players can contribute to the overall microenvironment. It can help also predict potential changes in tailoring the concentrations of proteins in selected protoplasmic astrocyte ECM mimetic material that can overcome the injured microenvironment to promote axon growth.

4.2.3 Harnessing astrocyte-neuron interactions for axon growth

This thesis explores the effects of selected astrocyte phenotypes on V2a interneurons with a simple metric of average neurite length. Axon extension is a result of complex receptor-ligand binding events between astrocytes and neurons that lead to growth cone changes. Astrocytes secrete ECM proteins and growth factors that can interact with neural cell adhesion molecules (NCAM), integrin receptors, and N-cadherin on neurons. RNA-sequencing of V2a interneurons can elucidate the presence of certain genes for receptors and CAMs that might specifically interact with the 5 proteins utilized in the selected protoplasmic ECM hydrogel[336]. These interactions potentially drive axon growth effects of the defined mixtures of proteins in hydrogel. Blocking antibody experiments targeting either the selected protoplasmic astrocyte ECM protein or corresponding neural receptor can potentially affect the axon growth of V2a interneurons. This will help us to understand the roles of astrocytes in neuronal connectivity[112,337]. Utilizing selected protoplasmic astrocyte ECM proteins in the hydrogel that could bind to specific receptors found on V2a interneurons can allow for synthesis of more targeted protein hydrogel design for axon growth. It would be interesting to conduct actin filament staining in the growth cone area with time-lapse super resolution microscopy for qualitative observations of growth cone dynamics in response to selected astrocyte ECM proteins[197]. Another key aspect is the role of

calcium oscillations in glia promoting transmitter release that can influence synapse plasticity and strength. It is possible that modulation of gap junction proteins, such as connexin 43 and 30, for selected protoplasmic astrocytes and purinergic receptors for selected fibrous astrocytes might alter the calcium oscillatory activity to increase synapse formation[338]. Thus, axon growth and growth cone dynamics can serve as readouts for blocking connexin activity and purinergic receptor, such as P2X7[339].

4.2.4 Changes in astrocyte reactivity to a more repair phenotype

Astrocytes respond to different types of CNS injuries by 1) adopting A1 reactivity where changes can be detrimental to neurons and 2) adopting A2 reactivity where changes can be neuroprotective. It would be advantageous to identify and apply factors that can drive switch from A1 reactivity to A2 reactivity for potential increase in neuroprotection in the harmful lesion microenvironment. RNA-sequencing and proteomic datasets of A1 astrocytes and the data gathered in this thesis about selected astrocyte phenotypes can provide a starting point of identifying signals that can be manipulated for driving the change from A1 to A2[40,106]. The blocking of certain inflammatory pathways, such as mTOR and mitogen activated protein kinase (MAPK), stimulated by TNF-α and LPS, that drive A1 reactivity, might increase the axon growth support of fibrous astrocytes[40,106]. After identifying a key molecule in blocking these inflammatory pathways, lentiviral transduction can create knockdown of pathway activity in primary or stem cell-derived astrocytes to test effects on axon growth. Astrocyte reactivity can be assessed using C3 levels as a readout for A1 reactivity and S100a10 for A2 reactivity[340]. Another quality that can be tuned to change astrocyte reactivity *in vivo* is the material stiffness of an implantable biomaterial[341]. The astrocyte reactivity

can also be affected by materials with lower stiffness potentially reversing astrogliosis. The stiffness of HA-mF-PEG-diMal hydrogel could be modulated with less amounts of crosslinker to decrease the material stiffness for implantation studies. The impacts of implantation could be evaluated with GFAP, IL-1β, and Yes-associated protein (YAP) staining to visualize the decrease of A1 astrocyte reactivity, S100a10 staining to indicate increases in A2 reactive astrocyte presence, and neurofilament staining to observe axon growth[44,341]. In addition, astrocytic GTPase ras homolog gene family member A (RhoA) can modulate or restrict astrocyte reactivity through activating myosin, compacting actin, and increasing F-actin content to lower GFAP and CSPG expression[342]. This suggests that cytoskeletal dynamics in astrocytes could be targeted with application of actin inhibitors and RhoA agonists/stimulants to promote a more reparative astrocyte phenotype. Development of SCI therapies that can deliver astrocyte-derived factors promoting A2 astrocyte reactive response may generate a more pro-regenerative microenvironment for axon growth.

4.2.5 Protein engineering in biomaterial studies

This thesis developed a hydrogel with defined mixtures of a few specific protoplasmic ECM proteins that can support high levels of average neurite length of V2a interneurons and be a potential controlled selected protoplasmic astrocyte ECM mimetic. The biomaterial was synthesized with the addition of commercially available mouse or human versions of ECM proteins at different concentrations in HAmF-PEGdiMal hydrogels. The ECM mimetic was a simplified version since it contained only 5 specific proteins in combination, while the ECM is composed of thousands of proteins.

However, the combination of a relatively few proteins in a hydrogel platform captured ECM effects on axon growth and could be a scalable biomaterial solution.

While we observed high axon growth within these protein hydrogels, it would be helpful to further characterize the interactions of the proteins and material. The biomaterial is modular with parameters that can be tuned to study the impacts on axon growth. Each of the 5 proteins could interact with HA in solution before addition of the PEG cross-linker based on protein isoelectric point[343,344]. Thus, the binding coefficient for each protein should be determined for HAmF. Understanding these protein dynamics might affect the mechanical properties of the hydrogel and how it can facilitate axon extension from V2a interneuron aggregates[343]. In addition, protein distribution in the hydrogel can dictate protein interactions and presentation of cell-binding sites to V2a interneuron aggregates for axon extension[345]. The protein release can be evaluated with BCA assay and specific protein ELISAs to understand the timing of bioactivity for each protein that can impact axon growth for longer translational studies *in vivo*[309]. Overall, these parameters can affect biomaterial stiffness in supporting neuron viability and be modulated to ensure softer protein-based hydrogels[343].

4.2.6 Investigating effects of matrix metalloproteinases (MMPs) for axon growth *in vitro*

Secreted and membrane-bound MMPs have been found to degrade ECM proteins to lead axons to grow over various substrates[346,347]. The levels of different MMPs in healthy and injured CNS may regulate neurite extension and synaptic stability of different neuron populations. Specifically, MMP2 and MMP9 have been identified as critical proteases that cleave inhibitory proteoglycan protein cores enriched in the SCI lesion core and aid in recovering axon growth[347–351]. While neurons can express MMPs

2 and 9 for ECM remodeling, it has been found that astrocytes in the healthy and injured spinal cord can secrete MMPs[351]. It would be interesting to apply MMP 2 and 9 inhibitors to V2a interneurons seeded on selected protoplasmic astrocyte ECM substrate to determine if the MMPs play a role in V2a interneurons remodeling ECM as a way for promoting axon growth.

4.2.7 Combinatorial therapies in SCI models

The main concern with astrocyte transplantation in the SCI lesion site is that quiescent or A2 reactive astrocytes can potentially change into A1 reactive astrocytes and become detrimental to functional recovery. Thus, it is important to consider utilizing stem-cell derived glia to identify beneficial components that are translational without the need for astrocyte transplantation. These glial cues can be incorporated into biomaterial systems and can directly activate pathways that shift A1 to A2 astrocytes. These combinatorial therapies can be tested in rat cervical hemisection SCI models to study more impacts on V2a interneuron axon growth and CST sprouting for functional respiratory and forelimb improvements in open-field behavioral tests[145].

Specifically, it would be important to test the effects of the selected protoplasmic ECM mimetic on particularly V2a interneurons in the SCI model. The V2a interneurons from lamina VII of the lumbar spinal cord can be identified in isolated rat spinal cord preparations with the dorsal surface of the lumbar segments removed[352]. Whole-cell patch clamp recordings with electrodes on the spinal cord sections can measure firing properties for identification of bursting and rhythmic patterns for V2a interneurons[353]. These parameters could affect diaphragm muscle activity and ventilation[156]. This can be supported with GFAP, S100a10, Chx10, and neurofilament staining to understand the

microenvironment response to protein-hydrogel. It would further be important to see if there are increases in rhythmic generation parameters contributing to motor neuron outputs due to increased axon growth of V2a interneurons. It would be interesting to modify the hydrogel to contain both selected fibrous and protoplasmic ECM proteins that can target axon growth of white and gray matter neuron populations *in vivo*. The dual nature of the selected astrocyte ECM mimetic biomaterial might increase axon growth of both V2a interneurons and CST neurons and increase potential sprouting in spared tissue[138].

To modulate concentrations of 5 proteins in the hydrogel for axon growth, it might be important to consider the changes of the 5 proteins post SCI model. This can increase our understanding of the certain proteins to be at high versus low concentrations in the hydrogel. Immunohistochemical staining of the 5 proteins and neurofilaments in tissue from injured rats could indicate the potential levels and distribution of the proteins at the injury site and how they might localize in relation to neural extensions. The levels of the 5 proteins in the injury microenvironment could be affected by severity and timescale post the rat cervical hemisection SCI. Hydrogels can contain either low or high concentrations of the 5 proteins depending on the presence of proteins post-injury to form a pro-regenerative microenvironment.

4.3 Concluding Remarks

As more methodologies of RNA-sequencing and proteomics are being developed and utilized, astrocyte phenotypic gene and protein expression can be investigated in different native and injury environments both *in vitro* and *in vivo*. These discovery studies can allow better definitions of astrocyte phenotypes and changes that might be

critical in generating astrocyte phenotypes that support repair. The astrocyte-derived factors can further be studied as targets for promoting neuronal connections to improve functional recovery after SCI. I am excited to see future research that continues evolving our understanding of astrocyte complexities and shines light on the beneficial functions and characteristics of non-reactive and reactive astrocytes on different neuron populations affected by CNS diseases.

Appendix A: Supplemental figures for Chapter 2

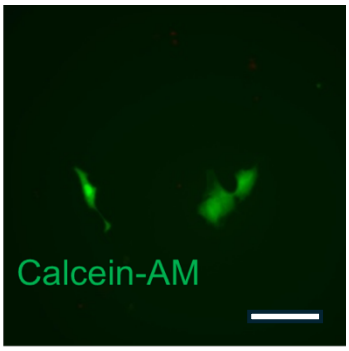

Supplemental Figure 2.1: Selected protoplasmic astrocytes at day 18 post 4μg/mL puromycin 1 day exposure stained by calcein-AM to demonstrate morphology; Scale bar=100μm

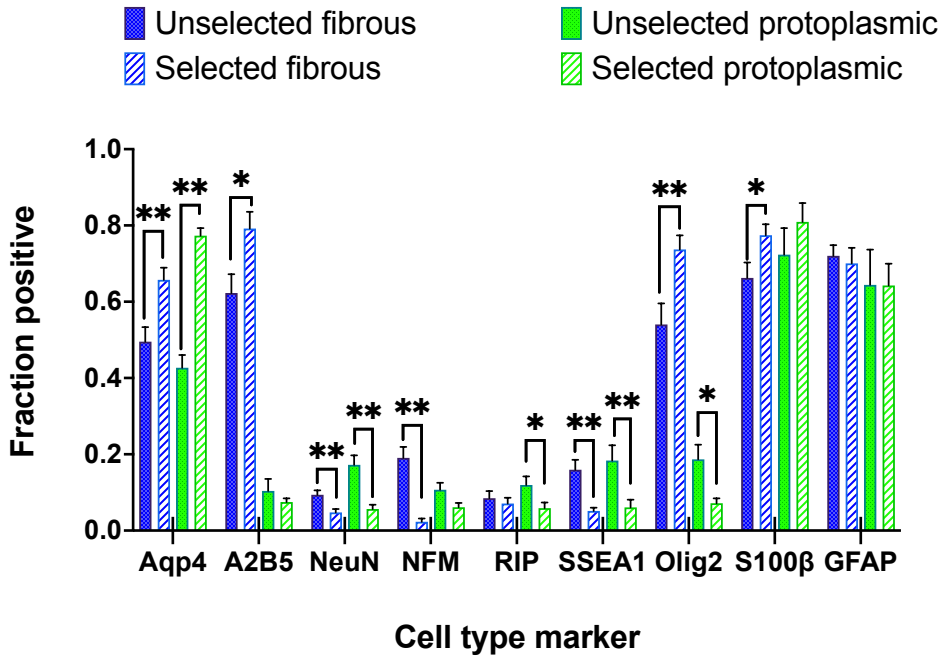

Supplemental Figure 2.2: Immunocytochemistry analysis of astrocyte phenotypic markers at day 21 for protoplasmic astrocytes and day 23 for fibrous astrocytes (N=3-4; ** p<0.01; Error bars= SEM).

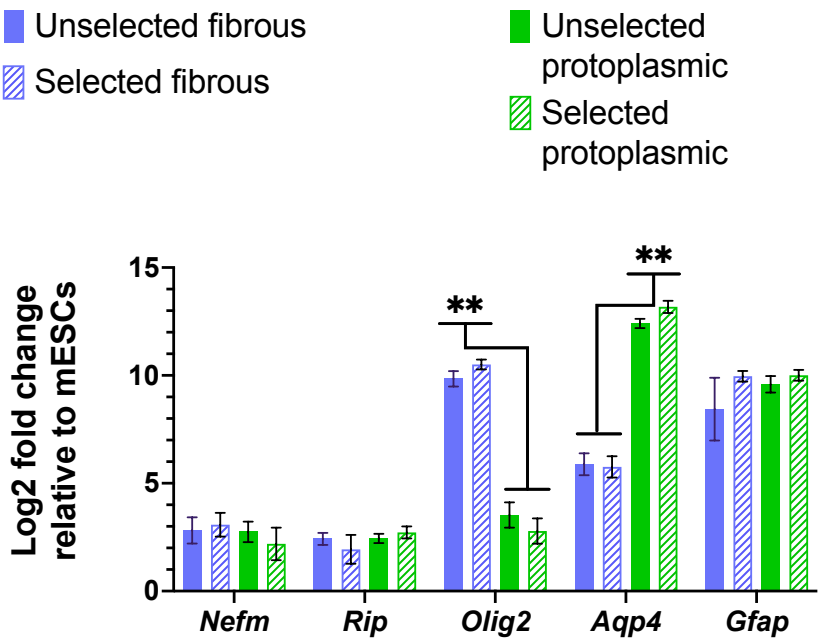

Supplemental Figure 2.3: Gene expression of astrocyte phenotypic markers and markers for other cell types; low mRNA expression levels present for other cell types while high mRNA expression levels present for astrocytes (N=5-6; ** p<0.01; Error bars= SEM).

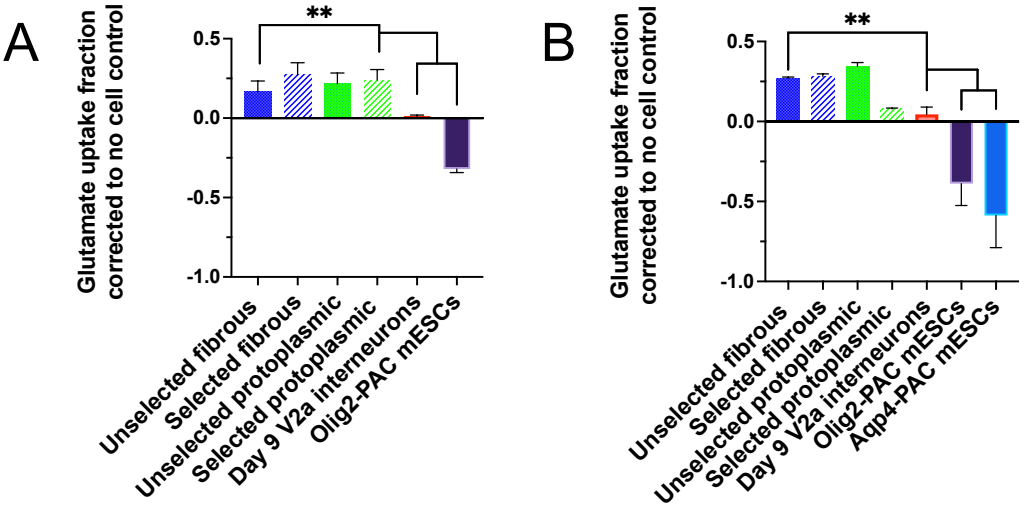

Supplemental Figure 2.4: Glutamate uptake fraction of unselected and selected astrocytes **A)** Using the Sigma Aldrich kit, glutamate uptake fraction of unselected and selected astrocyte subtype cultures with starting amount as 200μM glutamate and corrected for non-specific glutamate uptake in cell free control (glutamate uptake fraction of 0.37) that demonstrates astrocyte functionality post-puromycin selection (N=3 for astrocyte subtypes, N=1 with 2 technical replicates for neurons, N=2 for Olig2-PAC mESCs; ** p<0.01, Error bars= S.E.M). **B)** Using the Abcam kit, glutamate uptake fraction of unselected and selected astrocyte subtype cultures with starting amount as 200μM glutamate and corrected for non-specific glutamate uptake in cell free control (glutamate uptake fraction of 0.35) that demonstrates astrocyte functionality post-puromycin selection (N=1 for astrocyte subtypes with 2 technical replicates, N=3 for neurons, N=3 for Olig2-PAC mESCs and Aqp4-PAC mESCs; ** p<0.01, Error bars= S.E.M).

A

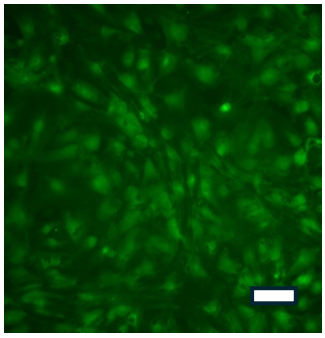

B

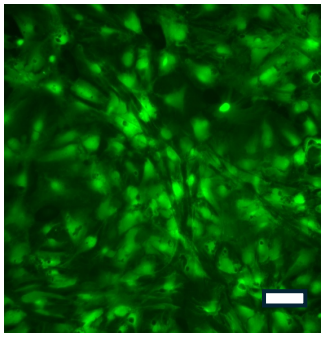

C

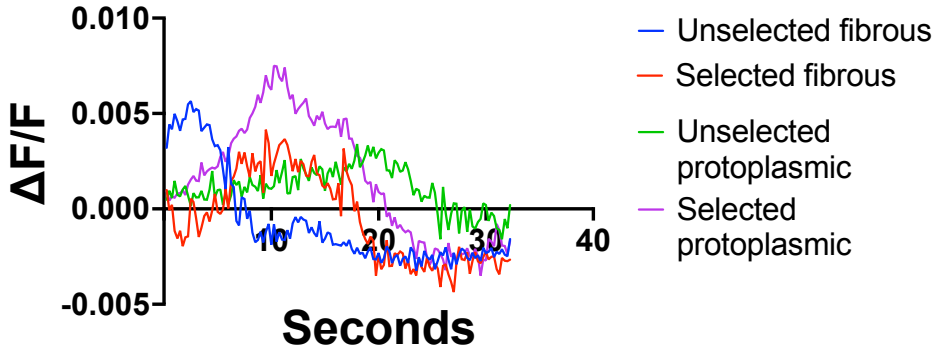
0.010
0.005
0.000
-0.005
ΔF/F
10
20
30
40
Seconds
Unselected fibrous
Selected fibrous
Unselected protoplasmic
Selected protoplasmic

D

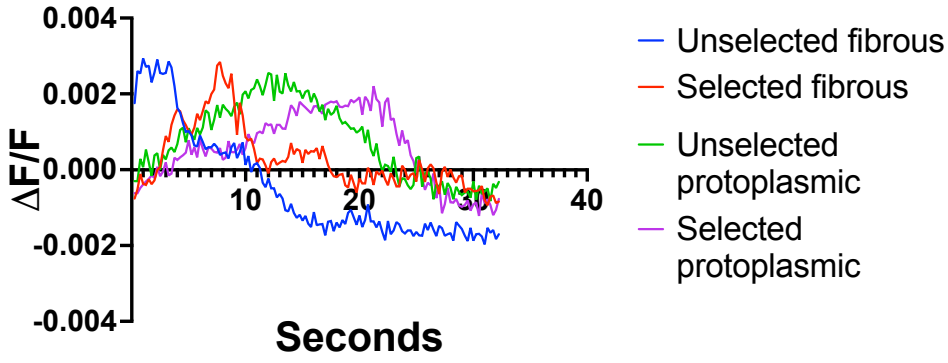
0.004
0.002
0.000
-0.002
-0.004
ΔF/F
10
20
30
40
Seconds
Unselected fibrous
Selected fibrous
Unselected protoplasmic
Selected protoplasmic

E

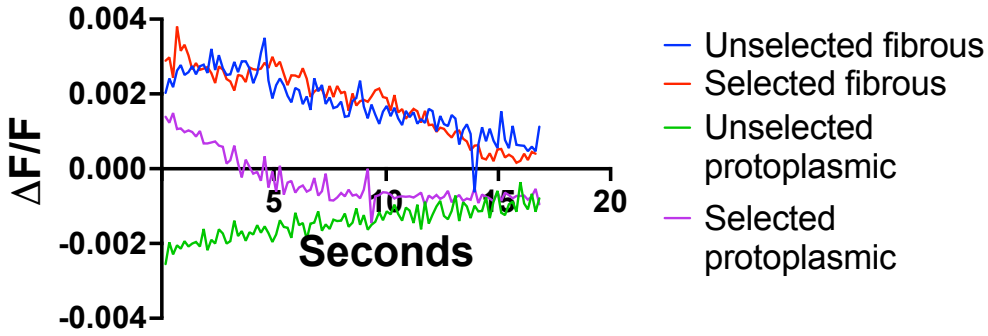
0.004
0.002
0.000
-0.002
-0.004
ΔF/F
5
10
15
20
Seconds
Unselected fibrous
Selected fibrous
Unselected protoplasmic
Selected protoplasmic

Supplemental Figure 2.5: A) Fluorescent image of Fluo-4AM (green) in selected protoplasmic astrocytes at time of 0 seconds (Scale= 100μm). **B)** Fluorescent image of Fluo-4AM (green) in selected protoplasmic astrocytes at a time of 28 seconds (Scale= 100μm). **C)** Average metric of ΔF/F over time of 32.5 seconds for 5 ROIs in unselected and selected astrocytes with ATP addition **D)** Average calcium transients of 20 ROIs over 32.5 seconds imaging for unselected and selected astrocyte phenotypes **E)** Average ΔF/F over time of 15 seconds for each unselected and selected astrocyte phenotype without any ATP addition

Supplemental Table 2.1. Least squared means, p-value, and FDR step-ups for certain genes upregulated in selected protoplasmic astrocytes compared to selected fibrous astrocytes

Gene name	Selected protoplasmic astrocyte LS mean	Selected fibrous astrocyte LS mean	P-value	False discovery rate (FDR) step-up
Tlr2	21.37	3.47	8.65×10^{-5}	$7.\times 10^{-3}$
Tlr3	40.90	11.23	6.11×10^{-4}	0.02
Casp1	9.34	1.01	7.58×10^{-4}	0.02
Ccl2	109.67	6.31	2.22×10^{-3}	0.03
Cfap126	17.12	0.87	1.71×10^{-4}	0.01
Cryab	138.14	15.27	2.61×10^{-4}	0.01
Igfbp5	6778.88	1239.31	2.43×10^{-4}	0.01
Tagln	503.95	14.58	7.96×10^{-4}	0.02
C3	1383.38	0.74	6.45×10^{-7}	3.61×10^{-3}
S100a6	201.66	13.51	1.95×10^{-4}	0.01
Ccn3	17.05	0.68	1.54×10^{-5}	4.66×10^{-3}
Cxcl10	54.69	1.33	4.63×10^{-5}	6.53×10^{-3}
Igfbp7	60.38	2.03	1.16×10^{-3}	0.02

Supplemental Table 2.2. P-values for top 20 significantly expressed identified genes in comparing RNA-sequencing data of selected protoplasmic astrocytes to selected fibrous astrocytes with mouse genome

Gene name	P-value
Slc43a3	2.15×10^{-7}
C3	6.45×10^{-7}
Ece2	1.04×10^{-6}
Snx10	1.46×10^{-6}
Rasgrf1	1.78×10^{-6}
Slco1a5	2.20×10^{-6}
Ttc12	2.25×10^{-6}
Ngf	3.14×10^{-6}
Pitpnm3	3.14×10^{-6}
Tep1	3.19×10^{-6}
Plpp2	3.31×10^{-6}
Eno2	3.62×10^{-6}
Rsph1	3.63×10^{-6}
Pdlim2	3.68×10^{-6}
Cers4	3.74×10^{-6}

Agbl2	$3.81x10^{-6}$
Gch1	$3.88x10^{-6}$
Myadm	$4.21x10^{-6}$
Micall2	$5.20x10^{-6}$

Appendix B: Supplemental figures for Chapter 3

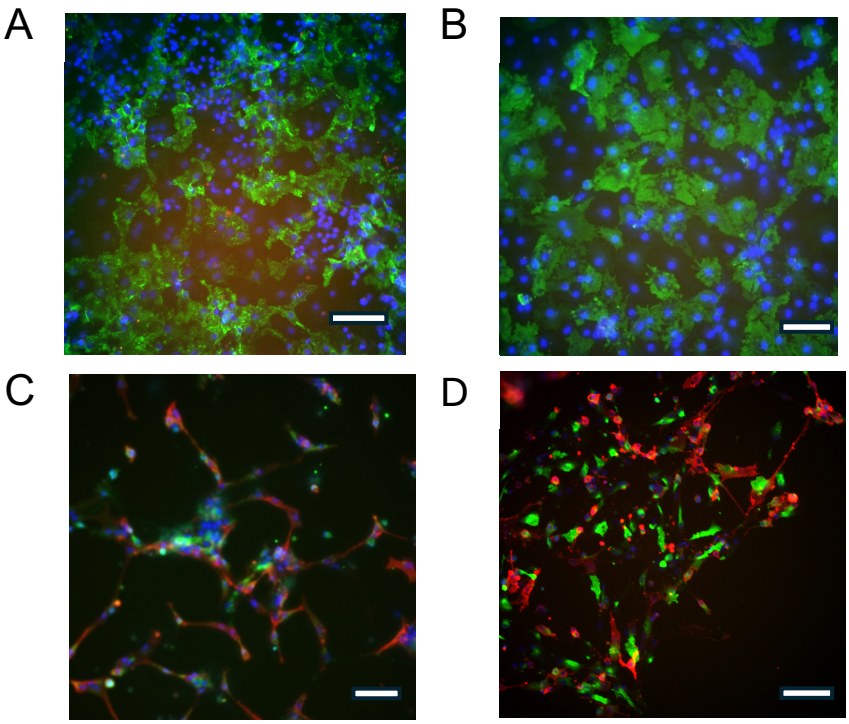

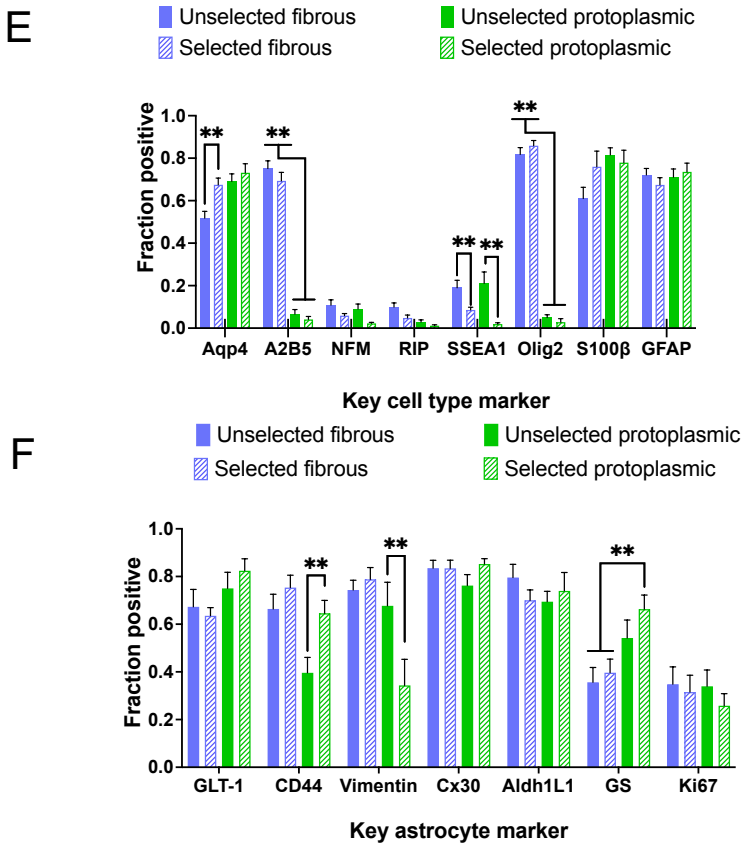

Supplemental Figure 3.1. Astrocytes cultured post-selection maintain expression astrocyte phenotypic markers and low fraction of cells positive for other cell types A, B) Representative images of Aqp4 (green), A2B5 (red) stained at day 27 for unselected and selected protoplasmic cultures respectively with maintenance of $Aqp4^{+}/A2B5^{-}$ staining in selected protoplasmic astrocytes (Scale bar= 100μm). **C, D)** Representative images of Aqp4 (green), A2B5 (red) staining at day 27 unselected and selected fibrous cultures showing high double positive staining post-selection indicative of maintenance of fibrous phenotype at that time point (Scale bar= 100μm). **E)** ICC analysis with fraction positive for neural cell type markers in day 27 unselected and selected astrocyte cultures. *p<0.05, **p<0.01 compared to respective unselected astrocyte phenotypes (N=5, Error bars= S.E.M.). The analysis showed an overall decrease in other cell types and maintenance of astrocyte-specific markers at a later time point in the differentiation protocol. **F)** ICC analysis with fraction positive for astrocytic markers in day 27 unselected and selected astrocyte cultures. *p<0.05, **p<0.01 compared to respective unselected astrocyte phenotypes (N=5, Error bars= S.E.M.). The analysis showed an overall decrease in other cell types and maintenance of astrocyte-specific markers at mature time point

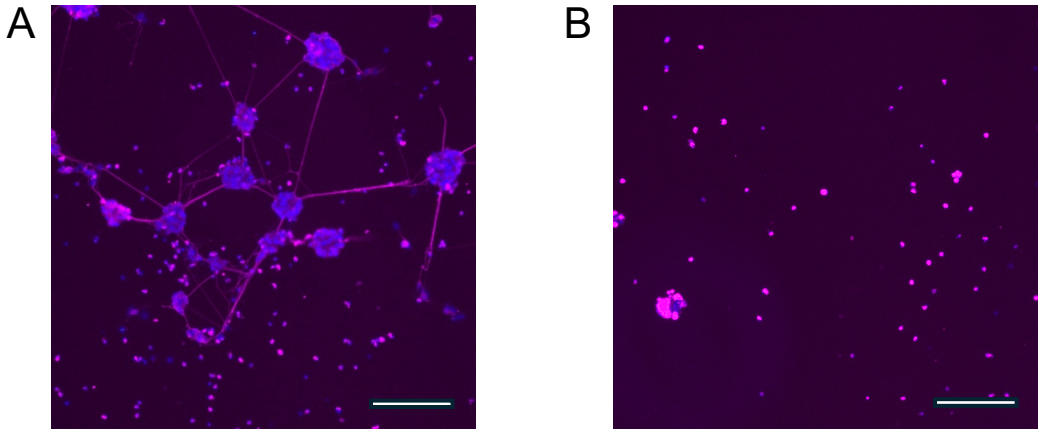

Supplemental Figure 3.2. Characterization of astrocyte phenotype substrates used to study axon growth effects A) Representative image of V2a interneurons seeded on decellularized selected protoplasmic astrocytes; these neurons are stained with βIII-Tubulin (red) and DAPI (blue); Scale bar= 100μm. **B)** Representative image of V2a interneurons seeded on decellularized selected fibrous astrocytes; these neurons are stained with βIII-Tubulin (red) and DAPI (blue); Scale bar= 100μm

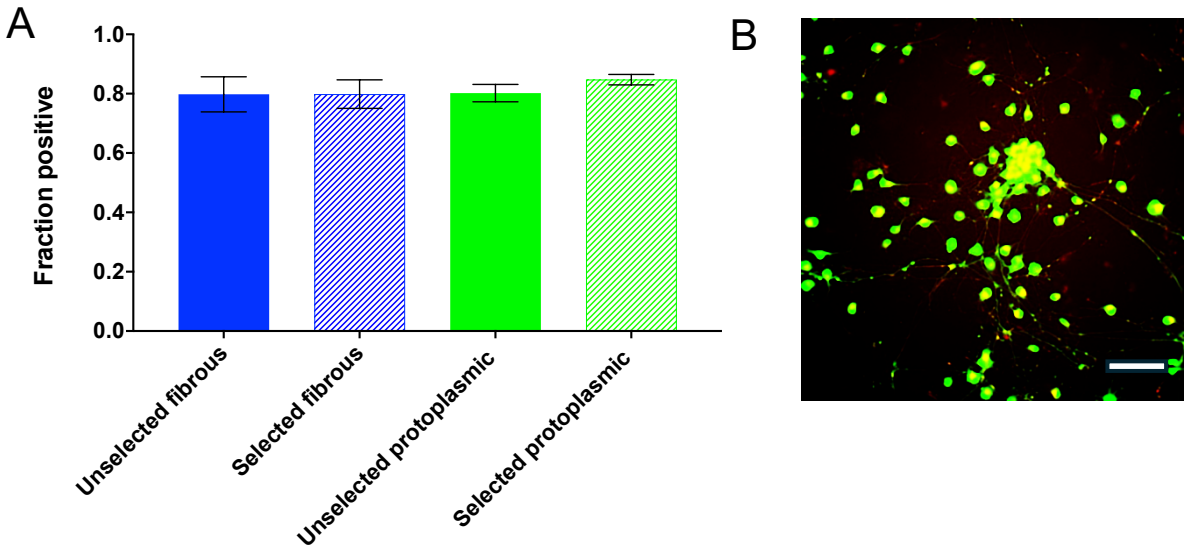

Supplemental Figure 3.3. Characterization of astrocyte phenotype substrates used to study axon growth effects A) There are high fraction of V2a interneurons positive for N=3 **B)** Representative image of SV2 (red) staining in V2a interneurons (green) seeded on live selected protoplasmic astrocytes Scale bar= 100μm

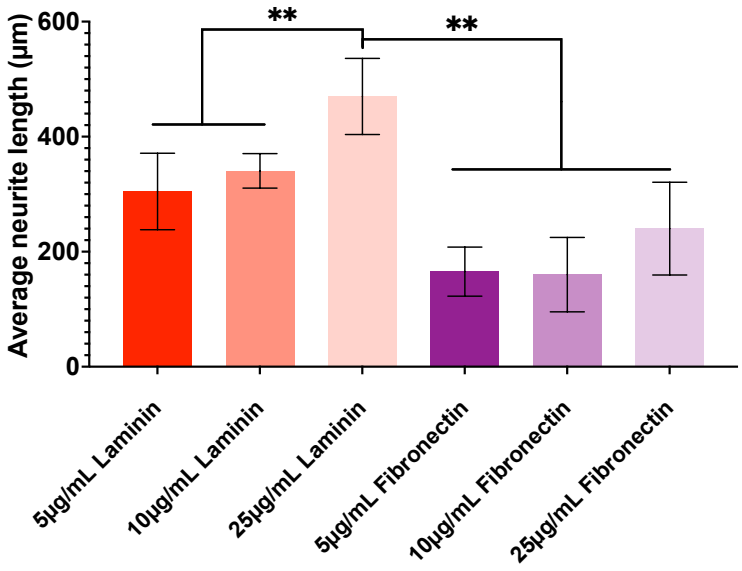

Supplemental Figure 3.4. 25μg/mL laminin significantly increases axon growth compared to other laminin and all of fibronectin concentrations
Single proteins at different concentrations in hydrogel-based system on V2a interneuron aggregates for axon growth potential with high laminin concentration having the most significant effect on axon growth; ** $p<0.01$

Supplemental Table 3.1. Growth factors upregulated in selected protoplasmic astrocyte ECM.

Protein	Ratio of AdjNSAF for selected protoplasmic to AdjNSAF for selected fibrous
Ciliary neurotrophic factor	1000

Pro-epidermal growth factor	1000
Bone morphogenic protein-4	7.67
Pleiotrophin	1.6
Insulin-like growth factor 2	0.83
Fibroblast growth factor 2	0.45
Brain-derived growth factor	0.33
Beta nerve growth factor	0

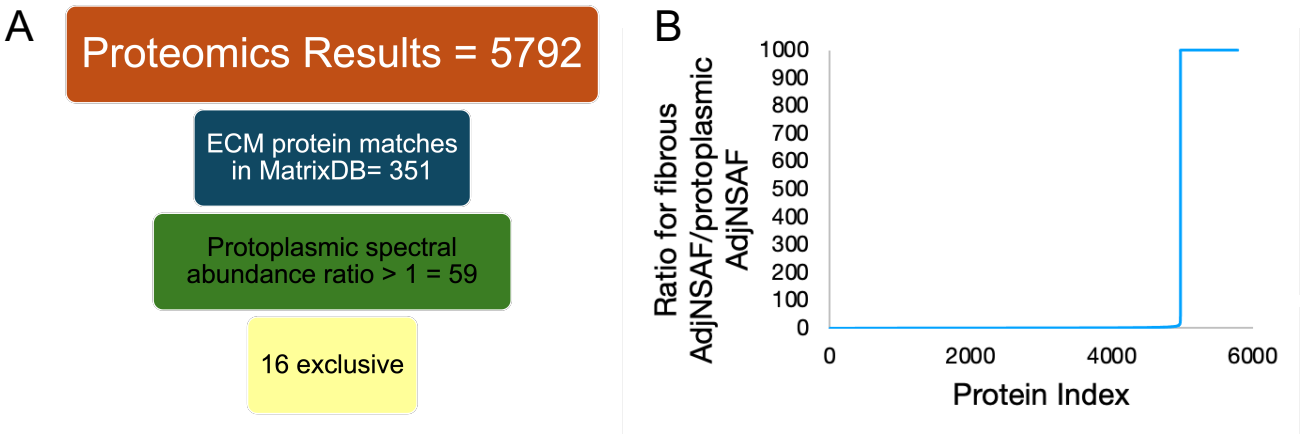

Supplemental Figure 3.5. Certain proteins are upregulated and are only present in selected fibrous ECM A) Schematic flow diagram that details the number of ECM proteins that can be identified from proteomic results and the number of protein candidates for selected protoplasmic astrocytes that highly upregulated for future studies. **B)** Proteins sorted by ratio of AdjNSAF in selected fibrous to selected protoplasmic demonstrate that there are proteins that are at low abundance in selected fibrous ECM and proteins with index after around 5000 are more prevalent in selected fibrous ECM compared to selected protoplasmic ECM.

Supplemental Table 3.2. Custom DoE output for fifth-order interactions between perlecan, laminin-1, fibronectin, col18a1, and anti-thrombin-III at low for K_d and high for 5 times K_d; The last column provides an abbreviation to denote high and low concentrations for each protein in a particular combination as capital first letter of protein and lower-case first letter of protein respectively

Combination number	Col18a1 (µg/mL)	Perlecan (µg/mL)	Laminin-1 (µg/mL)	Fibronectin (µg/mL)	Anti-thrombin III (µg/mL)	Abbreviation
1	2	10.3	10	55	1.49	C P I F a
2	2	2.06	10	55	1.49	C p I F a
3	2	10.3	50	11	1.49	C P L f a
4	2	2.06	50	11	1.49	C p L f a
5	0.4	2.06	10	55	7.45	c p I F A
6	0.4	2.06	50	11	1.49	c p L f a
7	0.4	2.06	10	11	7.45	c p I f A
8	2	10.3	50	55	7.45	C P L F A
9	2	10.3	50	11	7.45	C P L f A
10	2	2.06	50	55	7.45	C p L F A

11	2	10.3	50	55	7.45	C P L F A
12	0.4	10.3	10	11	1.49	c P l f a
13	2	2.06	10	55	7.45	C p l F A
14	0.4	2.06	50	55	1.49	c p L F a
15	2	2.06	10	11	7.45	C p l f A
16	0.4	10.3	50	55	1.49	c P L F a
17	0.4	2.06	10	11	1.49	c p l f a
18	2	10.3	10	11	1.49	C P l f a
19	0.4	10.3	10	55	7.45	c P l F A
20	0.4	10.3	10	55	1.49	c P l F a
21	2	2.06	50	55	7.45	C p L F A
22	0.4	10.3	50	55	1.49	c P L F a
23	2	2.06	10	11	1.49	C p l f a
24	2	10.3	10	11	7.45	C P l f A
25	0.4	2.06	50	55	1.49	c p L F a
26	0.4	10.3	50	11	7.45	c P L f A
27	2	10.3	10	55	1.49	C P l F a
28	0.4	2.06	10	11	1.49	c p l f a
29	2	10.3	50	55	1.49	C P L F a
30	0.4	10.3	50	11	1.49	c P L f a
31	2	10.3	10	11	1.49	C P l f a
32	0.4	2.06	10	55	1.49	c p l F a
33	0.4	2.06	50	11	7.45	c p L f A
34	0.4	10.3	10	11	7.45	c P l f A
35	2	10.3	10	11	7.45	C P l f A
36	2	2.06	50	11	7.45	C p L f A

Supplemental Table 3.3. Custom DoE output for fifth-order interactions perlecan, col18a1, laminin-1, fibronectin, and anti-thrombin-III at low for K_d and high at 50µg/mL; The last column provides an abbreviation to denote high and low concentrations for each protein in a particular combination as capital first letter of protein and lower-case first letter of protein respectively

Combination number	Col18a1 (µg/mL)	Perlecan (µg/mL)	Laminin-1 (µg/mL)	Fibronectin (µg/mL)	Anti-thrombin III (µg/mL)	Abbreviation
1	50	50	10	50	1.49	C P l F a
2	50	2.06	10	50	50	C p l F a
3	50	50	50	11	1.49	C P L f a
4	50	2.06	50	11	1.49	C p L f a
5	0.4	2.06	10	50	50	c p l F A
6	0.4	2.06	50	11	1.49	c p L f a
7	0.4	2.06	10	11	50	c p l f A
8	50	50	50	50	50	C P L F A
9	50	50	50	11	50	C P L f A
10	50	2.06	50	50	50	C p L F A
11	50	50	50	50	50	C P L F A

12	0.4	50	10	11	1.49	c P l f a
13	50	2.06	10	50	50	C p l F A
14	0.4	2.06	50	50	1.49	c p L F a
15	50	2.06	10	11	50	C p l f A
16	0.4	50	50	50	1.49	c P L F a
17	0.4	2.06	10	11	1.49	c p l f a
18	50	50	10	11	1.49	C P l f a
19	0.4	50	10	50	50	c P l F A
20	0.4	50	10	50	1.49	c P l F a
21	2	2.06	50	50	50	C p L F A
22	0.4	50	50	50	1.49	c P L F a
23	50	2.06	10	11	1.49	C p l f a
24	50	50	10	11	50	C P l f A
25	0.4	2.06	50	50	1.49	c p L F a
26	0.4	50	50	11	50	c P L F a
27	50	50	10	50	1.49	C P l F a
28	0.4	2.06	10	11	1.49	c p l f a
29	50	50	50	50	1.49	C P L F a
30	0.4	50	50	11	1.49	c P L f a
31	50	50	10	11	1.49	C P l f a
32	0.4	2.06	10	50	1.49	c p l F a
33	0.4	2.06	50	11	50	c p L f A
34	0.4	50	10	11	50	c P l f A
35	50	50	10	11	50	C P l f A
36	50	2.06	50	11	50	C p L f A

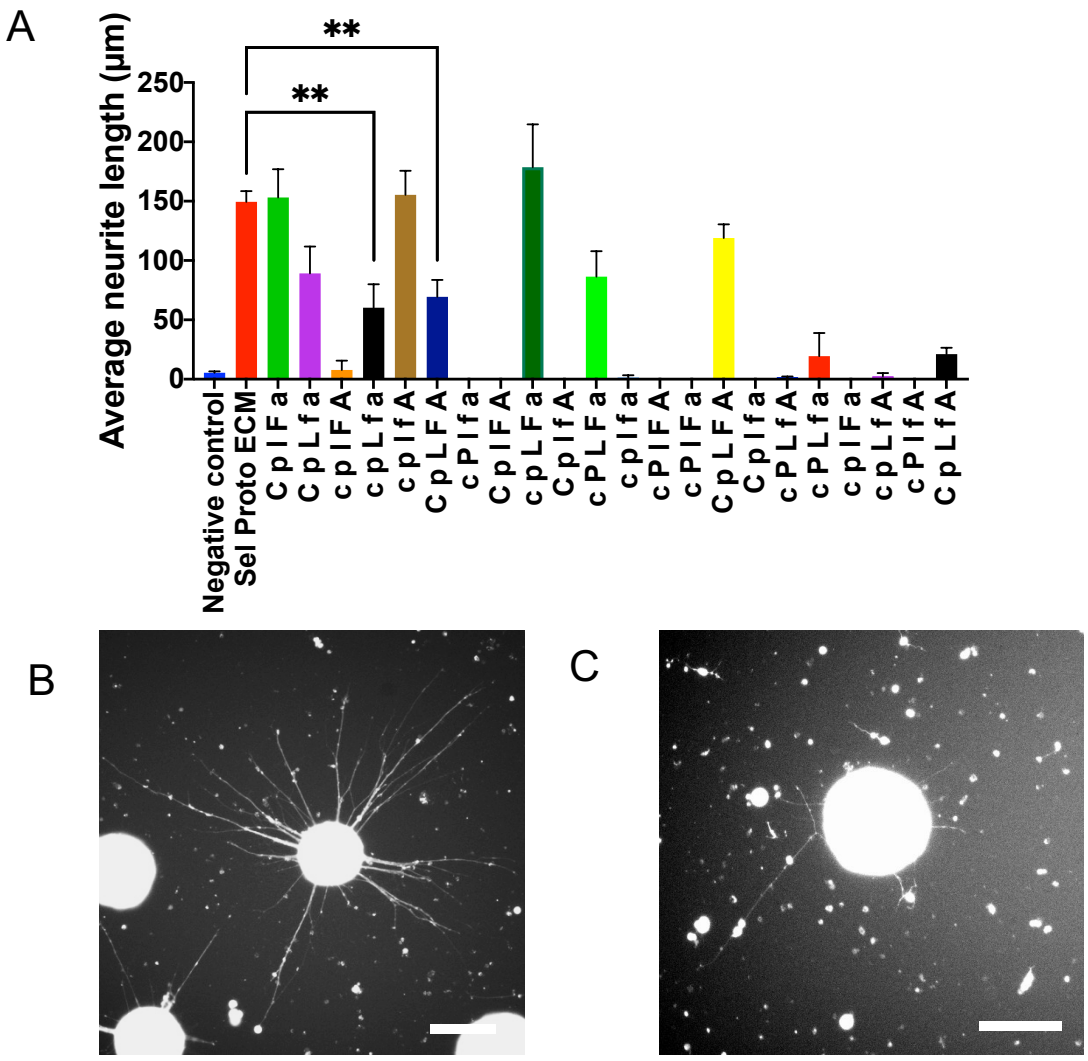

Supplemental Figure 3.6. Numerous low priority combinations with for same high concentrations (all around 50µg/mL) for all proteins in HA-based hydrogel demonstrated no growth with combination of 0.4µg/mL col18a1, 50µg/mL perlecan, 50µg/mL laminin-1, 50µg/mL fibronectin, and 1.49 µg/mL anti-thrombin III producing the maximum axon growth of V2a interneurons A) Combination of low priority demonstrated the highest axon growth with at least 10 neuroaggregates in 2 trials; * $p<0.05$ and ** $p<0.01$ comparison to selected protoplasmic ECM (Sel Proto ECM) in hydrogel **B)** Representative image of V2a interneuron aggregates in hydrogel with 50 µg/mL col18a1 (C), 2.06 µg/mL perlecan (p), 10µg/mL laminin-1 (L), 50µg/mL fibronectin (F), and 1.49 µg/mL anti-thrombin III (a); Scale bar=100µm **C)** Representative image of V2a interneuron aggregates in hydrogel with 50 µg/mL col18a1 (C), 2.06 µg/mL perlecan (p), 50µg/mL laminin-1 (L), 50µg/mL fibronectin (F), and 1.49 µg/mL anti-thrombin III (a); Scale bar=100µm

A

Effect Summary

Source	Logworth	PValue
Perlecan(2.06,10.3)	2.736	0.00184
Col18a1*Laminin-1	2.495	0.00320
Col18a1*Laminin-1*Anti-thrombin III	1.896	0.01271
Fibronectin*Anti-thrombin III	1.700	0.01993
Col18a1*Perlecan*Laminin-1*Anti-thrombin III	1.592	0.02556
Col18a1*Fibronectin*Anti-thrombin III	1.592	0.02561
Perlecan*Anti-thrombin III	1.517	0.03039 ^
Laminin-1*Fibronectin*Anti-thrombin III	1.373	0.04237
Col18a1*Perlecan*Laminin-1	1.195	0.06381 ^
Laminin-1(10,50)	1.132	0.07378 ^
Col18a1*Perlecan*Fibronectin	1.067	0.08564
Laminin-1*Anti-thrombin III	1.063	0.08654 ^
Anti-thrombin III(1.49,7.45)	0.840	0.14464 ^
Col18a1*Perlecan*Anti-thrombin III	0.763	0.17270 ^
Laminin-1*Fibronectin	0.718	0.19122 ^
Perlecan*Laminin-1*Fibronectin	0.693	0.20290
Col18a1*Perlecan*Laminin-1*Fibronectin*Anti-thrombin III	0.662	0.21760
Col18a1*Perlecan	0.630	0.23419 ^
Col18a1*Perlecan*Laminin-1*Fibronectin	0.628	0.23571 ^
Col18a1*Fibronectin	0.616	0.24189 ^
Col18a1(0.4,2)	0.616	0.24231 ^
Col18a1*Perlecan*Fibronectin*Anti-thrombin III	0.502	0.31458 ^
Fibronectin(11,55)	0.424	0.37654 ^
Perlecan*Laminin-1*Fibronectin*Anti-thrombin III	0.346	0.45107 ^
Perlecan*Laminin-1*Anti-thrombin III	0.244	0.57008 ^
Col18a1*Anti-thrombin III	0.114	0.76918 ^
Perlecan*Fibronectin*Anti-thrombin III	0.097	0.79996 ^
Perlecan*Laminin-1	0.092	0.80817 ^
Perlecan*Fibronectin	0.078	0.83479 ^
Col18a1*Laminin-1*Fibronectin	0.042	0.90724 ^
Col18a1*Laminin-1*Fibronectin*Anti-thrombin III	0.019	0.95769 ^

B

Effect Summary

Source	Logworth	PValue
Perlecan(2.06,10.3)	4.843	0.00001
Col18a1*Laminin-1	4.297	0.00005
Col18a1*Laminin-1*Anti-thrombin III	2.982	0.00104
Fibronectin*Anti-thrombin III	2.646	0.00226
Col18a1*Perlecan*Laminin-1*Anti-thrombin III	2.347	0.00450
Perlecan*Anti-thrombin III	2.291	0.00511 ^
Col18a1*Fibronectin*Anti-thrombin III	2.283	0.00521
Laminin-1*Fibronectin*Anti-thrombin III	1.787	0.01632
Col18a1*Perlecan*Laminin-1	1.695	0.02016 ^
Laminin-1(10,50)	1.588	0.02585 ^
Col18a1*Perlecan*Fibronectin	1.404	0.03942
Laminin-1*Anti-thrombin III	1.388	0.04093 ^
Col18a1*Perlecan*Anti-thrombin III	1.009	0.09789 ^
Anti-thrombin III(1.49,7.45)	0.972	0.10668 ^
Laminin-1*Fibronectin	0.946	0.11316 ^
Perlecan*Laminin-1*Fibronectin	0.764	0.17216
Col18a1*Fibronectin	0.725	0.18841 ^
Col18a1*Perlecan	0.624	0.23774 ^
Col18a1(0.4,2)	0.603	0.24922 ^
Fibronectin(11,55)	0.486	0.32680 ^
Perlecan*Laminin-1*Anti-thrombin III	0.272	0.53489 ^
Col18a1*Anti-thrombin III	0.169	0.67729 ^
Perlecan*Fibronectin	0.082	0.82834 ^
Perlecan*Laminin-1	0.061	0.86802 ^

C

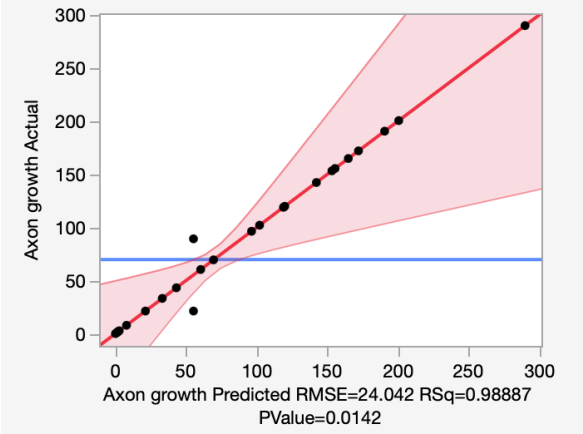

D

Source	Logworth	PValue
Laminin-1(10,50)	2.451	0.00354
Col18a1*Anti-thrombin III	2.373	0.00423
Laminin-1*Fibronectin*Anti-thrombin III	2.342	0.00455
Col18a1*Perlecan	2.326	0.00472
Col18a1(0.4,50)	2.325	0.00474 ^
Fibronectin(11,50)	2.028	0.00938 ^
Laminin-1*Fibronectin	1.997	0.01006 ^
Col18a1*Laminin-1*Fibronectin	1.960	0.01097
Col18a1*Laminin-1*Fibronectin*Anti-thrombin III	1.842	0.01437
Perlecan*Fibronectin*Anti-thrombin III	1.716	0.01923
Col18a1*Fibronectin*Anti-thrombin III	1.672	0.02129 ^
Perlecan*Laminin-1*Anti-thrombin III	1.610	0.02454
Perlecan(2.06,50)	1.511	0.03083 ^
Col18a1*Perlecan*Fibronectin	1.484	0.03280
Laminin-1*Anti-thrombin III	1.455	0.03507 ^
Perlecan*Laminin-1	1.448	0.03564 ^
Anti-thrombin III(1.49,50)	1.180	0.06601 ^
Perlecan*Laminin-1*Fibronectin*Anti-thrombin III	1.096	0.08013
Col18a1*Perlecan*Laminin-1*Anti-thrombin III	0.848	0.14195
Fibronectin*Anti-thrombin III	0.824	0.14994 ^
Perlecan*Anti-thrombin III	0.751	0.17723 ^
Col18a1*Perlecan*Laminin-1*Fibronectin*Anti-thrombin III	0.554	0.27895
Col18a1*Perlecan*Anti-thrombin III	0.528	0.29640 ^
Perlecan*Fibronectin	0.424	0.37678 ^
Col18a1*Perlecan*Laminin-1	0.203	0.62605 ^
Col18a1*Perlecan*Fibronectin*Anti-thrombin III	0.166	0.68236 ^
Col18a1*Perlecan*Laminin-1*Fibronectin	0.129	0.74340 ^
Col18a1*Laminin-1*Anti-thrombin III	0.121	0.75719 ^
Col18a1*Fibronectin	0.051	0.89000 ^
Col18a1*Laminin-1	0.044	0.90351 ^
Perlecan*Laminin-1*Fibronectin	0.004	0.99089 ^

E

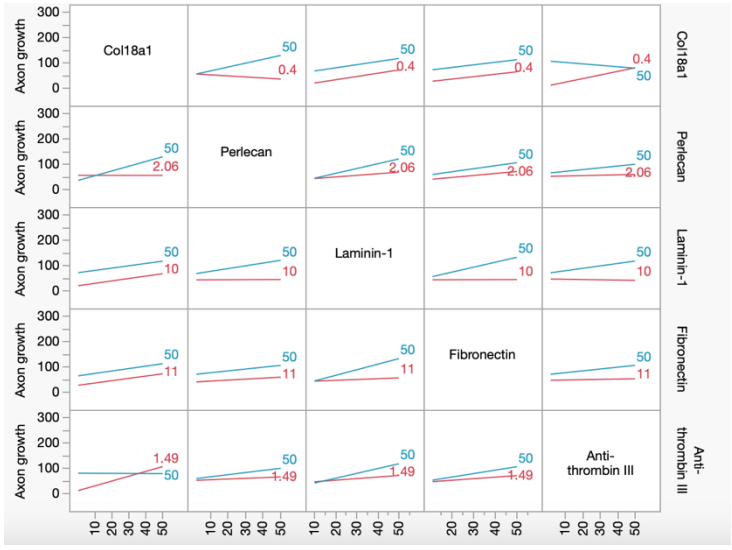

F

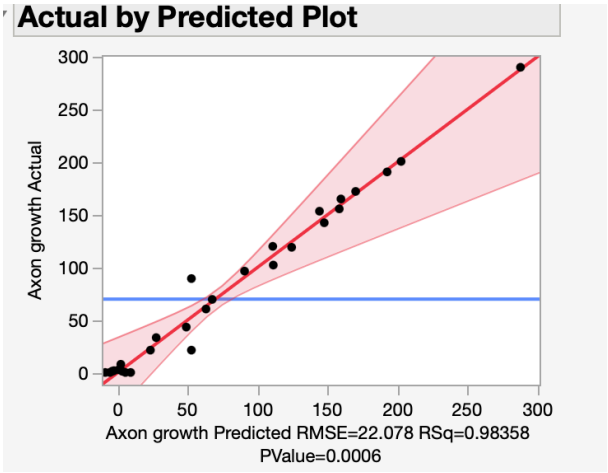

G

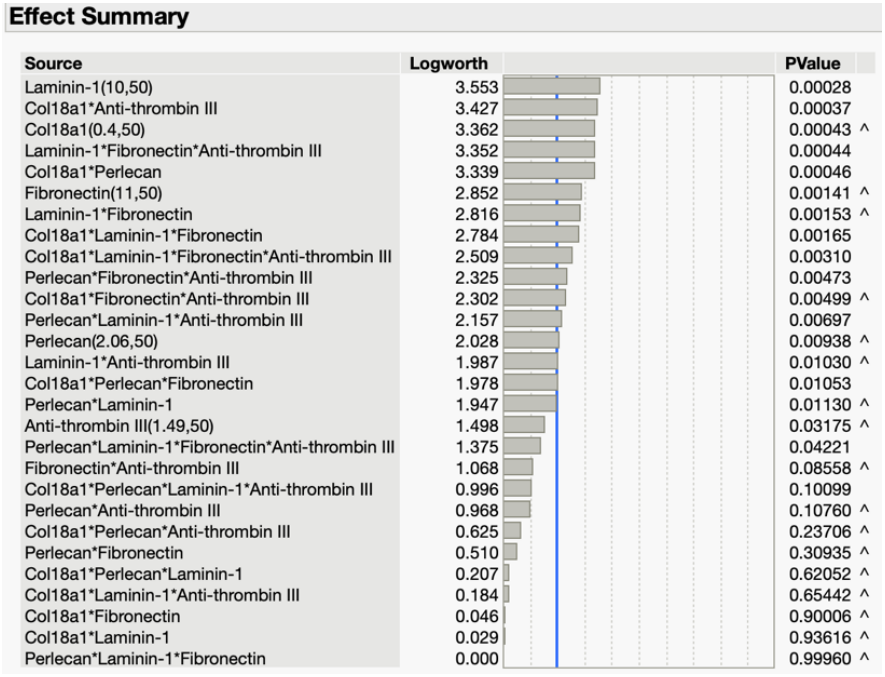

Source	Logworth	PValue	
Laminin-1(10,50)	3.553	0.00028	
Col18a1*Anti-thrombin III	3.427	0.00037	
Col18a1(0.4,50)	3.362	0.00043	^
Laminin-1*Fibronectin*Anti-thrombin III	3.352	0.00044	
Col18a1*Perlecan	3.339	0.00046	
Fibronectin(11,50)	2.852	0.00141	^
Laminin-1*Fibronectin	2.816	0.00153	^
Col18a1*Laminin-1*Fibronectin	2.784	0.00165	
Col18a1*Laminin-1*Fibronectin*Anti-thrombin III	2.509	0.00310	
Perlecan*Fibronectin*Anti-thrombin III	2.325	0.00473	
Col18a1*Fibronectin*Anti-thrombin III	2.302	0.00499	^
Perlecan*Laminin-1*Anti-thrombin III	2.157	0.00697	
Perlecan(2.06,50)	2.028	0.00938	^
Laminin-1*Anti-thrombin III	1.987	0.01030	^
Col18a1*Perlecan*Fibronectin	1.978	0.01053	
Perlecan*Laminin-1	1.947	0.01130	^
Anti-thrombin III(1.49,50)	1.498	0.03175	^
Perlecan*Laminin-1*Fibronectin*Anti-thrombin III	1.375	0.04221	
Fibronectin*Anti-thrombin III	1.068	0.08558	^
Col18a1*Perlecan*Laminin-1*Anti-thrombin III	0.996	0.10099	
Perlecan*Anti-thrombin III	0.968	0.10760	^
Col18a1*Perlecan*Anti-thrombin III	0.625	0.23706	^
Perlecan*Fibronectin	0.510	0.30935	^
Col18a1*Perlecan*Laminin-1	0.207	0.62052	^
Col18a1*Laminin-1*Anti-thrombin III	0.184	0.65442	^
Col18a1*Fibronectin	0.046	0.90006	^
Col18a1*Laminin-1	0.029	0.93616	^
Perlecan*Laminin-1*Fibronectin	0.000	0.99960	^

Supplemental Figure 3.7. Effect summaries of the least squares model with stepwise reduction generated by DoE observations A) Effect summary that demonstrates impact of specific interactions with corresponding p-values; $p<0.05$ interactions between proteins with significance from 36 combinations of 5 proteins at low concentration being K_d and high concentration being 5* K_d **B)** Effect summary that demonstrates impact of specific interactions from reduction least regression model of 36 combinations with low concentration being K_d and high concentration being 5* K_d and the corresponding p-values; $p<0.05$ interactions between proteins with significance **C)** Actual by predicted plot that demonstrates a best fit line by least squares model with significant p-value and small error for the model based on the average axon growth values for each of the 36 combinations with low concentration being K_d and high concentration being 50µg/mL **D)** Effect summary that demonstrates impact of specific interactions of the 36 combinations with low concentration being K_d and high concentration being 50µg/mL and the corresponding p-values; $p<0.05$ interactions between proteins with significance **E)** Interaction profiler output that displays the predictions of axon growth based on two-way interactions at varying concentrations of specific protein pair from observations of the 36 combinations with low concentration

being K_d and high concentration being 50µg/mL **F)** Actual by predicted plot resulting from stepwise regression model for model reduction and demonstrated a best fit line with significant p-value and small error for the model involving observations of the 36 combinations with low concentration being K_d and high concentration being 50µg/mL **G)** Effect summary of the stepwise regression model reduction that demonstrates key sets of interactions from the total 5^{th} order interactions in observations of the 36 combinations with low concentration being K_d and high concentration being 50µg/mL corresponding p-values; $p<0.05$ interactions between proteins being significant

References

1. Silva, N. A., Sousa, N., Reis, R. L. & Salgado, A. J. From basics to clinical: A comprehensive review on spinal cord injury. *Prog. Neurobiol.* **114**, 25–57 (2014).
2. Ahuja, C. S. *et al.* Traumatic spinal cord injury. *Nat. Rev. Dis. Primer* **3**, 17018 (2017).
3. Alizadeh, A., Dyck, S. M. & Karimi-Abdolrezaee, S. Traumatic Spinal Cord Injury: An Overview of Pathophysiology, Models and Acute Injury Mechanisms. *Front. Neurol.* **10**, 282 (2019).
4. Squair, J. W., Gautier, M., Sofroniew, M. V., Courtine, G. & Anderson, M. A. Engineering spinal cord repair. *Curr. Opin. Biotechnol.* **72**, 48–53 (2021).
5. Jain, N. B. *et al.* Traumatic Spinal Cord Injury in the United States, 1993-2012. *JAMA* **313**, 2236 (2015).
6. Fan, B., Wei, Z. & Feng, S. Progression in translational research on spinal cord injury based on microenvironment imbalance. *Bone Res.* **10**, 35 (2022).
7. Punjani, N., Deska-Gauthier, D., Hachem, L. D., Abramian, M. & Fehlings, M. G. Neuroplasticity and regeneration after spinal cord injury. *North Am. Spine Soc. J. NASSJ* **15**, 100235 (2023).
8. O'Shea, T. M., Burda, J. E. & Sofroniew, M. V. Cell biology of spinal cord injury and repair. *J. Clin. Invest.* **127**, 3259–3270 (2017).
9. Fan, B. *et al.* Microenvironment Imbalance of Spinal Cord Injury. *Cell Transplant.* **27**, 853–866 (2018).
10. Karsy, M. & Hawryluk, G. Modern Medical Management of Spinal Cord Injury. *Curr. Neurol. Neurosci. Rep.* **19**, 65 (2019).
11. Rowland, J. W., Hawryluk, G. W. J., Kwon, B. & Fehlings, M. G. Current status of acute spinal cord injury pathophysiology and emerging therapies: promise on the horizon. *Neurosurg. Focus* **25**, E2 (2008).
12. Burda, J. E. & Sofroniew, M. V. Reactive Gliosis and the Multicellular Response to CNS Damage and Disease. *Neuron* **81**, 229–248 (2014).
13. Vardhan, S., Jordan, T. & Sakiyama-Elbert, S. Stem cell engineering approaches for investigating glial cues in central nervous system disorders. *Curr. Opin. Biotechnol.* **87**, 103131 (2024).
14. Barres, B. A. The Mystery and Magic of Glia: A Perspective on Their Roles in Health and Disease. *Neuron* **60**, 430–440 (2008).
15. Roybon, L. *et al.* Human Stem Cell-Derived Spinal Cord Astrocytes with Defined Mature or Reactive Phenotypes. *Cell Rep.* **4**, 1035–1048 (2013).
16. Chu, T. *et al.* Astrocyte transplantation for spinal cord injury: Current status and perspective. *Brain Res. Bull.* **107**, 18–30 (2014).
17. Verkhratsky, A. *et al.* Astrocytes in human central nervous system diseases: a frontier for new therapies. *Signal Transduct. Target. Ther.* **8**, 396 (2023).
18. Bradbury, E. J. & Burnside, E. R. Moving beyond the glial scar for spinal cord repair. *Nat. Commun.* **10**, 3879 (2019).
19. Sofroniew, M. V. Astrocyte Reactivity: Subtypes, States, and Functions in CNS Innate Immunity. *Trends Immunol.* **41**, 758–770 (2020).
20. Sofroniew, M. V. Astrocyte cells in the brain have immune memory. *Nature* **627**, 744–745 (2024).

21. Liddelow, S. A. & Barres, B. A. Reactive Astrocytes: Production, Function, and Therapeutic Potential. *Immunity* **46**, 957–967 (2017).
22. Bush, T. G. *et al.* Leukocyte Infiltration, Neuronal Degeneration, and Neurite Outgrowth after Ablation of Scar-Forming, Reactive Astrocytes in Adult Transgenic Mice. *Neuron* **23**, 297–308 (1999).
23. Pekny, M. *et al.* Abnormal Reaction to Central Nervous System Injury in Mice Lacking Glial Fibrillary Acidic Protein and Vimentin. *J. Cell Biol.* **145**, 503–514 (1999).
24. Okada, S. *et al.* Conditional ablation of Stat3 or Socs3 discloses a dual role for reactive astrocytes after spinal cord injury. *Nat. Med.* **12**, 829–834 (2006).
25. White, R. E. Don't fence me in: Harnessing the beneficial roles of astrocytes for spinal cord repair. (2010).
26. Anderson, M. A. *et al.* Astrocyte scar formation aids central nervous system axon regeneration. *Nature* **532**, 195–200 (2016).
27. Yu, G., Zhang, Y. & Ning, B. Reactive Astrocytes in Central Nervous System Injury: Subgroup and Potential Therapy. *Front. Cell. Neurosci.* **15**, 792764 (2021).
28. Batiuk, M. Y. *et al.* Identification of region-specific astrocyte subtypes at single cell resolution. *Nat. Commun.* **11**, 1220 (2020).
29. Anderson, M. A., Ao, Y. & Sofroniew, M. V. Heterogeneity of reactive astrocytes. *Neurosci. Lett.* **565**, 23–29 (2014).
30. Bergles, D. E. & Richardson, W. D. Oligodendrocyte Development and Plasticity. *Cold Spring Harb. Perspect. Biol.* **8**, a020453 (2016).
31. Beattie, M. S., Li, Q. & Bresnahan, J. C. Cell death and plasticity after experimental spinal cord injury. in *Progress in Brain Research* vol. 128 9–21 (Elsevier, 2000).
32. Almad, A. A. & Maragakis, N. J. Glia: an emerging target for neurological disease therapy. *Stem Cell Res. Ther.* **3**, 37 (2012).
33. Sellers, D. L., Maris, D. O. & Horner, P. J. Postinjury Niches Induce Temporal Shifts in Progenitor Fates to Direct Lesion Repair after Spinal Cord Injury. *J. Neurosci.* **29**, 6722–6733 (2009).
34. Fawcett, J. W. & Asher, Richard. A. The glial scar and central nervous system repair. *Brain Res. Bull.* **49**, 377–391 (1999).
35. Colonna, M. & Butovsky, O. Microglia Function in the Central Nervous System During Health and Neurodegeneration. *Annu. Rev. Immunol.* **35**, 441–468 (2017).
36. Olson, J. K. & Miller, S. D. Microglia Initiate Central Nervous System Innate and Adaptive Immune Responses through Multiple TLRs. *J. Immunol.* **173**, 3916–3924 (2004).
37. Zhang, C. *et al.* Spatiotemporal dynamics of the cellular components involved in glial scar formation following spinal cord injury. *Biomed. Pharmacother.* **153**, 113500 (2022).
38. Timofeeva, A. V., Akhmetzyanova, E. R., Rizvanov, A. A. & Mukhamedshina, Y. O. Interaction of microglia with the microenvironment in spinal cord injury. *Neuroscience* **565**, 594–603 (2025).
39. Bretheau, F. *et al.* The alarmin interleukin-1α triggers secondary degeneration through reactive astrocytes and endothelium after spinal cord injury. *Nat. Commun.* **13**, 5786 (2022).

40. Liddelow, S. A. *et al.* Neurotoxic reactive astrocytes are induced by activated microglia. *Nature* **541**, 481–487 (2017).
41. Oberheim, N. A. *et al.* Uniquely Hominid Features of Adult Human Astrocytes. *J. Neurosci.* **29**, 3276–3287 (2009).
42. Davies, S. J. A. *et al.* Transplantation of Specific Human Astrocytes Promotes Functional Recovery after Spinal Cord Injury. *PLoS ONE* **6**, e17328 (2011).
43. Haas, C., Neuhuber, B., Yamagami, T., Rao, M. & Fischer, I. Phenotypic analysis of astrocytes derived from glial restricted precursors and their impact on axon regeneration. *Exp. Neurol.* **233**, 717–732 (2012).
44. Thompson, R. E. *et al.* Different Mixed Astrocyte Populations Derived from Embryonic Stem Cells Have Variable Neuronal Growth Support Capacities. *Stem Cells Dev.* **26**, 1597–1611 (2017).
45. Hochstim, C., Deneen, B., Lukaszewicz, A. & Zhou, Q. The spinal cord contains positionally distinct astrocyte subtypes whose identities are specified by a homeodomain transcriptional code. (2008).
46. Rowitch, D. H. & Kriegstein, A. R. Developmental genetics of vertebrate glial–cell specification. *Nature* **468**, 214–222 (2010).
47. Westergard, T. & Rothstein, J. D. Astrocyte Diversity: Current Insights and Future Directions. *Neurochem. Res.* **45**, 1298–1305 (2020).
48. Malatesta, P., Appolloni, I. & Calzolari, F. Radial glia and neural stem cells. *Cell Tissue Res.* **331**, 165–178 (2008).
49. Anthony, T. E., Mason, H. A., Gridley, T., Fishell, G. & Heintz, N. Brain lipid-binding protein is a direct target of Notch signaling in radial glial cells. *Genes Dev.* **19**, 1028–1033 (2005).
50. Lu, Q. R. *et al.* Common Developmental Requirement for Olig Function Indicates a Motor Neuron/Oligodendrocyte Connection. *Cell* **109**, 75–86 (2002).
51. McCreedy, D. A., Rieger, C. R., Gottlieb, D. I. & Sakiyama-Elbert, S. E. Transgenic enrichment of mouse embryonic stem cell-derived progenitor motor neurons. *Stem Cell Res.* **8**, 368–378 (2012).
52. Ohayon, D., Aguirrebengoa, M., Escalas, N., Jungas, T. & Soula, C. Transcriptome profiling of the Olig2-expressing astrocyte subtype reveals their unique molecular signature. *iScience* **24**, 102806 (2021).
53. Tabata, H. Diverse subtypes of astrocytes and their development during corticogenesis. *Front. Neurosci.* **9**, (2015).
54. Wang, H. *et al.* Region-specific distribution of Olig2-expressing astrocytes in adult mouse brain and spinal cord. *Mol. Brain* **14**, 36 (2021).
55. Barbar, L. *et al.* CD49f Is a Novel Marker of Functional and Reactive Human iPSC-Derived Astrocytes. *Neuron* **107**, 436-453.e12 (2020).
56. Krencik, R., Weick, J. P., Liu, Y., Zhang, Z.-J. & Zhang, S.-C. Specification of transplantable astroglial subtypes from human pluripotent stem cells. *Nat. Biotechnol.* **29**, 528–534 (2011).
57. Rajan, P. & McKay, R. D. G. Multiple Routes to Astrocytic Differentiation in the CNS. *J. Neurosci.* **18**, 3620–3629 (1998).
58. Kleiderman, S. *et al.* Functional and phenotypic differences of pure populations of stem cell-derived astrocytes and neuronal precursor cells. *Glia* **64**, 695–715 (2016).

59. Magistri, M. *et al.* A comparative transcriptomic analysis of astrocytes differentiation from human neural progenitor cells. *Eur. J. Neurosci.* **44**, 2858–2870 (2016).
60. Thompson, R. E. *et al.* Effect of hyaluronic acid hydrogels containing astrocyte-derived extracellular matrix and/or V2a interneurons on histologic outcomes following spinal cord injury. *Biomaterials* **162**, 208–223 (2018).
61. Sun, D. & Jakobs, T. C. Structural Remodeling of Astrocytes in the Injured CNS. *The Neuroscientist* **18**, 567–588 (2012).
62. Raff, M. C., Miller, R. H. & Noble, M. A glial progenitor cell that develops in vitro into an astrocyte or an oligodendrocyte depending on culture medium. *Nature* **303**, 390–396 (1983).
63. Raff, M. C., Abney, E. R. & Miller, R. H. Two glial cell lineages diverge prenatally in rat optic nerve. *Dev. Biol.* **106**, 53–60 (1984).
64. Emsley, J. G. & Macklis, J. D. Astroglial heterogeneity closely reflects the neuronal-defined anatomy of the adult murine CNS. *Neuron Glia Biol.* **2**, 175–186 (2006).
65. Stogsdill, J. A., Harwell, C. C. & Goldman, S. A. Astrocytes as master modulators of neural networks: Synaptic functions and disease-associated dysfunction of astrocytes. *Ann. N. Y. Acad. Sci.* **1525**, 41–60 (2023).
66. Bushong, E. A., Martone, M. E., Jones, Y. Z. & Ellisman, M. H. Protoplasmic Astrocytes in CA1 Stratum Radiatum Occupy Separate Anatomical Domains. *J. Neurosci.* **22**, 183–192 (2002).
67. Sun, D., Lye-Barthel, M., Masland, R. H. & Jakobs, T. C. The morphology and spatial arrangement of astrocytes in the optic nerve head of the mouse. *J. Comp. Neurol.* **516**, 1–19 (2009).
68. Sofroniew, M. V. & Vinters, H. V. Astrocytes: biology and pathology. *Acta Neuropathol. (Berl.)* **119**, 7–35 (2010).
69. Köhler, S., Winkler, U. & Hirrlinger, J. Heterogeneity of Astrocytes in Grey and White Matter. *Neurochem. Res.* **46**, 3–14 (2021).
70. Salman, M. M. *et al.* Emerging roles for dynamic aquaporin-4 subcellular relocalization in CNS water homeostasis. *Brain* **145**, 64–75 (2022).
71. Stokum, J. A. *et al.* Heterogeneity of aquaporin-4 localization and expression after focal cerebral ischemia underlies differences in white versus grey matter swelling. *Acta Neuropathol. Commun.* **3**, 61 (2015).
72. Skucas, V. A. *et al.* Impairment of Select Forms of Spatial Memory and Neurotrophin-Dependent Synaptic Plasticity by Deletion of Glial Aquaporin-4. *J. Neurosci.* **31**, 6392–6397 (2011).
73. Duan, S., Anderson, C. M., Stein, B. A. & Swanson, R. A. Glutamate Induces Rapid Upregulation of Astrocyte Glutamate Transport and Cell-Surface Expression of GLAST. *J. Neurosci.* **19**, 10193–10200 (1999).
74. Lovatt, D. *et al.* The Transcriptome and Metabolic Gene Signature of Protoplasmic Astrocytes in the Adult Murine Cortex. *J. Neurosci.* **27**, 12255–12266 (2007).
75. Furuta, A., Rothstein, J. D. & Martin, L. J. Glutamate Transporter Protein Subtypes Are Expressed Differentially during Rat CNS Development. *J. Neurosci.* **17**, 8363–8375 (1997).
76. Shibata, T. *et al.* Glutamate Transporter GLAST Is Expressed in the Radial Glia–Astrocyte Lineage of Developing Mouse Spinal Cord. *J. Neurosci.* **17**, 9212–9219 (1997).

77. Bernstein, H.-G. *et al.* Distribution of immunoreactive glutamine synthetase in the adult human and mouse brain. Qualitative and quantitative observations with special emphasis on extra-astroglial protein localization. *J. Chem. Neuroanat.* **61–62**, 33–50 (2014).
78. Ben Haim, L. *et al.* Evidence for glutamine synthetase function in mouse spinal cord oligodendrocytes. *Glia* **69**, 2812–2827 (2021).
79. Anlauf, E. & Derouiche, A. Glutamine Synthetase as an Astrocytic Marker: Its Cell Type and Vesicle Localization. *Front. Endocrinol.* **4**, (2013).
80. Orthmann-Murphy, J. L., Abrams, C. K. & Scherer, S. S. Gap Junctions Couple Astrocytes and Oligodendrocytes. *J. Mol. Neurosci.* **35**, 101–116 (2008).
81. Lutz, S. E. *et al.* Deletion of Astrocyte Connexins 43 and 30 Leads to a Dysmyelinating Phenotype and Hippocampal CA1 Vacuolation. *J. Neurosci.* **29**, 7743–7752 (2009).
82. Dermietzel, R. *et al.* Connexin43 null mice reveal that astrocytes express multiple connexins. *Brain Res. Rev.* **32**, 45–56 (2000).
83. Nagy, J. I., Ionescu, A. -V., Lynn, B. D. & Rash, J. E. Coupling of astrocyte connexins Cx26, Cx30, Cx43 to oligodendrocyte Cx29, Cx32, Cx47: Implications from normal and connexin32 knockout mice. *Glia* **44**, 205–218 (2003).
84. Cornell-Bell, A. H. & Finkbeiner, S. M. Ca2+ waves in astrocytes. *Cell Calcium* **12**, 185–204 (1991).
85. Tatsumi, K. *et al.* Olig2-Lineage Astrocytes: A Distinct Subtype of Astrocytes That Differs from GFAP Astrocytes. *Front. Neuroanat.* **12**, 8 (2018).
86. Du, J. *et al.* S100B is selectively expressed by gray matter protoplasmic astrocytes and myelinating oligodendrocytes in the developing CNS. *Mol. Brain* **14**, 154 (2021).
87. Steiner, J. *et al.* Evidence for a wide extra-astrocytic distribution of S100B in human brain. *BMC Neurosci.* **8**, 2 (2007).
88. Su, X., Vasilkovska, T., Fröhlich, N. & Garaschuk, O. Characterization of cell type-specific S100B expression in the mouse olfactory bulb. *Cell Calcium* **94**, 102334 (2021).
89. White, R. E., McTigue, D. M. & Jakeman, L. B. Regional heterogeneity in astrocyte responses following contusive spinal cord injury in mice. *J. Comp. Neurol.* **518**, 1370–1390 (2010).
90. Scolding, N. J., Rayner, P. J. & Compston, D. A. S. IDENTIFICATION OF A2BS-POSITIVE PUTATIVE OLIGODENDROCYTE PROGENITOR CELLS AND A2B5-POSITIVE ASTROCYTES IN ADULT HUMAN WHITE MATTER.
91. Smith, G. M. & Silver, J. Chapter 45 Transplantation of immature and mature astrocytes and their effect on scar formation in the lesioned central nervous system. in *Progress in Brain Research* vol. 78 353–361 (Elsevier, 1988).
92. Jiang, P. *et al.* Human iPSC-Derived Immature Astroglia Promote Oligodendrogenesis by Increasing TIMP-1 Secretion. *Cell Rep.* **15**, 1303–1315 (2016).
93. Hemati-Gourabi, M., Cao, T., Romprey, M. K. & Chen, M. Capacity of astrocytes to promote axon growth in the injured mammalian central nervous system. *Front. Neurosci.* **16**, 955598 (2022).

94. Cai, N., Kurachi, M., Shibasaki, K., Okano-Uchida, T. & Ishizaki, Y. CD44-Positive Cells Are Candidates for Astrocyte Precursor Cells in Developing Mouse Cerebellum. *The Cerebellum* **11**, 181–193 (2012).
95. Naruse, M., Shibasaki, K., Yokoyama, S., Kurachi, M. & Ishizaki, Y. Dynamic Changes of CD44 Expression from Progenitors to Subpopulations of Astrocytes and Neurons in Developing Cerebellum. *PLoS ONE* **8**, e53109 (2013).
96. Zhang, Y. *et al.* Purification and Characterization of Progenitor and Mature Human Astrocytes Reveals Transcriptional and Functional Differences with Mouse. *Neuron* **89**, 37–53 (2016).
97. Reddy, A. S. *et al.* A Comprehensive Analysis of Cell Type–Specific Nuclear RNA From Neurons and Glia of the Brain. *Biol. Psychiatry* **81**, 252–264 (2017).
98. Werkman, I. L. *et al.* Transcriptional heterogeneity between primary adult grey and white matter astrocytes underlie differences in modulation of in vitro myelination. *J. Neuroinflammation* **17**, 373 (2020).
99. Herrero-Navarro, Á. *et al.* Astrocytes and neurons share region-specific transcriptional signatures that confer regional identity to neuronal reprogramming. *Sci. Adv.* **7**, eabe8978 (2021).
100. Andersen, J. *et al.* Single-cell transcriptomic landscape of the developing human spinal cord. *Nat. Neurosci.* **26**, 902–914 (2023).
101. Boisvert, M. M., Erikson, G. A., Shokhirev, M. N. & Allen, N. J. The Aging Astrocyte Transcriptome from Multiple Regions of the Mouse Brain. *Cell Rep.* **22**, 269–285 (2018).
102. Wei, H. *et al.* Systematic analysis of purified astrocytes after SCI unveils Zeb2os function during astrogliosis. *Cell Rep.* **34**, 108721 (2021).
103. Frazel, P. W. *et al.* Longitudinal scRNA-seq analysis in mouse and human informs optimization of rapid mouse astrocyte differentiation protocols. *Nat. Neurosci.* **26**, 1726–1738 (2023).
104. Lafon-Cazal, M. *et al.* Proteomic Analysis of Astrocytic Secretion in the Mouse. *J. Biol. Chem.* **278**, 24438–24448 (2003).
105. Dowell, J. A., Johnson, J. A. & Li, L. Identification of Astrocyte Secreted Proteins with a Combination of Shotgun Proteomics and Bioinformatics. *J. Proteome Res.* **8**, 4135–4143 (2009).
106. Dozio, V. & Sanchez, J.-C. Profiling the proteomic inflammatory state of human astrocytes using DIA mass spectrometry. *J. Neuroinflammation* **15**, 331 (2018).
107. Galarza, S., Crosby, A. J., Pak, C. & Peyton, S. R. Control of Astrocyte Quiescence and Activation in a Synthetic Brain Hydrogel. *Adv. Healthc. Mater.* **9**, 1901419 (2020).
108. Chai, H. *et al.* Neural Circuit-Specialized Astrocytes: Transcriptomic, Proteomic, Morphological, and Functional Evidence. *Neuron* **95**, 531-549.e9 (2017).
109. Keene, S. D. *et al.* Mass spectrometric and computational analysis of cytokine-induced alterations in the astrocyte secretome. *PROTEOMICS* **9**, 768–782 (2009).
110. Mason, C., Edmondson, J. & Hatten, M. The extending astroglial process: development of glial cell shape, the growing tip, and interactions with neurons. *J. Neurosci.* **8**, 3124–3134 (1988).
111. Fawcett, J. W., Housden, E., Smith-Thomas, L. & Meyer, R. L. The growth of axons in three-dimensional astrocyte cultures. *Dev. Biol.* **135**, 449–458 (1989).

112. Smith, G. M., Rutishauser, U., Silver, J. & Miller, R. H. Maturation of astrocytes in vitro alters the extent and molecular basis of neurite outgrowth. *Dev. Biol.* **138**, 377–390 (1990).
113. Fok-Seang, J. *et al.* An analysis of astrocytic cell lines with different abilities to promote axon growth. *Brain Res.* **689**, 207–223 (1995).
114. Christopherson, K. S. *et al.* Thrombospondins Are Astrocyte-Secreted Proteins that Promote CNS Synaptogenesis. *Cell* **120**, 421–433 (2005).
115. Kucukdereli, H. *et al.* Control of excitatory CNS synaptogenesis by astrocyte-secreted proteins Hevin and SPARC. *Proc. Natl. Acad. Sci.* **108**, (2011).
116. Allen, N. J. *et al.* Astrocyte glypicans 4 and 6 promote formation of excitatory synapses via GluA1 AMPA receptors. *Nature* **486**, 410–414 (2012).
117. Blanco-Suarez, E., Liu, T.-F., Kopelevich, A. & Allen, N. J. Astrocyte-Secreted Chordin-like 1 Drives Synapse Maturation and Limits Plasticity by Increasing Synaptic GluA2 AMPA Receptors. *Neuron* **100**, 1116-1132.e13 (2018).
118. McCarthy, K. D. & De Vellis, J. Preparation of separate astroglial and oligodendroglial cell cultures from rat cerebral tissue. *J. Cell Biol.* **85**, 890–902 (1980).
119. Aguirrebengoa, M. & Ohayon, D. Purification of astrocyte subtype based on a double reporter mice approach for downstream transcription profiling. *STAR Protoc.* **2**, 101009 (2021).
120. Lindsay, R. M., Barber, P. C., Sherwood, M. R. C., Zimmer, J. & Raisman, G. Astrocyte cultures from adult rat brain. Derivation, characterization and neurotrophic properties of pure astroglial cells from corpus callosum. *Brain Res.* **243**, 329–343 (1982).
121. Freitag, K. *et al.* Diverse but unique astrocytic phenotypes during embryonic stem cell differentiation, culturing and development. *Commun. Biol.* **6**, 40 (2023).
122. Batiuk, M. Y. *et al.* An immunoaffinity-based method for isolating ultrapure adult astrocytes based on ATP1B2 targeting by the ACSA-2 antibody. *J. Biol. Chem.* **292**, 8874–8891 (2017).
123. Kantzer, C. G. *et al.* Anti-ACSA-2 defines a novel monoclonal antibody for prospective isolation of living neonatal and adult astrocytes: Kantzer et al. *Glia* **65**, 990–1004 (2017).
124. Luna, S. D. L., Soria, I., Pulido, D., Ortín, J. & Jiménez, A. Efficient transformation of mammalian cells with constructs containing a puromycin-resistance marker. *Gene* **62**, 121–126 (1988).
125. Iwamoto, M., Mori, C., Hiraoka, Y. & Haraguchi, T. Puromycin resistance gene as an effective selection marker for ciliate Tetrahymena. *Gene* **534**, 249–255 (2014).
126. Sánchez-Puig, J. M. & Blasco, R. Puromycin resistance (pac) gene as a selectable marker in vaccinia virus. *Gene* **257**, 57–65 (2000).
127. Fatima, A. *et al.* Murine transgenic iPS cell line for monitoring and selection of cardiomyocytes. *Stem Cell Res.* **17**, 266–272 (2016).
128. Steyer, B. *et al.* Scarless Genome Editing of Human Pluripotent Stem Cells via Transient Puromycin Selection. *Stem Cell Rep.* **10**, 642–654 (2018).
129. Tsujisaka, Y. *et al.* Purification of human iPSC-derived cells at large scale using microRNA switch and magnetic-activated cell sorting. *Stem Cell Rep.* **17**, 1772–1785 (2022).

130. McCreedy, D. A. *et al.* A new method for generating high purity motoneurons from mouse embryonic stem cells. *Biotechnol. Bioeng.* **111**, 2041–2055 (2014).
131. Xu, H., Iyer, N., Huettner, J. E. & Sakiyama-Elbert, S. E. A puromycin selectable cell line for the enrichment of mouse embryonic stem cell-derived V3 interneurons. *Stem Cell Res. Ther.* **6**, 220 (2015).
132. Iyer, N. R., Huettner, J. E., Butts, J. C., Brown, C. R. & Sakiyama-Elbert, S. E. Generation of highly enriched V2a interneurons from mouse embryonic stem cells. *Exp. Neurol.* **277**, 305–316 (2016).
133. Pardieck, J., Harb, M. & Sakiyama-Elbert, S. E. A transgenic mouse embryonic stem cell line for puromycin selection of V0V interneurons from heterogenous induced cultures. *Stem Cell Res. Ther.* **13**, 131 (2022).
134. Choo, A. M.-T. *et al.* Modeling spinal cord contusion, dislocation, and distraction: Characterization of vertebral clamps, injury severities, and node of Ranvier deformations. *J. Neurosci. Methods* **181**, 6–17 (2009).
135. Inman, D. M. & Steward, O. Ascending sensory, but not other long-tract axons, regenerate into the connective tissue matrix that forms at the site of a spinal cord injury in mice. *J. Comp. Neurol.* **462**, 431–449 (2003).
136. Anderson, M. A. *et al.* Natural and targeted circuit reorganization after spinal cord injury. *Nat. Neurosci.* **25**, 1584–1596 (2022).
137. Bareyre, F. M. *et al.* The injured spinal cord spontaneously forms a new intraspinal circuit in adult rats. *Nat. Neurosci.* **7**, 269–277 (2004).
138. Courtine, G. *et al.* Recovery of supraspinal control of stepping via indirect propriospinal relay connections after spinal cord injury. *Nat. Med.* **14**, 69–74 (2008).
139. Hansen, C. N. *et al.* Sparing of Descending Axons Rescues Interneuron Plasticity in the Lumbar Cord to Allow Adaptive Learning After Thoracic Spinal Cord Injury. *Front. Neural Circuits* **10**, (2016).
140. Zholudeva, L. V. *et al.* Spinal Interneurons as Gatekeepers to Neuroplasticity after Injury or Disease. *J. Neurosci.* **41**, 845–854 (2021).
141. Goulding, M. Circuits controlling vertebrate locomotion: moving in a new direction. *Nat. Rev. Neurosci.* **10**, 507–518 (2009).
142. Kathe, C. *et al.* The neurons that restore walking after paralysis. *Nature* **611**, 540–547 (2022).
143. Francius, C. *et al.* Identification of Multiple Subsets of Ventral Interneurons and Differential Distribution along the Rostrocaudal Axis of the Developing Spinal Cord. *PLoS ONE* **8**, e70325 (2013).
144. Ziskind-Conhaim, L. & Hochman, S. Diversity of molecularly defined spinal interneurons engaged in mammalian locomotor pattern generation. *J. Neurophysiol.* **118**, 2956–2974 (2017).
145. Zavvarian, M.-M., Hong, J. & Fehlings, M. G. The Functional Role of Spinal Interneurons Following Traumatic Spinal Cord Injury. *Front. Cell. Neurosci.* **14**, 127 (2020).
146. White, N. & Sakiyama-Elbert, S. E. Derivation of Specific Neural Populations From Pluripotent Cells for Understanding and Treatment of Spinal Cord Injury. *Dev. Dyn.* **248**, 78–87 (2019).

147. Ericson, J. *et al.* Pax6 Controls Progenitor Cell Identity and Neuronal Fate in Response to Graded Shh Signaling. *Cell* **90**, 169–180 (1997).
148. Li, W.-Y. *et al.* Chx10+V2a interneurons in spinal motor regulation and spinal cord injury. *Neural Regen. Res.* **18**, 933 (2023).
149. Lu, D. C., Niu, T. & Alaynick, W. A. Molecular and cellular development of spinal cord locomotor circuitry. *Front. Mol. Neurosci.* **8**, (2015).
150. Clovis, Y. M. *et al.* Chx10 Consolidates V2a Interneuron Identity through Two Distinct Gene Repression Modes. *Cell Rep.* **16**, 1642–1652 (2016).
151. Brown, C. R., Butts, J. C., McCreedy, D. A. & Sakiyama-Elbert, S. E. Generation of V2a Interneurons from Mouse Embryonic Stem Cells. *Stem Cells Dev.* **23**, 1765–1776 (2014).
152. Butts, J. C. *et al.* V2a interneuron differentiation from mouse and human pluripotent stem cells. *Nat. Protoc.* **14**, 3033–3058 (2019).
153. Eklöf-Ljunggren, E. *et al.* Origin of excitation underlying locomotion in the spinal circuit of zebrafish. *Proc. Natl. Acad. Sci.* **109**, 5511–5516 (2012).
154. Dougherty, K. J. & Kiehn, O. Firing and Cellular Properties of V2a Interneurons in the Rodent Spinal Cord. *J. Neurosci.* **30**, 24–37 (2010).
155. Crone, S. A. *et al.* Genetic Ablation of V2a Ipsilateral Interneurons Disrupts Left-Right Locomotor Coordination in Mammalian Spinal Cord. *Neuron* **60**, 70–83 (2008).
156. Jensen, V. N., Seedle, K., Turner, S. M., Lorenz, J. N. & Crone, S. A. V2a Neurons Constrain Extradiaphragmatic Respiratory Muscle Activity at Rest. *eneuro* **6**, ENEURO.0492-18.2019 (2019).
157. Jensen, V. N. *et al.* V2a neurons restore diaphragm function in mice following spinal cord injury. *Proc. Natl. Acad. Sci.* **121**, e2313594121 (2024).
158. Salamatina, A. *et al.* Differential Loss of Spinal Interneurons in a Mouse Model of ALS. *Neuroscience* **450**, 81–95 (2020).
159. Romer, S. H. *et al.* Accessory respiratory muscles enhance ventilation in ALS model mice and are activated by excitatory V2a neurons. *Exp. Neurol.* **287**, 192–204 (2017).
160. Lau, L. W., Cua, R., Keough, M. B., Haylock-Jacobs, S. & Yong, V. W. Pathophysiology of the brain extracellular matrix: a new target for remyelination. *Nat. Rev. Neurosci.* **14**, 722–729 (2013).
161. Gaudet, A. D. & Popovich, P. G. Extracellular matrix regulation of inflammation in the healthy and injured spinal cord. *Exp. Neurol.* **258**, 24–34 (2014).
162. Long, K. R. & Huttner, W. B. How the extracellular matrix shapes neural development. *Open Biol.* **9**, 180216 (2019).
163. Novak, U. & Kaye, A. H. Extracellular matrix and the brain: components and function. *J. Clin. Neurosci.* **7**, 280–290 (2000).
164. Haggerty, A. E., Maldonado-Lasunción, I. & Oudega, M. Biomaterials for revascularization and immunomodulation after spinal cord injury. *Biomed. Mater.* **13**, 044105 (2018).
165. Busch, S. A. & Silver, J. The role of extracellular matrix in CNS regeneration. *Curr. Opin. Neurobiol.* **17**, 120–127 (2007).
166. Wang, D. & Fawcett, J. The perineuronal net and the control of CNS plasticity. *Cell Tissue Res.* **349**, 147–160 (2012).

167. Powell, E. M., Meiners, S., DiProspero, N. A. & Geller, H. M. Mechanisms of astrocyte-directed neurite guidance.
168. Wilems, T., Vardhan, S., Wu, S. & Sakiyama-Elbert, S. The influence of microenvironment and extracellular matrix molecules in driving neural stem cell fate within biomaterials. *Brain Res. Bull.* **148**, 25–33 (2019).
169. Sanes, J. R., Engvall, E., Butkowski, R. & Hunter, D. D. Molecular heterogeneity of basal laminae: isoforms of laminin and collagen IV at the neuromuscular junction and elsewhere. *J. Cell Biol.* **111**, 1685–1699 (1990).
170. Powell, S. K. & Kleinman, H. K. Neuronal laminins and their cellular receptors. *Int. J. Biochem. Cell Biol.* **29**, 401–414 (1997).
171. Lein, P. J., Banker, G. A. & Higgins, D. Laminin selectively enhances axonal growth and accelerates the development of polarity by hippocampal neurons in culture. *Dev. Brain Res.* **69**, 191–197 (1992).
172. Plantman, S. *et al.* Integrin-laminin interactions controlling neurite outgrowth from adult DRG neurons in vitro. *Mol. Cell. Neurosci.* **39**, 50–62 (2008).
173. Franco, S. J. & Müller, U. Extracellular matrix functions during neuronal migration and lamination in the mammalian central nervous system. *Dev. Neurobiol.* **71**, 889–900 (2011).
174. Hasel, P. *et al.* Defining the molecular identity and morphology of glia limitans superficialis astrocytes in vertebrates. *Cell Rep.* **44**, 115344 (2025).
175. Rautavuoma, K. *et al.* Premature aggregation of type IV collagen and early lethality in lysyl hydroxylase 3 null mice. *Proc. Natl. Acad. Sci.* **101**, 14120–14125 (2004).
176. Schneider, V. A. & Granato, M. The Myotomal diwanka (lh3) Glycosyltransferase and Type XVIII Collagen Are Critical for Motor Growth Cone Migration. *Neuron* **50**, 683–695 (2006).
177. Leclere, P. G. *et al.* Impaired Axonal Regeneration by Isolectin B4-Binding Dorsal Root Ganglion Neurons *In Vitro*. *J. Neurosci.* **27**, 1190–1199 (2007).
178. Risling, M., Fried, K., Lindå, H., Carlstedt, T. & Cullheim, S. Regrowth of motor axons following spinal cord lesions: Distribution of laminin and collagen in the CNS scar tissue. *Brain Res. Bull.* **30**, 405–414 (1993).
179. Lein, P. J. & Higgins, D. The NC1 Domain of Type IV Collagen Promotes Axonal Growth in Sympathetic Neurons through Interaction with the 1B1 IntеglSn.
180. Blackshaw, S. E., Arkison, S., Cameron, C. & Davies, J. A. Promotion of regeneration and axon growth following injury in an invertebrate nervous system by the use of three–dimensional collagen gels. *Proc. R. Soc. Lond. B Biol. Sci.* **264**, 657–661 (1997).
181. O'Connor, S. M., Stenger, D. A., Shaffer, K. M. & Ma, W. Survival and neurite outgrowth of rat cortical neurons in three-dimensional agarose and collagen gel matrices. *Neurosci. Lett.* **304**, 189–193 (2001).
182. Bozkurt, A. *et al. In Vitro* Assessment of Axonal Growth Using Dorsal Root Ganglia Explants in a Novel Three-Dimensional Collagen Matrix. *Tissue Eng.* **13**, 2971–2979 (2007).
183. Krolo, M., Vilovi, K., Sapunar, D., Vrdoljak, E. & Saraga-Babi, M. Fibronectin Expression in the Developing Human Spinal Cord, Nerves, and Ganglia.
184. Tonge, D. A. *et al.* Fibronectin supports neurite outgrowth and axonal regeneration of adult brain neurons in vitro. *Brain Res.* **1453**, 8–16 (2012).

185. Stoffels, J. M. J., Hoekstra, D., Franklin, R. J. M., Baron, W. & Zhao, C. The EIIIA domain from astrocyte-derived fibronectin mediates proliferation of oligodendrocyte progenitor cells following CNS demyelination. *Glia* **63**, 242–256 (2015).
186. Sutherland, T. C. & Geoffroy, C. G. The Influence of Neuron-Extrinsic Factors and Aging on Injury Progression and Axonal Repair in the Central Nervous System. *Front. Cell Dev. Biol.* **8**, 190 (2020).
187. Melrose, J. Hyaluronan hydrates and compartmentalises the CNS / PNS extracellular matrix and provides niche environments conducive to the optimisation of neuronal activity. *J. Neurochem.* **166**, 637–653 (2023).
188. Tammi, M. I., Day, A. J. & Turley, E. A. Hyaluronan and Homeostasis: A Balancing Act. *J. Biol. Chem.* **277**, 4581–4584 (2002).
189. Fowke, T. M. *et al.* Hyaluronan synthesis by developing cortical neurons in vitro. *Sci. Rep.* **7**, 44135 (2017).
190. Casini, P., Nardi, I. & Ori, M. RHAMM mRNA expression in proliferating and migrating cells of the developing central nervous system. *Gene Expr. Patterns* **10**, 93–97 (2010).
191. Preston, M. & Sherman, L. S. Neural Stem Cell Niches: Critical Roles for the Hyaluronan- Based Extracellular Matrix in Neural Stem Cell Proliferation and Differentiation. *Front Biosci* (2012).
192. Cui, H., Freeman, C., Jacobson, G. A. & Small, D. H. Proteoglycans in the central nervous system: Role in development, neural repair, and Alzheimer's disease. *IUBMB Life* **65**, 108–120 (2013).
193. Kerever, A. *et al.* Perlecan is required for FGF-2 signaling in the neural stem cell niche. *Stem Cell Res.* **12**, 492–505 (2014).
194. Hayes, A. J., Farrugia, B. L., Biose, I. J., Bix, G. J. & Melrose, J. Perlecan, A Multi-Functional, Cell-Instructive, Matrix-Stabilizing Proteoglycan With Roles in Tissue Development Has Relevance to Connective Tissue Repair and Regeneration. *Front. Cell Dev. Biol.* **10**, 856261 (2022).
195. Cho, J. Y., Chak, K., Andreone, B. J., Wooley, J. R. & Kolodkin, A. L. The extracellular matrix proteoglycan perlecan facilitates transmembrane semaphorin-mediated repulsive guidance. *Genes Dev.* **26**, 2222–2235 (2012).
196. Snow, D. M., Smith, J. D., Cunningham, A. T., McFarlin, J. & Goshorn, E. C. Neurite elongation on chondroitin sulfate proteoglycans is characterized by axonal fasciculation. *Exp. Neurol.* **182**, 310–321 (2003).
197. Nakajima, C. *et al.* Identification of the growth cone as a probe and driver of neuronal migration in the injured brain. *Nat. Commun.* **15**, 1877 (2024).
198. Silver, D. J. & Silver, J. Contributions of chondroitin sulfate proteoglycans to neurodevelopment, injury, and cancer. *Curr. Opin. Neurobiol.* **27**, 171–178 (2014).
199. Bradbury, E. J. *et al.* Chondroitinase ABC promotes functional recovery after spinal cord injury. *Nature* **416**, 636–640 (2002).
200. Bartus, K. *et al.* Large-Scale Chondroitin Sulfate Proteoglycan Digestion with Chondroitinase Gene Therapy Leads to Reduced Pathology and Modulates Macrophage Phenotype following Spinal Cord Contusion Injury. *J. Neurosci.* **34**, 4822–4836 (2014).

201. Hu, H. Z., Granger, N., Pai, S. B., Bellamkonda, R. V. & Jeffery, N. D. Therapeutic efficacy of microtube-embedded chondroitinase ABC in a canine clinical model of spinal cord injury. *Brain* **141**, 1017–1027 (2018).
202. Fitch, M. T. & Silver, J. CNS injury, glial scars, and inflammation: Inhibitory extracellular matrices and regeneration failure. *Exp. Neurol.* **209**, 294–301 (2008).
203. Jakeman, L., Williams, K. & Brautigam, B. In the presence of danger: the extracellular matrix defensive response to central nervous system injury. *Neural Regen. Res.* **9**, 377 (2014).
204. Fitch, M. T. & Silver, J. Glial cell extracellular matrix: boundaries for axon growth in development and regeneration.
205. McRae, P. A. & Porter, B. E. The perineuronal net component of the extracellular matrix in plasticity and epilepsy. *Neurochem. Int.* **61**, 963–972 (2012).
206. Jones, L. L., Margolis, R. U. & Tuszynski, M. H. The chondroitin sulfate proteoglycans neurocan, brevican, phosphacan, and versican are differentially regulated following spinal cord injury. *Exp. Neurol.* **182**, 399–411 (2003).
207. Ughrin, Y. M., Chen, Z. J. & Levine, J. M. Multiple Regions of the NG2 Proteoglycan Inhibit Neurite Growth and Induce Growth Cone Collapse. *J. Neurosci.* **23**, 175–186 (2003).
208. Hara, M. *et al.* Interaction of reactive astrocytes with type I collagen induces astrocytic scar formation through the integrin–N-cadherin pathway after spinal cord injury. *Nat. Med.* **23**, 818–828 (2017).
209. Liesi, P. & Kauppila, T. Induction of Type IV Collagen and Other Basement-Membrane-Associated Proteins after Spinal Cord Injury of the Adult Rat May Participate in Formation of the Glial Scar. *Exp. Neurol.* **173**, 31–45 (2002).
210. Lin, J., Duan, M., Lin, N. & Zhao, W. The emerging role of the chondroitin sulfate proteoglycan family in neurodegenerative diseases. *Rev. Neurosci.* **32**, 737–750 (2021).
211. Straley, K. S., Foo, C. W. P. & Heilshorn, S. C. Biomaterial Design Strategies for the Treatment of Spinal Cord Injuries. *J. Neurotrauma* **27**, 1–19 (2010).
212. Smith, L. J. *et al.* Diels–Alder Click-Cross-Linked Hydrogels with Increased Reactivity Enable 3D Cell Encapsulation. *Biomacromolecules* **19**, 926–935 (2018).
213. Taylor, S. J., Rosenzweig, E. S., McDonald, J. W. & Sakiyama-Elbert, S. E. Delivery of neurotrophin-3 from fibrin enhances neuronal fiber sprouting after spinal cord injury. *J. Controlled Release* **113**, 226–235 (2006).
214. Johnson, P. J., Tatara, A., McCreedy, D. A., Shiu, A. & Sakiyama-Elbert, S. E. Tissue-engineered fibrin scaffolds containing neural progenitors enhance functional recovery in a subacute model of SCI. *Soft Matter* **6**, 5127 (2010).
215. Zeng, X. *et al.* A biocompatible gelatin sponge scaffold confers robust tissue remodeling after spinal cord injury in a non-human primate model. *Biomaterials* **299**, 122161 (2023).
216. Kourgiantaki, A. *et al.* Neural stem cell delivery via porous collagen scaffolds promotes neuronal differentiation and locomotion recovery in spinal cord injury. *Npj Regen. Med.* **5**, 12 (2020).
217. Wang, H. *et al.* Injectable hydrogels for spinal cord injury repair. *Eng. Regen.* **3**, 407–419 (2022).

218. Cai, M. *et al.* Hydrogel scaffolds in the treatment of spinal cord injury: a review. *Front. Neurosci.* **17**, 1211066 (2023).
219. Sun, Z. *et al.* Recent advance in bioactive hydrogels for repairing spinal cord injury: material design, biofunctional regulation, and applications. *J. Nanobiotechnology* **21**, 238 (2023).
220. Jia, Z. *et al.* Hydrogel-based treatments for spinal cord injuries. *Heliyon* **9**, e19933 (2023).
221. Jain, A., Kim, Y.-T., McKeon, R. J. & Bellamkonda, R. V. In situ gelling hydrogels for conformal repair of spinal cord defects, and local delivery of BDNF after spinal cord injury. *Biomaterials* **27**, 497–504 (2006).
222. Gupta, D., Tator, C. H. & Shoichet, M. S. Fast-gelling injectable blend of hyaluronan and methylcellulose for intrathecal, localized delivery to the injured spinal cord. *Biomaterials* **27**, 2370–2379 (2006).
223. Khaing, Z. Z. *et al.* High molecular weight hyaluronic acid limits astrocyte activation and scar formation after spinal cord injury. *J. Neural Eng.* **8**, 046033 (2011).
224. Mothe, A. J., Tam, R. Y., Zahir, T., Tator, C. H. & Shoichet, M. S. Repair of the injured spinal cord by transplantation of neural stem cells in a hyaluronan-based hydrogel. *Biomaterials* **34**, 3775–3783 (2013).
225. Romano, N. H., Sengupta, D., Chung, C. & Heilshorn, S. C. Protein-engineered biomaterials: Nanoscale mimics of the extracellular matrix. *Biochim. Biophys. Acta BBA - Gen. Subj.* **1810**, 339–349 (2011).
226. Schense, J. C., Bloch, J., Aebischer, P. & Hubbell, J. A. Enzymatic incorporation of bioactive peptides into fibrin matrices enhances neurite extension. *Nat. Biotechnol.* **18**, 415–419 (2000).
227. Tysseling-Mattiace, V. M. *et al.* Self-Assembling Nanofibers Inhibit Glial Scar Formation and Promote Axon Elongation after Spinal Cord Injury. *J. Neurosci.* **28**, 3814–3823 (2008).
228. Tibbitt, M. W. & Anseth, K. S. Hydrogels as extracellular matrix mimics for 3D cell culture. *Biotechnol. Bioeng.* **103**, 655–663 (2009).
229. Ho, M. T., Teal, C. J. & Shoichet, M. S. A hyaluronan/methylcellulose-based hydrogel for local cell and biomolecule delivery to the central nervous system. *Brain Res. Bull.* **148**, 46–54 (2019).
230. Lutolf, M. P. & Hubbell, J. A. Synthetic biomaterials as instructive extracellular microenvironments for morphogenesis in tissue engineering. *Nat. Biotechnol.* **23**, 47–55 (2005).
231. Volpato, F. Z., Führmann, T., Migliaresi, C., Hutmacher, D. W. & Dalton, P. D. Using extracellular matrix for regenerative medicine in the spinal cord. *Biomaterials* **34**, 4945–4955 (2013).
232. Jiang, W. *et al.* Decellularized extracellular matrix in the treatment of spinal cord injury. *Exp. Neurol.* **368**, 114506 (2023).
233. Hu, J. *et al.* Decellularization alters the unfavorable regenerative adverse microenvironment of the injured spinal cord to support neurite outgrowth. *Ann. Transl. Med.* **10**, 934–934 (2022).
234. Hong, J. Y. *et al.* Decellularized brain matrix enhances macrophage polarization and functional improvements in rat spinal cord injury. *Acta Biomater.* **101**, 357–371 (2020).

235. Zholudeva, L. V. *et al.* Transplantation of Neural Progenitors and V2a Interneurons after Spinal Cord Injury. *J. Neurotrauma* **35**, 2883–2903 (2018).
236. Zholudeva, L. V. *et al.* Human spinal interneurons repair the injured spinal cord through synaptic integration. Preprint at https://doi.org/10.1101/2024.01.11.575264 (2024).
237. Sankavaram, S. R. *et al.* Adult Neural Progenitor Cells Transplanted into Spinal Cord Injury Differentiate into Oligodendrocytes, Enhance Myelination, and Contribute to Recovery. *Stem Cell Rep.* **12**, 950–966 (2019).
238. Fischer, I., Dulin, J. N. & Lane, M. A. Transplanting neural progenitor cells to restore connectivity after spinal cord injury. *Nat. Rev. Neurosci.* **21**, 366–383 (2020).
239. Aceves, M. *et al.* Developmental stage of transplanted neural progenitor cells influences anatomical and functional outcomes after spinal cord injury in mice. *Commun. Biol.* **6**, 544 (2023).
240. Kamata, Y. *et al.* A robust culture system to generate neural progenitors with gliogenic competence from clinically relevant induced pluripotent stem cells for treatment of spinal cord injury. *Stem Cells Transl. Med.* **10**, 398–413 (2021).
241. Rosenzweig, E. S. *et al.* Chondroitinase improves anatomical and functional outcomes after primate spinal cord injury. *Nat. Neurosci.* **22**, 1269–1275 (2019).
242. Burnside, E. R. *et al.* Immune-evasive gene switch enables regulated delivery of chondroitinase after spinal cord injury. *Brain* **141**, 2362–2381 (2018).
243. Warren, P. M. *et al.* Rapid and robust restoration of breathing long after spinal cord injury. *Nat. Commun.* **9**, 4843 (2018).
244. Chu, P.-H. *et al.* Astrocyte-associated fibronectin promotes the proinflammatory phenotype of astrocytes through β1 integrin activation. *Mol. Cell. Neurosci.* **125**, 103848 (2023).
245. Fehlings, M. G. & Perrin, R. G. The role and timing of early decompression for cervical spinal cord injury: Update with a review of recent clinical evidence. *Injury* **36**, S13–S26 (2005).
246. Escartin, C. & Bonvento, G. Targeted Activation of Astrocytes: A Potential Neuroprotective Strategy. *Mol. Neurobiol.* **38**, 231–241 (2008).
247. Silver, J. & Miller, J. H. Regeneration beyond the glial scar. *Nat. Rev. Neurosci.* **5**, 146–156 (2004).
248. Karimi-Abdolrezaee, S. & Billakanti, R. Reactive Astrogliosis after Spinal Cord Injury—Beneficial and Detrimental Effects. *Mol. Neurobiol.* **46**, 251–264 (2012).
249. Voskuhl, R. R. *et al.* Reactive Astrocytes Form Scar-Like Perivascular Barriers to Leukocytes during Adaptive Immune Inflammation of the CNS. *J. Neurosci.* **29**, 11511–11522 (2009).
250. Ferrer-Acosta, Y., Gonzalez-Vega, M. N., Rivera-Aponte, D. E., Martinez-Jimenez, S. M. & Martins, A. H. Monitoring Astrocyte Reactivity and Proliferation in Vitro Under Ischemic-Like Conditions. *J. Vis. Exp.* 55108 (2017) doi:10.3791/55108.
251. Gottipati, M. K., Zuidema, J. M. & Gilbert, R. J. Biomaterial strategies for creating in vitro astrocyte cultures resembling in vivo astrocyte morphologies and phenotypes. *Curr. Opin. Biomed. Eng.* **14**, 67–74 (2020).
252. Wang, J. *et al.* Inhibition of A1 Astrocytes and Activation of A2 Astrocytes for the Treatment of Spinal Cord Injury. *Neurochem. Res.* **48**, 767–780 (2023).

253. Prah, J. *et al.* A novel serum free primary astrocyte culture method that mimic quiescent astrocyte phenotype. *J. Neurosci. Methods* **320**, 50–63 (2019).
254. Kerstetter, A. E. & Miller, R. H. Isolation and Culture of Spinal Cord Astrocytes. in *Astrocytes* (ed. Milner, R.) vol. 814 93–104 (Humana Press, Totowa, NJ, 2012).
255. Foo, L. C. *et al.* Development of a Method for the Purification and Culture of Rodent Astrocytes. *Neuron* **71**, 799–811 (2011).
256. Lanjewar, S. N. & Sloan, S. A. Growing Glia: Cultivating Human Stem Cell Models of Gliogenesis in Health and Disease. *Front. Cell Dev. Biol.* **9**, 649538 (2021).
257. Nolle, A. *et al.* Enrichment of Glial Cells From Human Post-mortem Tissue for Transcriptome and Proteome Analysis Using Immunopanning. *Front. Cell. Neurosci.* **15**, 772011 (2021).
258. Thompson, R. E. Elucidating the Roles of Astrocyte-derived Factors in Recovery and Regeneration Following Spinal Cord Injury.
259. Schindelin, J. *et al.* Fiji: an open-source platform for biological-image analysis. *Nat. Methods* **9**, 676–682 (2012).
260. Tcw, J. *et al.* An Efficient Platform for Astrocyte Differentiation from Human Induced Pluripotent Stem Cells. *Stem Cell Rep.* **9**, 600–614 (2017).
261. Sloan, S. A. *et al.* Human Astrocyte Maturation Captured in 3D Cerebral Cortical Spheroids Derived from Pluripotent Stem Cells. *Neuron* **95**, 779-790.e6 (2017).
262. Clayton, B. L. L. *et al.* A phenotypic screening platform for identifying chemical modulators of astrocyte reactivity. *Nat. Neurosci.* **27**, 656–665 (2024).
263. Lundgaard, I., Osório, M. J., Kress, B. T., Sanggaard, S. & Nedergaard, M. White matter astrocytes in health and disease. *Neuroscience* **276**, 161–173 (2014).
264. Morita, K. *et al.* BMP signaling alters aquaporin-4 expression in the mouse cerebral cortex. *Sci. Rep.* **11**, 10540 (2021).
265. Tan, B. *et al.* The Olig family affects central nervous system development and disease. *Neural Regen. Res.* **9**, 329 (2014).
266. Gleiser, C. *et al.* Aquaporin-4 in Astroglial Cells in the CNS and Supporting Cells of Sensory Organs—A Comparative Perspective. *Int. J. Mol. Sci.* **17**, 1411 (2016).
267. Keirstead, H. S. *et al.* Human Embryonic Stem Cell-Derived Oligodendrocyte Progenitor Cell Transplants Remyelinate and Restore Locomotion after Spinal Cord Injury. *J. Neurosci.* **25**, 4694–4705 (2005).
268. Wang, J. *et al.* Oligodendrocyte/Type-2 Astrocyte Progenitor Cells and Glial-Restricted Precursor Cells Generate Different Tumor Phenotypes in Response to the Identical Oncogenes. *J. Neurosci.* **33**, 16805–16817 (2013).
269. Raff, M., Abney, E., Cohen, J., Lindsay, R. & Noble, M. Two types of astrocytes in cultures of developing rat white matter: differences in morphology, surface gangliosides, and growth characteristics. *J. Neurosci.* **3**, 1289–1300 (1983).
270. Gusel'nikova, V. V. & Korzhevskiy, D. E. NeuN As a Neuronal Nuclear Antigen and Neuron Differentiation Marker. *Acta Naturae* **7**, 42–47 (2015).
271. Baumann, N. & Pham-Dinh, D. Biology of Oligodendrocyte and Myelin in the Mammalian Central Nervous System. *Physiol. Rev.* **81**, 871–927 (2001).
272. Willerth, S. M., Faxel, T. E., Gottlieb, D. I. & Sakiyama-Elbert, S. E. The Effects of Soluble Growth Factors on Embryonic Stem Cell Differentiation Inside of Fibrin Scaffolds. *Stem Cells* **25**, 2235–2244 (2007).

273. Nakajima-Koyama, M., Lee, J., Ohta, S., Yamamoto, T. & Nishida, E. Induction of Pluripotency in Astrocytes through a Neural Stem Cell-like State. *J. Biol. Chem.* **290**, 31173–31188 (2015).
274. Vanhoutte, N., De Hemptinne, I., Vermeiren, C., Maloteaux, J.-M. & Hermans, E. In vitro differentiated neural stem cells express functional glial glutamate transporters. *Neurosci. Lett.* **370**, 230–235 (2004).
275. Yang, Y. *et al.* Molecular comparison of GLT1$^+$ and ALDH1L1$^+$ astrocytes *in vivo* in astroglial reporter mice. *Glia* **59**, 200–207 (2011).
276. Cuellar-Santoyo, A. O. *et al.* Revealing the contribution of astrocytes to glutamatergic neuronal transmission. *Front. Cell. Neurosci.* **16**, 1037641 (2023).
277. Van Wagoner, N. J., Oh, J.-W., Repovic, P. & Benveniste, E. N. Interleukin-6 (IL-6) Production by Astrocytes: Autocrine Regulation by IL-6 and the Soluble IL-6 Receptor. *J. Neurosci.* **19**, 5236–5244 (1999).
278. Hung, J. & Colicos, M. A. Astrocytic Ca2+ Waves Guide CNS Growth Cones to Remote Regions of Neuronal Activity. *PLoS ONE* **3**, e3692 (2008).
279. Hastings, N. *et al.* Electrophysiological In Vitro Study of Long-Range Signal Transmission by Astrocytic Networks. *Adv. Sci.* **10**, 2301756 (2023).
280. Tiberi, A. *et al.* Reduced levels of NGF shift astrocytes toward a neurotoxic phenotype. *Front. Cell Dev. Biol.* **11**, 1165125 (2023).
281. O'Shea, T. M. *et al.* Derivation and transcriptional reprogramming of border-forming wound repair astrocytes after spinal cord injury or stroke in mice. *Nat. Neurosci.* **27**, 1505–1521 (2024).
282. Cameron, E. G. *et al.* A molecular switch for neuroprotective astrocyte reactivity. *Nature* **626**, 574–582 (2024).
283. Krencik, R. *et al.* Dysregulation of astrocyte extracellular signaling in Costello syndrome. *Sci. Transl. Med.* **7**, (2015).
284. Pathak, D. & Sriram, K. Neuron-astrocyte omnidirectional signaling in neurological health and disease. *Front. Mol. Neurosci.* **16**, 1169320 (2023).
285. Brandebura, A. N., Paumier, A., Onur, T. S. & Allen, N. J. Astrocyte contribution to dysfunction, risk and progression in neurodegenerative disorders. *Nat. Rev. Neurosci.* **24**, 23–39 (2023).
286. Cunningham, C., Dunne, A. & Lopez-Rodriguez, A. B. Astrocytes: Heterogeneous and Dynamic Phenotypes in Neurodegeneration and Innate Immunity. *The Neuroscientist* **25**, 455–474 (2019).
287. Forrest, S. L. *et al.* Distribution Patterns of Astrocyte Populations in the Human Cortex. *Neurochem. Res.* **48**, 1222–1232 (2023).
288. Ghézali, G. *et al.* Connexin 30 controls astroglial polarization during postnatal brain development. *Development* **145**, dev155275 (2018).
289. Pajarillo, E., Rizor, A., Lee, J., Aschner, M. & Lee, E. The role of astrocytic glutamate transporters GLT-1 and GLAST in neurological disorders: Potential targets for neurotherapeutics. *Neuropharmacology* **161**, 107559 (2019).
290. Brozzi, F., Arcuri, C., Giambanco, I. & Donato, R. S100B Protein Regulates Astrocyte Shape and Migration via Interaction with Src Kinase. *J. Biol. Chem.* **284**, 8797–8811 (2009).
291. Dzwonek, J. & Wilczynski, G. M. CD44: molecular interactions, signaling and functions in the nervous system. *Front. Cell. Neurosci.* **9**, (2015).

292. Kim, J., Yoo, I. D., Lim, J. & Moon, J.-S. Pathological phenotypes of astrocytes in Alzheimer's disease. *Exp. Mol. Med.* **56**, 95–99 (2024).
293. Ali, F. & Kwan, A. C. Interpreting in vivo calcium signals from neuronal cell bodies, axons, and dendrites: a review. *Neurophotonics* **7**, 1 (2019).
294. Guérit, S. *et al.* Astrocyte-derived Wnt growth factors are required for endothelial blood-brain barrier maintenance. *Prog. Neurobiol.* **199**, 101937 (2021).
295. Rupprecht, P. *et al.* Centripetal integration of past events in hippocampal astrocytes regulated by locus coeruleus. *Nat. Neurosci.* **27**, 927–939 (2024).
296. Shkryl, V. M. The spatio-temporal properties of calcium transients in hippocampal pyramidal neurons in vitro. *Front. Cell. Neurosci.* **16**, 1054950 (2022).
297. Khakh, B. S. & Sofroniew, M. V. Diversity of astrocyte functions and phenotypes in neural circuits. *Nat. Neurosci.* **18**, 942–952 (2015).
298. Wakida, N. M. *et al.* Calcium Dynamics in Astrocytes During Cell Injury. *Front. Bioeng. Biotechnol.* **8**, 912 (2020).
299. Rungta, R. L. *et al.* Ca^{2+} transients in astrocyte fine processes occur via Ca^{2+} influx in the adult mouse hippocampus: Ca^{2+} Transients in Astrocyte Fine Processes. *Glia* **64**, 2093–2103 (2016).
300. Neo, S. & Tang, B. Collagen 1 signaling at the central nervous system injury site and astrogliosis. *Neural Regen. Res.* **12**, 1600 (2017).
301. Song, S. *et al.* Activation of endothelial Wnt/β-catenin signaling by protective astrocytes repairs BBB damage in ischemic stroke. *Prog. Neurobiol.* **199**, 101963 (2021).
302. McRae, J., Smith, C., Emmanuel, A. & Beeke, S. The experiences of individuals with cervical spinal cord injury and their family during post-injury care in non-specialised and specialised units in UK. *BMC Health Serv. Res.* **20**, 783 (2020).
303. Zholudeva, L. V. & Lane, M. A. Harnessing Spinal Interneurons for Spinal Cord Repair. *Neurosci. Insights* **17**, 26331055221101607 (2022).
304. Crone, S. A. *et al.* Irregular Breathing in Mice following Genetic Ablation of V2a Neurons. *J. Neurosci.* **32**, 7895–7906 (2012).
305. Allen, N. J. & Eroglu, C. Cell Biology of Astrocyte-Synapse Interactions. *Neuron* **96**, 697–708 (2017).
306. Farhy-Tselnicker, I. & Allen, N. J. Astrocytes, neurons, synapses: a tripartite view on cortical circuit development. *Neural Develop.* **13**, 7 (2018).
307. Bonvento, G. & Bolaños, J. P. Astrocyte-neuron metabolic cooperation shapes brain activity. *Cell Metab.* **33**, 1546–1564 (2021).
308. Perez-Catalan, N. A., Doe, C. Q. & Ackerman, S. D. The role of astrocyte-mediated plasticity in neural circuit development and function. *Neural Develop.* **16**, 1 (2021).
309. Ramos Ferrer, P., Vardhan, S. & Sakiyama-Elbert, S. Sustained neurotrophin-3 delivery from hyaluronic acid hydrogels for neural tissue regeneration. *J. Biomed. Mater. Res. A* **112**, 1188–1199 (2024).
310. Goretzki, L., Burg, M. A., Grako, K. A. & Stallcup, W. B. High-affinity Binding of Basic Fibroblast Growth Factor and Platelet-derived Growth Factor-AA to the Core Protein of the NG2 Proteoglycan. *J. Biol. Chem.* **274**, 16831–16837 (1999).
311. Takeuchi, M. *et al.* Type IV Collagen Controls the Axogenesis of Cerebellar Granule Cells by Regulating Basement Membrane Integrity in Zebrafish. *PLOS Genet.* **11**, e1005587 (2015).

312. Chen, Y. *et al.* Nidogen-2 is a Novel Endogenous Ligand of LGR4 to Inhibit Vascular Calcification. *Circ. Res.* **131**, 1037–1054 (2022).
313. Walia, A. *et al.* Endostatin's emerging roles in angiogenesis, lymphangiogenesis, disease, and clinical applications. *Biochim. Biophys. Acta BBA - Gen. Subj.* **1850**, 2422–2438 (2015).
314. Brunetti, J. *et al.* Unraveling Heparan Sulfate Proteoglycan Binding Motif for Cancer Cell Selectivity. *Front. Oncol.* **9**, 843 (2019).
315. Fermin, D., Basrur, V., Yocum, A. K. & Nesvizhskii, A. I. Abacus: A computational tool for extracting and pre-processing spectral count data for label-free quantitative proteomic analysis. *PROTEOMICS* **11**, 1340–1345 (2011).
316. Rossi, R., Arjmand, S., Bærentzen, S. L., Gjedde, A. & Landau, A. M. Synaptic Vesicle Glycoprotein 2A: Features and Functions. *Front. Neurosci.* **16**, 864514 (2022).
317. Zhu, W., Smith, J. W. & Huang, C.-M. Mass Spectrometry-Based Label-Free Quantitative Proteomics. *J. Biomed. Biotechnol.* **2010**, 1–6 (2010).
318. Florens, L. *et al.* Analyzing chromatin remodeling complexes using shotgun proteomics and normalized spectral abundance factors. *Methods* **40**, 303–311 (2006).
319. O'Connor, C. *et al.* Neurotrophic extracellular matrix proteins promote neuronal and iPSC astrocyte progenitor cell- and nano-scale process extension for neural repair applications. *J. Anat.* **246**, 585–601 (2025).
320. Zhang, Z. *et al.* Neurite outgrowth on well-characterized surfaces: preparation and characterization of chemically and spatially controlled fibronectin and RGD substrates with good bioactivity. *Biomaterials* **26**, 47–61 (2005).
321. Akers, R. M., Mosher, D. F. & Lilien, J. E. Promotion of retinal neurite outgrowth by substratum-bound fibronectin. *Dev. Biol.* **86**, 179–188 (1981).
322. Weston, C. A., Anova, L., Rialas, C., Prives, J. M. & Weeks, B. S. Laminin-1 Activates Cdc42 in the Mechanism of Laminin-1-Mediated Neurite Outgrowth. *Exp. Cell Res.* **260**, 374–378 (2000).
323. Hager, G., Pawelzik, H., Kreutzberg, G. W. & Zieglga, W. A PEPTIDE DERIVED FROM A NEURITE OUTGROWTH-PROMOTING DOMAIN ON THE 1 CHAIN OF LAMININ MODULATES THE ELECTRICAL PROPERTIES OF NEOCORTICAL NEURONS.
324. Guss, E. J., Akbergenova, Y., Cunningham, K. L. & Littleton, J. T. Loss of the extracellular matrix protein Perlecan disrupts axonal and synaptic stability during Drosophila development. *eLife* **12**, RP88273 (2023).
325. Balasubramani, M., Bier, M. E., Hummel, S., Schneider, W. J. & Halfter, W. Perlecan and its immunoglobulin like domain IV are abundant in vitreous and serum of the chick embryo. *Matrix Biol.* **23**, 143–152 (2004).
326. Seppinen, L. & Pihlajaniemi, T. The multiple functions of collagen XVIII in development and disease. *Matrix Biol.* **30**, 83–92 (2011).
327. Harvey, B. M., Baxter, M., Garcia, A. M. & Granato, M. Glial cell derived pathway directs regenerating optic nerve axons toward the CNS midline. Preprint at https://doi.org/10.1101/2024.10.15.618346 (2024).
328. Gould, T. W. *et al.* Glial cells maintain synapses by inhibiting an activity-dependent retrograde protease signal. *PLOS Genet.* **15**, e1007948 (2019).

329. Friedmann, I., Hauben, E., Yoles, E., Kardash, L. & Schwartz, M. T cell-mediated neuroprotection involves antithrombin activity. *J. Neuroimmunol.* **121**, 12–21 (2001).
330. Fox, M. A., Ho, M. S., Smyth, N. & Sanes, J. R. A synaptic nidogen: Developmental regulation and role of nidogen-2 at the neuromuscular junction. *Neural Develop.* **3**, 24 (2008).
331. Köhler, S. *et al.* Gray and white matter astrocytes differ in basal metabolism but respond similarly to neuronal activity. *Glia* **71**, 229–244 (2023).
332. Guertin, P. A. Central Pattern Generator for Locomotion: Anatomical, Physiological, and Pathophysiological Considerations. *Front. Neurol.* **3**, (2013).
333. Mladinic, M. & Nistri, A. Microelectrode arrays in combination with in vitro models of spinal cord injury as tools to investigate pathological changes in network activity: facts and promises. *Front. Neuroengineering* **6**, (2013).
334. Goshi, N., Morgan, R. K., Lein, P. J. & Seker, E. A primary neural cell culture model to study neuron, astrocyte, and microglia interactions in neuroinflammation. *J. Neuroinflammation* **17**, 155 (2020).
335. Luchena, C. *et al.* A Neuron, Microglia, and Astrocyte Triple Co-culture Model to Study Alzheimer's Disease. *Front. Aging Neurosci.* **14**, 844534 (2022).
336. Tomaselli, K. J., Neugebauer, K. M., Bixby, J. L., Lilien, J. & Reichard, L. F. N-cadherin and integrins: Two receptor systems that mediate neuronal process outgrowth on astrocyte surfaces. *Neuron* **1**, 33–43 (1988).
337. Rigby, M. J., Gomez, T. M. & Puglielli, L. Glial Cell-Axonal Growth Cone Interactions in Neurodevelopment and Regeneration. *Front. Neurosci.* **14**, 203 (2020).
338. Scemes, E. & Giaume, C. Astrocyte calcium waves: What they are and what they do. *Glia* **54**, 716–725 (2006).
339. Fields, R. D. & Burnstock, G. Purinergic signalling in neuron–glia interactions. *Nat. Rev. Neurosci.* **7**, 423–436 (2006).
340. Fei, X. *et al.* Homer1 promotes the conversion of A1 astrocytes to A2 astrocytes and improves the recovery of transgenic mice after intracerebral hemorrhage. *J. Neuroinflammation* **19**, 67 (2022).
341. Hu, Y. *et al.* Matrix stiffness changes affect astrocyte phenotype in an in vitro injury model. *NPG Asia Mater.* **13**, 35 (2021).
342. Stern, S. *et al.* RhoA drives actin compaction to restrict axon regeneration and astrocyte reactivity after CNS injury. *Neuron* **109**, 3436-3455.e9 (2021).
343. Hughes, M. D. G., Cussons, S., Mahmoudi, N., Brockwell, D. J. & Dougan, L. Tuning Protein Hydrogel Mechanics through Modulation of Nanoscale Unfolding and Entanglement in Postgelation Relaxation. *ACS Nano* **16**, 10667–10678 (2022).
344. Mout, R. *et al.* De novo design of modular protein hydrogels with programmable intra- and extracellular viscoelasticity. *Proc. Natl. Acad. Sci.* **121**, e2309457121 (2024).
345. Khoury, L. R. & Popa, I. Chemical unfolding of protein domains induces shape change in programmed protein hydrogels. *Nat. Commun.* **10**, 5439 (2019).
346. Andries, L., Van Hove, I., Moons, L. & De Groef, L. Matrix Metalloproteinases During Axonal Regeneration, a Multifactorial Role from Start to Finish. *Mol. Neurobiol.* **54**, 2114–2125 (2017).

347. Chan, Z. C.-K., Oentaryo, M. J. & Lee, C. W. MMP-mediated modulation of ECM environment during axonal growth and NMJ development. *Neurosci. Lett.* **724**, 134822 (2020).
348. Zuo, J., Ferguson, T. A., Hernandez, Y. J., Stetler-Stevenson, W. G. & Muir, D. Neuronal Matrix Metalloproteinase-2 Degrades and Inactivates a Neurite-Inhibiting Chondroitin Sulfate Proteoglycan. *J. Neurosci.* **18**, 5203–5211 (1998).
349. Szklarczyk, A., Lapinska, J., Rylski, M., McKay, R. D. G. & Kaczmarek, L. Matrix Metalloproteinase-9 Undergoes Expression and Activation during Dendritic Remodeling in Adult Hippocampus. *J. Neurosci.* **22**, 920–930 (2002).
350. Hsu, J.-Y. C. *et al.* Matrix Metalloproteinase-2 Facilitates Wound Healing Events That Promote Functional Recovery after Spinal Cord Injury. *J. Neurosci.* **26**, 9841–9850 (2006).
351. Ogier, C. *et al.* Matrix metalloproteinase-2 (MMP-2) regulates astrocyte motility in connection with the actin cytoskeleton and integrins. *Glia* **54**, 272–284 (2006).
352. Zhong, G., Sharma, K. & Harris-Warrick, R. M. Frequency-dependent recruitment of V2a interneurons during fictive locomotion in the mouse spinal cord. *Nat. Commun.* **2**, 274 (2011).
353. Hochman, S., Garraway, S. M. & Pockett, S. Membrane properties of deep dorsal horn neurons from neonatal rat spinal cord in vitro. *Brain Res.* **767**, 214–219 (1997).

Figures Created in BioRender. Vardhan, S. (2025)

Enrichment plot in Chapter 2 software citation: Yu G (2025). *enrichplot: Visualization of Functional Enrichment Result*. R package version 1.26.6, https://yulab-smu.top/biomedical-knowledge-mining-book/.

Vita

EDUCATION

University of Washington Seattle, WA

PhD, Bioengineering July 2025

Characterization of enriched astrocyte phenotypes and ECM generation for *in vitro* axon growth of V2a interneurons

The University of Texas at Austin Austin, TX

Masters, Biomedical Engineering Aug 2019

Cornell University Ithaca, NY

Major in Biological Engineering and Minor in Biomedical Engineering Dec 2016

RESEARCH EXPERIENCE

Graduate Research Assistant at Sakiyama-Elbert Lab
Seattle, WA and Austin, TX

UW Seattle Bioengineering, UT Austin Biomedical Engineering Aug 2017-August 2025

- Worked in cell-culture setting with mESC cell line maintenance and differentiation into astrocyte and neuron subtypes
- Developed and made critical decisions for puromycin selection protocol of astrocyte subtypes based on experiments with cell viability and qPCR
- Characterized selectable stem cell line derived enriched astrocyte phenotypes with imaging, qPCR, flow cytometry, proteomics, and RNA-sequencing
- Evaluated therapeutic potential of astrocyte-derived ECM proteins in hydrogel for axon growth of V2a interneurons
- Prepared oral presentations and posters to share research findings to scientific community at 5 conferences; wrote manuscripts for journal submissions and grant figures with conveying our results for the broader goal of advancing understanding of spinal cord biology
- Presented thesis project progress at research updates in lab group meeting for help in troubleshooting and read publications to keep updated on astrocyte field progress
- Conducted and designed *in vitro* studies with necessary controls for comparison to experimental groups with ensuring timeline planning for meeting thesis and manuscript deadliness and requirements
- Mentored two undergraduate students on various projects involving stem cell culture, imaging, data analysis, and hydrogels and helped them gain experiences for medical and graduate school acceptances
- Set up a lab space and cell culture rooms with equipment ordering by reviewing products from different company representatives; managed safety procedures

regarding use of chemicals in lab and record the chemicals used; this was done for the lab move from UT Austin to UW
- Worked and communicated with collaborators at UW Genomics and Proteomics Core for conducting RNA-sequencing and proteomics

Visiting Graduate Researcher at Shoichet Lab
Toronto, Ontario, Canada
University of Toronto, externship portion of NIH Ruth L. Kirschstein Imaging Fellowship
May 2018-August 2018

- Synthesized peptides for incorporation in hyaluronic acid-based hydrogels to model glioblastoma stem cell niche
- Gained experience in chemistry and HPLC skill sets for verification of peptide synthesis
- Collected and summarized resources to start a review on glioblastoma models for graduate student mentor

Research Technician and Undergraduate Research Student at Zipfel Lab
Ithaca, NY
Cornell Biomedical Engineering January 2015 – June 2017

- Constructed flow chambers to compare GFP aptamers and antibody in single molecular pulldown trials in determining dimerization of protein complexes
- Utilized protein purification methods and spectroscopy to optimize a fluorescent biosensor to detect ATP:ADP ratio as measure of cancer metabolism
- Presented the biosensor progress at scientific poster competition
- Collaborated with different labs to incorporate ideas for the biosensor improvement

Research Assistant at Parthasarathy Lab
Orlando, Florida
University of Central Florida Medicine Oct 2012 – April 2013; May 2016-August 2016

- Tuned chemistry of cypate-conjugated methods to utilize in detecting atherosclerosis plaques and other features
- Performed and analyzed enzymatic assays that demonstrated beneficial effects of Holy Basil on reducing harmful enzymatic activity that contributes to atherosclerosis progression

ENTREPRENEURSHIP EXPERIENCE

Texas Biodesign Program *(Spring 2022)*

- Worked in a team to develop a startup idea of 3D reconstruction of cervical lymph nodes for aiding in surgery and interacted with clinicians to discuss patient needs in this idea space
    - Identified a gap in the clinical space regarding cervical cancer and expanded on the research need to develop startup idea

Principal of Texas Venture Labs Practicum *(Spring 2022)*

- Led a team of associate student consultants on conducting market validation with surveys for Quimby (pre-revenue company) and pricing research for Dreamland (post-revenue company)
- Managed customer-client interactions and tracked team progress to reach our weekly goals/deliverables for our clients, which most of these interactions included communicating on virtual meeting platforms
- Communicated the team progress to company clients and facilitated discussion for completion of tasks
- Motivated team building for members to help drive their interests in respective tasks and help them to see it to completion
- Able to modify tasks based on client's feedback

Associate of Texas Venture Labs Practicum *(Fall 2021)*

- Worked in team of student consultants to build financial model for SkyStations (pre-revenue) and create a slide deck for investors
- Researched medical school curriculums in Saudi Arabia for potential international market expansion for OnlineMedEd (post-revenue company)
- Learned business concepts along with a patent law course to understand the fundamentals of different phases of a startup and company growth

PUBLICATIONS AND PRESENTATIONS

Publications:

- Vardhan,S., & Sakiyama-Elbert, S. (2025) Investigation of astrocyte phenotypic components and extracellular matrix (ECM) proteins on supporting axon growth of V2a interneurons *in vitro*. In Preparation.
- Vardhan, S., Thompson, R., Kenny, P., & Sakiyama-Elbert, S. (2025). Utilization of transgenic selectable mouse embryonic stem cell lines for puromycin selection of astrocyte phenotypes from heterogeneous astrocyte cultures. In Preparation.
- Vardhan, S., Jordan, T., & Sakiyama-Elbert, S. (2024). Stem cell engineering approaches for investigating glial cues in central nervous system disorders. *Current Opinion in Biotechnology.* Accepted for publication.
- Ferrer, P.R., Vardhan, S., & Sakiyama-Elbert, S. (2023). Sustained Neurotrophin-3 Delivery from Hyaluronic-Acid Hydrogels for Neural Tissue Regeneration. *Journal of Biomedical Materials Research*.
- Wilems, T., Vardhan, S., Wu, S., & Sakiyama-Elbert, S. (2019). The influence of microenvironment and extracellular matrix molecules in driving neural stem cell fate within biomaterials. *Brain research bulletin*.
- Narasimhulu, C. A., & Vardhan, S. (2015). Therapeutic Potential of Ocimum tenuiflorum as MPO Inhibitor with Implications for Atherosclerosis Prevention. *Journal of medicinal food*, *18*(5), 507-515.

Presentations:

- Vardhan, S., & Sakiyama-Elbert, S., 2023. Utilizing hyaluronic acid (HA)-based hydrogel platforms for testing effects of enriched astrocyte extracellular

matrix (ECM) on axon growth of V2a interneurons. *UW Biomaterial Seminar*. Seattle, 16 Dec.

- Vardhan, S., & Sakiyama-Elbert, S., 2023. Enriched grey matter astrocytes support greater axon growth of V2a interneurons than enriched white matter astrocytes. *BMES Rapid-fire Presentation and Poster*. Seattle, 13 Oct.
- Vardhan, S., Merchant, A., and Sakiyama-Elbert, S., 2022. The effect of enriched astrocyte phenotypic cultures on ECM composition and interneuron axon growth. *TERMIS Oral Presentation*. Toronto, 11 July.
- Vardhan,S. and Sakiyama-Elbert, S., 2020. The effect of astrocyte phenotype enrichment as live, frozen, and decellularized substrates for Axonal Growth of V2a interneurons. *World Biomaterials Congress.* Virtual, 11 Dec.
- Vardhan, S. and Sakiyama-Elbert, S., 2019. The Effect Of Astrocyte Phenotype Enrichment On Axonal Growth Of Motor Neurons and V2a Interneurons. *Biomedical Engineering Society Oral Presentation*. Philadelphia, 18 Oct.

TEACHING ASSISTANT EXPERIENCE

UT Austin- mentored students in achieving their goals for classes: Transport in Living Guided students through their design projects with business concepts and modeling products at the start of the COVID pandemic

- Taught transport mathematical concepts to a class of 70-80 students in a virtual environment
- Planned weekly timelines for student progress in the design projects and consulted the professor to ensure tasks were met
- Maintained assignment and test records

LEADERSHIP & SERVICE

STEM Pals, Volunteer
Jan 2023- Current
UW Union, Working group member and housing justice committee Sept 2022 – Current
Graduate Society of Women in Engineering (SWE), President at UT Austin (2018-2019)
BME Representative of Graduate Student Assembly
Aug 2019-May 2022
UT BME Graduate Student Society Academic Chair and Retreat Committee
Jan 2018- May 2022
Financial Director of SAGES (Society of advancing gender equity in STEM)
March 2018-May 2022
Financial Director of Graduate Engineering Council, Graduate and Industry Networking Committee Aug 2020- May 2021

SKILLS

Wet Lab: Cloning, stem cell culture, fluorescence in situ hybridization, assays, viability staining, gel electrophoresis, western blots, ICC, flow cytometry, decellularization, hydrogel synthesis, bulk RNA-sequencing, proteomics

Microscopy: Fluorescence, calcium imaging, confocal, spectroscopy

Analysis and Software: R studio, JMP for design of experiments, Partek software, Abacus, Nikon microscope analysis, Cell Profiler, Image J, Graphpad Prism, Matlab, Basic python understanding and coding, Microsoft Office

Soft skills: scientific presentation, teamwork, problem solving, project management, mentorship, troubleshooting

AWARDS

Texas Biodesign Cohort Program 2022
Society of Biomaterials Tissue Engineering Special Interest Group Student Abstract Award 2020
NIH Ruth L. Kirschstein Imaging Fellowship 2017